



## Structural evolution of the superimposed Provençal and Subalpine fold-thrust belts (SE France)

Jocelyn Balansa, Nicolas Espurt, Jean-Claude Hippolyte, Jean Philip,  
Séverine Caritg

### ► To cite this version:

Jocelyn Balansa, Nicolas Espurt, Jean-Claude Hippolyte, Jean Philip, Séverine Caritg. Structural evolution of the superimposed Provençal and Subalpine fold-thrust belts (SE France). *Earth-Science Reviews*, 2022, 227, pp.103972. 10.1016/j.earscirev.2022.103972 . hal-03604262

HAL Id: hal-03604262

<https://hal.science/hal-03604262>

Submitted on 10 Mar 2022

**HAL** is a multi-disciplinary open access archive for the deposit and dissemination of scientific research documents, whether they are published or not. The documents may come from teaching and research institutions in France or abroad, or from public or private research centers.

L'archive ouverte pluridisciplinaire **HAL**, est destinée au dépôt et à la diffusion de documents scientifiques de niveau recherche, publiés ou non, émanant des établissements d'enseignement et de recherche français ou étrangers, des laboratoires publics ou privés.

1    **Structural evolution of the superimposed Provençal and**  
2    **Subalpine fold-thrust belts (SE France)**

3    Jocelyn Balansa<sup>1</sup>, Nicolas Espurt<sup>1,2\*</sup>, Jean-Claude Hippolyte<sup>1</sup>, Jean Philip<sup>1</sup>, Séverine Caritg<sup>3</sup>

4    <sup>1</sup>Aix Marseille Univ, CNRS, IRD, INRAE, Coll France, CEREGE, Aix-en-Provence, France

5    <sup>2</sup>Université Côte d'Azur, CNRS, Observatoire de la Côte d'Azur, IRD, GEOAZUR, France

6    <sup>3</sup>BRGM-French Geological Survey, Orléans, France

7    \*Corresponding author at: Campus Azur CNRS, GEOAZUR, 250 rue Albert Einstein, CS  
8    10269, 06905 Sophia Antipolis CEDEX, France.

9    *E-mail address:* espurt@geoazur.unice.fr (N. Espurt)

10    **Abstract**

11    Highlighting how crustal shortening is accommodated in space and time in fold-thrust belts is  
12    a major issue for understanding the long-term tectonic evolution of orogenic systems. In this  
13    study, we combine surface and subsurface data to build a 150 km-long sequentially restored  
14    balanced cross-section across two superimposed foreland fold-thrust belts in southeastern  
15    France: the upper Cretaceous-Eocene Provençal belt and Oligocene-Neogene Subalpine belt.  
16    These belts are composed of inverted Paleozoic-Mesozoic basins with Mesozoic halokinetic  
17    structures, basement thrusts, and cover thrusts-nappes detached in the Triassic evaporites. The  
18    multiphase growth of the Provençal and Subalpine belts has been constrained along the  
19    studied cross-section by syn-orogenic deposits and kinematic indicators of thrusting. The pre-  
20    orogenic palinspastic reconstruction of the cross-section to Late Santonian shows a large  
21    uplift zone in the center of the section (Durance and Valensole highs), which led to the  
22    separation of the Beausset basin (South Provence basin) to the south from the Barles-Digne  
23    basin (Vocontian basin) to the north. The Provençal shortening propagated ~NNE-ward from  
24    the Beausset basin up to folds in the Barles area during the Latest Santonian to Eocene times.  
25    Shortening value reaches 38 km and has been mainly accommodated by the inversion of the  
26    South Provence basin-Durance high. The Subalpine shortening propagated ~SW-ward from  
27    the Barles-Digne basin up to the Mediterranean coast during the Oligocene-Miocene to  
28    Quaternary times. It reaches 35 km and has been mainly consumed by the inversion of the  
29    thick Digne basin. The Provençal thrust wedge is characterized by distributed basement  
30    thrusts reworking numerous structures inherited from the Variscan belt and Permian-

31 Mesozoic rifts. This structural style might have favored the development of confined foreland  
32 basins, as the Arc and Rians basins. In contrast, the vertical stacking of the thick Digne Nappe  
33 and Barles basement triangle zone in the Subalpine thrust wedge might have controlled the  
34 large flexure of the Valensole foreland basin. The lack of Triassic evaporites in the Valensole  
35 high probably explains that shortening was not transferred into the cover of this domain.  
36 Consequently, the Provençal then the Subalpine shortenings might have been transferred more  
37 deeply to induce the reactivation of basement faults into the external zones. The Mesozoic  
38 halokinetic structures also strongly influenced the location of contractional deformation. This  
39 study highlights that the crustal structural inheritances influenced the structural styles and  
40 development of extensional basins and subsequent Provençal and Subalpine belts.

## 41 **Keywords**

42 Superimposed orogens; Thrust tectonics; Cross-section balancing; Sequential restoration;  
43 Structural inheritance; Provence-Alps

## 44 **1. Introduction**

45 The structural evolution of fold-thrust belts is systematically controlled by crustal  
46 heterogeneities (e.g., rheology, crust-mantle coupling and crustal thickness) which are mostly  
47 inherited from previous tectonic stages of extensional, compressional, or strike-slip  
48 deformation (e.g., Lutaud, 1957; Angelier and Aubouin, 1976; Zubieta-Rossetti et al., 1993;  
49 Coward, 1996; Roure and Colletta, 1996; Beauchamp et al., 1999; Branquet et al., 2002; Kley  
50 and Monaldi, 2002; Souquet et al., 2003; Mora et al., 2006; Alvarez-Marron et al., 2006;  
51 Vergés et al., 2007; Espurt et al., 2008; Malavieille and Konstantinovskaya, 2010; Bellahsen  
52 et al. 2012; Hinsch, 2013; Moutherneau et al., 2013; Tavani et al., 2015; Lacombe and  
53 Bellahsen, 2016; Bestani et al., 2016; Butler, 2017; Calderon et al., 2017; Espurt et al., 2019a;  
54 Jourdon et al., 2019, 2020; Spitz et al., 2020; Martín-González et al., 2021; Moutherneau et al.,  
55 2021). These elements generate anisotropic behavior of the crust during contractional  
56 deformation in the Provence, where the succession of geological events generated a complex  
57 structural framework since Paleozoic (Matte, 2001; Lacombe and Jolivet, 2005; Guillot and

58 Menot, 2009; Schreiber et al., 2011; Advokaat et al., 2014; Tavani et al., 2018; van  
59 Hinsbergen et al., 2020; Romagny et al., 2020; Angrand and Moutherieu, 2021). In this paper  
60 we have chosen to study and discuss the anisotropic behavior of Provence crust and its role on  
61 kinematic evolution of superimposed Provençal and the Subalpine fold-thrust belts (Fig. 1;  
62 Lemoine, 1972; Siddans, 1979).

63 The Provençal and southwestern Subalpine foreland thrust wedges have contrasting thrust  
64 vergences and time emplacement as recorded by structural data and well preserved syn-  
65 tectonic foreland strata. Both thrust wedges are characterized by a far-field transmission of the  
66 compressional stress into the most external zones that is still poorly characterized and not yet  
67 quantified because of complex overlap of extensional and compressional deformations (e.g.,  
68 Baudemont, 1985; Tempier, 1987; Delfaud et al., 1989; Guieu and Roussel, 1990; Philip,  
69 2012; Bestani et al., 2016; Tavani et al., 2018). Thrust-fold structures related to the Provençal  
70 compression develop at more than 180 km to the north from the Provence crystalline massifs  
71 (Fig. 1). They were described in the Valensole foreland basin (Dubois and Curneille, 1978), in  
72 the Castellane arc (de Lapparent, 1935; Goguel, 1937; Kerckhove and Antoine, 1963; Roux,  
73 1968; Roux, 1970; Campredon and Giannerini, 1982), in the Barles area (Lemoine, 1972;  
74 Haccard et al., 1989b), and in the Baronnies-Dévoluy area (Gidon et al., 1970; Lemoine,  
75 1972; Gidon and Pairis, 1976; Fabre et al., 1985; Montenat et al., 2005). Likewise, the  
76 occurrence of deformed Neogene to Quaternary rocks in southern Provence and the seismicity  
77 data, suggest far-field reactivation of inherited structures more than 100 km to the south to the  
78 Subalpine thrust front and as far as the Ligurian continental shelf (Guieu, 1968; Angelier and  
79 Aubouin, 1976; Weydert and Nury, 1978; Dupire, 1985; Hippolyte et al., 1993; Champion et  
80 al., 2000; Baroux et al., 2001; Chardon et al., 2005; Cushing et al., 2008; Béthoux et al., 2008;  
81 Larroque et al., 2021; Fig. 1).

82 Low-temperature thermochronology methods which are used to constrain the chronology  
83 of thrust propagation as in many fold-thrust belts (e.g., Ege et al., 2007; Jolivet et al., 2007;  
84 Espurt et al., 2011; Parra et al., 2012; Labaume et al., 2016; Rat et al., 2019; Hernandez et al.,  
85 2020), are poorly applicable in the study area because the Provençal and Subalpine thrust  
86 wedges have experienced insufficient Cenozoic burial and the exhumation history of the inner  
87 crystalline basement of the Provençal belt has been erased by the thermal event related to the  
88 Oligocene-Miocene Ligurian-Provençal rift (Lucazeau and Mailhe, 1986; Machhour et al.,  
89 1994; Morillon, 1997; Jakni, 2000; Bestani, 2015). The study of syn-tectonic strata with  
90 growth stratal pattern deposited during contractional deformations remains thus essential for  
91 reconstructing the chronology of successive deformational events, thrust propagation, and  
92 foreland basin evolution (Vergés and Munoz, 1990). This approach can be combined with  
93 fault slip analyses to constrain deformation regimes, thrust tectonic transport directions and  
94 particularly late fault reactivation in younger and in appearance undeformed foreland strata  
95 (Angelier, 1984, 1991). Balanced cross-section method has been used to restore  
96 compressional tectonic structures to their initial stages and the geometry of the basins before  
97 their deformation (Dahlstrom, 1969; Thomas and Bayona, 2002). Integration of precise timing  
98 of thrusting provided by syn-orogenic deposits with cross-section balancing can be a powerful  
99 tool for reconstructing shortening rates and restore deformation stages (Burbank and Vergés,  
100 1994; Zapata and Allmendinger, 1996; Meigs and Burbank, 1997; Echavarria et al., 2003;  
101 Heermance et al., 2008; Li et al., 2010).

102 This paper is a review and analysis of the geology and structure of the Provençal and  
103 Subalpine thrust wedges in Central Provence. To decipher the complex multistage thrusting  
104 history in space and time of these superimposed thrust wedges, we built a 150 km-long  
105 balanced and restored cross-section across the widespread dissected Provençal Beausset, Arc  
106 and Rians foreland basins, and broad Alpine Valensole foreland basin (Fig. 1) using available

107 surface and subsurface data. Foreland syn-tectonic deposits and fault slip data allow us to  
108 validate an accurate kinematics model of crustal shortening budget. We discuss the role of  
109 pre-existing basement-cover heterogeneities, and we confirm their dominance on long-term  
110 tectonic evolution of the orogenic belts.

111 **2. Structural framework**

112 From the Mediterranean coast to the south, to the Baronnies-Barles area to the north (Fig.  
113 1), the ~E-trending folds and thrusts mainly result from the ~northward Provençal  
114 compression (so-called Pyrenean-Provençal compression; Bertrand, 1888; Zürcher, 1891;  
115 Kilian, 1892; Lutaud, 1924; Philip and Allemann, 1982; Tempier, 1987). Shortening occurred  
116 from the Latest Santonian-Campanian to the Late Eocene (~50 m.y.) in response to the N-S  
117 convergence of the Eurasian and African plates through the Sardinia-Corsica continental  
118 block (Lacombe and Jolivet, 2005; Schreiber et al., 2011; Advokaat et al., 2014; van  
119 Hinsbergen et al., 2020; Fig. 2b). During Oligocene-Miocene times, the inner Provençal thrust  
120 wedge has been affected by the E-W opening of the West-European rift then the NW-SE  
121 opening of the Ligurian-Provençal back-arc basin between Provence and Corsica-Sardinia  
122 block (Hippolyte et al., 1993; Gattacceca et al., 2007; Bache et al., 2010; Oudet et al., 2010;  
123 Nury et al., 2016; Romagny et al., 2020; van Hinsbergen et al., 2020; Fig. 2c). A SW-ward  
124 migration of the Alpine deformation front into the southern Subalpine zone and Provençal  
125 zone occurred from the Oligocene-Miocene to the present day (~30 m.y.) in response to the  
126 eastward continental subduction of Eurasia beneath Adria (Fig. 2d). It is characterized by two  
127 major arcs detached above Triassic evaporites, the Diois-Baronnies-Western Provence Arc to  
128 the west and the Digne-Castellane Arc to the east (Goguel, 1937; Siddans, 1979; Villeger and  
129 Andrieux, 1987). These arcs are separated by the poorly deformed Neogene Valensole  
130 foreland basin (Figs. 1 and 2d). The thrust systems are accommodated by NNE-trending  
131 strike-slip faults (Middle Durance fault zone, Bès fault; Hippolyte et al., 2012; Guyonnet-

132 Benaize et al., 2015) inherited from the Paleozoic and Mesozoic extensional fault pattern  
133 (Roure and Colletta, 1996).

134 Many previous local studies have described the structural architecture of the thrust systems  
135 in the Provençal zone (Kilian, 1892; Mennessier, 1959; Aubouin and Mennessier, 1962;  
136 Aubouin and Chorowicz, 1967; Morabito, 1967; Guieu, 1968; Mennessier, 1970; Tempier,  
137 1987; Bestani et al., 2015; Guyonnet-Benaize et al., 2015; Bestani et al., 2016; Espurt et al.,  
138 2019b), in the Valensole foreland basin (Dubois and Curnelle, 1978; Hippolyte and Dumont,  
139 2000) and in the Subalpine zone of the Digne-Castellane arc (Goguel, 1937, 1939, 1944;  
140 Unalan, 1970; Lemoine, 1972; Gigot et al., 1974; Debelmas, 1974; Giannerini, 1978; Siddans,  
141 1979; Gidon and Pairis, 1992; Laurent et al., 2000; Graham et al., 2012; Célini et al., 2020).

142 North of the Paleozoic basement units outcropping in the Maures and Tanneron-Estérel  
143 massifs (Figs. 1 and 3), the Provençal zone consists in strongly deformed Mesozoic sediments  
144 and upper Cretaceous-Eocene foreland sedimentary units covered in places by Oligocene and  
145 Miocene-Pliocene rocks. Southward, it shows ENE-trending thrust sheets (Bandol, Sainte-  
146 Baume, Etoile-Pierresca, Aurélien Mount) associated with two large synclines (Beausset and  
147 Arc; Bestani et al., 2015). Northward, the structures are characterized by E- to ESE-trending  
148 thrusts (Sainte-Victoire Mountain, Pourrières, Pallières, Vinon, Les Maurras and Gréoux) and  
149 small synclines (e.g., Rians and Saint-Julien) interfering with NW- to NNE-trending zones of  
150 middle-upper Triassic evaporitic-carbonate (e.g., Barjols or Carcès Triassic zones; Fig. 3).

151 These Triassic sequences show significant internal fold systems and can be associated with  
152 halokinetic synclines (Angelier and Aubouin, 1976; Baudemont, 1985; Espurt et al., 2019b).  
153 Northward, Miocene-Pliocene sediments fill the Valensole foreland basin. Its morphology  
154 corresponds to a ~55 km long and up to ~30 km plateau dissected by Quaternary rivers (Gigot  
155 et al., 1974; Dubois and Curnelle, 1978; Mercier, 1979; Fig. 3). Westward, the basin is  
156 bordered by the NNE-trending Middle Durance fault system (e.g., Roure et al., 1992). This

157 fault controlled extensional subsidence to the northwest of the Manosque basin during the  
158 Mesozoic and the Oligocene, and transpressional uplift during its Miocene inversion (e.g.,  
159 Roure and Colletta, 1996; Guyonnet-Benaize et al., 2015). Along the northern and  
160 northeastern edges of the Valensole foreland basin, Mesozoic to Neogene strata are deformed  
161 by SW-verging anticlines (e.g., Lambruissier, Mirabeau-Mallemoisson, Aiglun, La Maurière)  
162 and overthrusted by the SW-verging Digne Nappe and Castellane arc (Goguel, 1963; Gigot et  
163 al., 1974; Dubois and Curnelle, 1978; Faucher et al., 1988, Hippolyte and Dumont, 2000; Fig.  
164 3).

165 **3. Stratigraphy**

166 The basement rocks and sedimentary successions in the Provençal and Subalpine zones are  
167 summarized in Figs. 4 and 5 and described hereafter.

168 **3.1. Variscan basement and upper Paleozoic sedimentary successions**

169 Paleozoic rocks are exposed in the Maures and Tanneron-Estérel massifs, Cap Sicié  
170 peninsula, and punctually in the eastern Provençal zone (Carcès) and Subalpine zone of  
171 Digne-Barles (St-Geniez, Verdaches and in tectonic slices at the base of the Digne Nappe)  
172 (Baudemont, 1985; Tempier, 1987; Guiomar, 1990; Crévola and Pupin, 1994; Fig. 3). In the  
173 Maures and Tanneron massifs, the Variscan belt is formed by E-verging thrust stacking of  
174 Cambrian-Silurian foliated metasediments including phyllites, micaschists and gneisses. The  
175 upper Carboniferous stage is associated with N-S orogen-parallel transpressional shearing  
176 synchronous with the opening of intramountain basin filled by terrigenous sediments and  
177 emplacement of granitoid and dome structures (Crévola and Pupin, 1994; Onézime et al.,  
178 1999; Rolland et al., 2009; Corsini et al., 2010; Schneider et al., 2014; Simonetti et al., 2020).  
179 During the continental break-up of Pangea, the Variscan framework was unconformably  
180 overlain by a more than 800 m-thick Permian detrital and volcanoclastic sequence

181 accumulated in a puzzle of intracontinental basins associated with NNE- to SE-trending  
182 steeply-dipping normal faults (Bathiard and Lambert, 1968; Baudemont, 1985; Delfaud et al.,  
183 1989; Toutin-Morin et al., 1993; Durand, 1993; Cassinis et al., 2003). Well data indicate a  
184 heterogenous distribution of the upper Carboniferous-Permian depocenters under the  
185 Mesozoic-Cenozoic cover of Provençal zone and Valensole foreland basin (e.g., Morabito,  
186 1967; Bathiard and Lambert, 1968; Dubois and Curneille, 1978; Baudemont, 1985).

### 187 **3.2. Triassic to upper Santonian Tethyan, Vocontian and South Provence rift successions**

188 Paleozoic rocks are unconformably overlain by ~30-120 m-thick lower-middle Triassic  
189 white to red fluvial conglomerates and sandstones, and red-green argillites of the  
190 Buntsandstein facies (Fig. 4). The opening of the Tethys Ocean started with the deposition of  
191 a middle-upper Triassic succession of dolomite, marls, cargneules, halite, anhydrite, and  
192 gypsum layers. The Muschelkalk facies is 100 to 600 m-thick. This unit is composed by the  
193 lower Anhydrittgruppe evaporites mainly developed in Provençal domain (Fig. 4), and upper  
194 Muschelkalk limestones (Mennessier, 1959; Caron, 1979; Brocard and Philip, 1989; Toutin-  
195 Morin et al., 1993; 1994; Espurt et al., 2019b). It is overlain by dolostones and evaporitic  
196 marls of Keuper facies, 40 to 450 m-thick in Provence and more than 1 km-thick in the Digne  
197 basin (Arnaud et al., 1976; Baudrimont and Dubois, 1977; de Graciansky et al., 1989; Fig. 4).  
198 Rhaetian rocks consist of 30 to 80 m-thick alternation of limestones and yellow-green marls.  
199 Middle-upper Triassic successions also contain ankaratrite intrusions and volcanoclastic  
200 levels (Caron, 1970).

201 Sedimentologic and structural studies in Provence (Philip et al., 1987; Espurt et al., 2019b)  
202 and southern Subalpine zone (Coadou et al., 1971; Rousset et al., 1983; Dardeau, 1988;  
203 Mascle et al., 1988; Lemoine and de Graciansky, 1988; Haccard et al., 1989b; Graham et al.,  
204 2012; Célini et al., 2020) suggest that the Jurassic-Santonian succession is associated with  
205 significant thickness and facies changes due to syn-rift basement faulting, thermal subsidence

206 and local halokinetic motions of the ductile Triassic evaporite layers. From Jurassic to  
207 Barremian, the Provençal domain consisted in dominantly marine carbonates that built huge  
208 platforms (Léonide et al., 2007; Masse et al., 2009) including shallow marine limestones,  
209 dolomites, calcareous breccias and lower Cretaceous rudist-bearing limestones with Urgonian  
210 facies (Fig. 4). The thickness of this carbonate succession varies from 300 m to 1 km. These  
211 platform sequences are superseded by pelagic facies in the Digne basin during Jurassic times.  
212 Major subsidence of the Digne basin is recorded by the deposition of up to 1.4 km-thick of  
213 lower Jurassic pelagic shales (Coadou et al., 1971; Fig. 4). During Middle Jurassic, the  
214 subsidence reaches the Barles area with the deposition of more than 1.8 km-thick upper  
215 Bathonian-lower Oxfordian black shales and turbidites (Black Shales Formation). The  
216 overlying upper Jurassic-lower Cretaceous pelagic sediments attest for persisting subsidence  
217 associated with gravitational instabilities. It consists of ~220 m-thick upper Oxfordian clayed  
218 limestones and Kimmeridgian-Tithonian limestones covered by ~350 m-thick Berriaskan-  
219 Barremian clayed limestones, breccias and turbidites (Rousset et al., 1983; de Graciansky and  
220 Lemoine, 1988; Célini et al., 2020).

221 From Latest Barremian to the beginning of Cenomanian and probably until Late Santonian,  
222 the opening of the Bay of Biscay is associated with the Valais Ocean through the Vocontian  
223 basin and led to NNE-SSW extension between Eurasia and Sardinia-Corsica block (Advokaat  
224 et al., 2014; Tavani et al., 2018; van Hinsbergen et al., 2020; Angrand and Mouthereau, 2021;  
225 Fig. 2a). During this period, the uplift of the Durance high separates the Digne-Barles basin to  
226 the north from the Beausset basin to the south. The Beausset basin can be interpreted as the  
227 eastern prolongation of the Pyrenean Rift System (Philip et al., 1987; Hennuy, 2003; Bestani  
228 et al., 2016; Tavani et al., 2018; Floquet et al., 2021; Angrand and Mouthereau, 2021; Fig.  
229 2a). ~350 m-thick of Aptian-Albian pelagic black shales and gravitational deposits  
230 accumulated in the southern edge of the Beausset basin (Philip et al., 1987), overlain by ~1.1

231 km-thick Cenomanian-Santonian marine rudist-rich carbonate including siliciclastic  
232 sediments (e.g., La Ciotat conglomerates) deposited into local troughs sourced from an  
233 emerged basement paleo-high between the Provence and the Sardinia-Corsica block (Philip,  
234 1970; Hennuy, 2003; Floquet et al., 2005, 2006). Northward, middle Cenomanian-upper  
235 Santonian sediments progressively onlap the Durance high from the Beausset basin to the  
236 southern edge of the Arc basin (Fig. 4). The Durance high corresponds to a large E-trending  
237 dome with low relief associated with major subaerial erosion and bauxite formation from  
238 uppermost Albian to lowermost Cenomanian at least, and till Santonian (Aubouin and  
239 Chorowicz, 1967; Masse and Philip, 1976; Laville, 1981; Guyonnet-Benaize et al., 2010;  
240 Figs. 2 and 4). North of the Durance high, Aptian-Albian deposits reach ~170 m-thick in the  
241 Digne-Barles basin (Rousset et al., 1983; Friès, 1987; Haccard et al., 1989b; Breheret, 1995),  
242 and consist of marine black shales. The overlying Cenomanian-Santonian strata dominantly  
243 consist of more than 1.5 km-thick marine marls and limestones in the Digne basin (Rousset et  
244 al., 1983).

### 245 **3.3. Uppermost Santonian to Eocene foreland successions in Provençal zone**

246 Plate reconstructions suggest the onset of N-S convergence between Africa and Eurasia  
247 that led to the contraction of Corsica-Sardinia block and Provence (Advokaat et al., 2014; van  
248 Hinsbergen et al., 2020; Angrand et Moutherieu, 2021; Fig. 2b), as illustrated by the  
249 transition from marine to continental environment in Latest Santonian in the Beausset basin.  
250 The growth of Provençal belt initiates at ~84 Ma and continues until the Late Eocene toward  
251 the north (Philip, 1970; Philip et al., 1987; Tempier, 1987; Lemoine et al., 2000; Lacombe  
252 and Jolivet, 2005; Montenat et al., 2005; Espurt et al., 2012; Philip et al., 2017). The  
253 Provençal foreland succession is characterized by local continental facies dated by  
254 magnetostratigraphy (Westphal and Durand, 1990; Cojan et al., 2003) and biostratigraphy  
255 (Garcia and Vianey-Liaud, 2001; Philip et al., 2017). Upper Cretaceous-lower Eocene

256 foreland sequences are exposed in the Beausset, Arc, Rians, Saint-Julien and Esparron-de-  
257 Verdon basins (Fig. 4). They are described in Fig. 5a. The Valdonnian and Fuvelian facies are  
258 of Latest Santonian-Early Campanian age and correspond to lacustrine and palustrine black  
259 limestones units including lignite beds (Fabre-Taxy and Philip, 1964; Durand, 1980; Fig. 5a).  
260 The Begudian facies is of Middle Campanian age and consists in lacustrine and fluvial  
261 deposits. The Rognacian facies is of Late Campanian-Maastrichtian age. It consists in  
262 dinosaur eggshells and bones-bearing red marls, sandstones and Rousset lacustrine limestone  
263 deposits (Cojan, 1989; 1993; Garcia and Vianney-Liaud, 2001). In the Arc basin, the  
264 Cretaceous-Cenozoic boundary is located inside the Galante Formation, a 5-10 m-thick fluvial  
265 conglomerates made of well-rounded pebbles of basement quartzite sourced from the Maures  
266 massif (Durand, 1962; Cojan, 1993). The Danian corresponds to the Vitrollian facies with red  
267 silty marls including lacustrine microcodium limestones. The Selandian-Thanetian Bird  
268 Eggshells Marls Formation comprises the lacustrine limestones of Meyreuil and Saint-Marc  
269 in the Arc basin. In the Rians basin it also includes the Touars conglomerates with clasts  
270 derived from the Maures massif. The Ypresian period includes deposition of the Langesse  
271 limestone and red-grey marls with gypsum in the Arc basin, and the fluvial Bluish Sands  
272 Formation including lacustrine *Bithynia* bearing limestones in the Rians basin and High Var  
273 area (de Lapparent, 1938a, 1938b; Corroy, 1957; Durand and Tempier, 1962; Angelier, 1971;  
274 Philip et al., 2017; Fig. 1). Finally, the Lutetian consists in Montaiguet and Cuques lacustrine  
275 limestones cropping out in the Arc basin. The upper Cretaceous-Eocene continental sequences  
276 of the Provençal foreland basin include locally massive syn-orogenic alluvial-fan deposits  
277 with growth strata recording thrust activity (Durand and Tempier, 1962; Guieu, 1968;  
278 Angelier, 1971; Leleu et al., 2009; Espurt et al., 2012). They correspond to upper Cretaceous  
279 Begudian-Rognacian breccias and Paleocene microcodium breccias with clasts derived  
280 generally from the nearby Jurassic-Cretaceous growing reliefs (Fig. 5a).

281     **3.4. Oligocene syn-rift and Miocene post-rift successions in Provençal zone**

282     The Oligocene is a transitional period between the end of the Provençal compression and  
283     the initial growth of the southern Subalpine zone (Nury, 1988). In the south and east of the  
284     study area, the Provençal compressional structures were affected by the E-W opening of the  
285     West-European rift then the NW-SE opening of the Ligurian-Provençal back-arc rift between  
286     Provence and Corsica-Sardinia block (Hippolyte et al, 1993; Gattaccea et al., 2007;  
287     Advokaat et al., 2014; van Hinsbergen et al., 2014; Bestani et al., 2016; Nury et al., 2016;  
288     Romagny et al., 2020, van Hinsbergen et al., 2020; Fig. 2c). The result of these successive  
289     extensional events is the formation of large intracontinental basins like the Marseille,  
290     Aubagne, Aix-en-Provence, and Manosque basins (Fig. 3; Hippolyte et al, 1993). Smaller  
291     Oligocene basins developed in southeastern Provence. They are the NE- to E-trending  
292     Bandol, Signes-Méounes, Peypin, Saint-Zacharie and Nans basins/troughs (Popoff, 1973;  
293     Nury, 1988) (Figs. 3, 4 and 5a). In the High Var area (Fig. 1), Oligocene sediments fill N- to  
294     NNW-trending narrow basins (Touraine, 1967; Angelier, 1971; Angelier and Aubouin, 1976;  
295     Giannerini, 1978; Philip et al., 2017) like the La Combe, Bourdas and Plan d'Auron troughs  
296     (Figs. 3, 4 and 5a). In the overall, syn-rift sediments correspond to lacustrine and clastic  
297     deposits including marls and locally gypsum intercalations as in the Manosque basin (Fig. 3),  
298     but the subsidence rate was ten times larger during the Ligurian-Provençal rifting than during  
299     the West-European rifting (Hippolyte et al., 1993).

300     The drifting of the Ligurian-Provençal basin associated with the counterclockwise rotation  
301     of the Corsica-Sardinia block during the Miocene times led to the flooding of the inner  
302     Provençal basement thrust wedge (Guieu and Roussel, 1990; Hippolyte et al, 1993;  
303     Gattaccea et al., 2007; Oudet et al., 2010; Bestani et al., 2016; Nury et al., 2016). In the  
304     onshore domain, Miocene (Burdigalian(?) to Tortonian) continental strata with marine  
305     intercalations filled N- to NW-trending incised valleys and basins (e.g., Les Maurras, Barjols,

306 Nans, Signes/Méounes and Bandol). These deposits consist of basal red breccias, sandstones  
307 and marls, and upper fluvial conglomerates (Mennessier, 1959; Cornet, 1965; Angelier and  
308 Aubouin, 1976) generally originated from the erosion of nearby Jurassic reliefs (Les Maurras  
309 basin) or from the Maures massif (Nans basin) (Figs. 3 and 4; Cornet, 1961). In the west of  
310 the study area (Luberon-Nerthe; Fig. 1), shallow marine environment is associated with the  
311 formation of concomitant wave-cut platforms overlain by marine molasse including  
312 limestones and grainstones (Champion et al., 2000; Besson, 2005; Oudet et al., 2010).  
313 Basaltic clasts related to Messinian intrusions and lava flows of Evenos are found in the upper  
314 conglomerate sequences (Pliocene?) of the Bandol basin (Coulon, 1967; Baubron, 1984).  
315 Pliocene to Quaternary sediments are mainly found within paleo-valleys that were incised  
316 during the Messinian and then filled by Gilbert type deltas after the reflooding of the  
317 Mediterranean Sea at 5.46 Ma (Clauzon, 1978; 1982, Bache et al., 2012).

318 **3.5. Cenozoic foreland successions in Subalpine zone: Barles zone and Valensole foreland  
319 basin**

320 In the Barles zone, folded Mesozoic sequences are unconformably overlain by the poorly  
321 dated (upper Eocene-lower Oligocene?) continental Basal Breccia Formation (Lemoine, 1972;  
322 Haccard et al., 1989a,b; Fig. 5b). It is composed of breccia channels interbedded with red  
323 shales. The breccia channels are composed of clasts and olistoliths, exclusively sourced from  
324 local Jurassic and Cretaceous limestone strata, included in a red shaly matrix with  
325 microcodium (Gigot et al., 1974; Haccard et al., 1989b). The Basal Breccia Formation is  
326 interpreted as sedimentary drape sequences (with differential compaction) sealing the paleo-  
327 morphology of E-trending Eocene Provençal folds (Lemoine, 1972; Maillart et al., 1987;  
328 Haccard et al., 1989b). However, the breccia beds also exhibit large sedimentary fans which  
329 could be interpreted as growth strata deformed by progressive tectonic uplift (Maillart et al.,  
330 1987). The Basal Breccia Formation might be laterally equivalent to upper Eocene

331 nummulitic limestones deposited immediately to the east in the Digne-Castellane basin  
332 (Haccard et al., 1989b; Fig. 4) or post-date it and of Early Oligocene age (Lichorish and Ford,  
333 1998).

334 The growth of the southwestern Subalpine zone started during the Oligocene and continued  
335 throughout the Neogene. Oligocene rocks belonging to the Barles zone and northern edge of  
336 the Valensole basin consist of basal fluvial sandstone and red clay named as the Red  
337 Continental Molasse Formation and the upper brackish deposits named as the Grey Molasse  
338 Formation (Haccard et al., 1989b; Fig. 5b). This succession reaching more than 450 m-thick is  
339 interpreted as deposited as the distal foreland sediments of the inner Alps (Maillart et al.,  
340 1987; Gidon, 1997; Ford et al., 1999). Like the Basal Breccia Formation, the Red Continental  
341 Molasse Formation includes large sedimentary fans in the Barles zone and northern edge of  
342 the Valensole basin which could be interpreted as growth strata deformed by progressive limb  
343 rotation (Gidon, 1997). The Valensole foreland basin is then filled by more than 3 km-thick  
344 marine to continental Miocene-Pliocene strata with strong facies and thickness variations  
345 (Gigot et al., 1974; Gidon and Pairis, 1988; Haccard et al., 1989a,b; Clauzon et al., 1989;  
346 Cojan et al., 2013). It is connected westward to the Forcalquier and Cucuron-Pertuis basins  
347 (Fig. 3). Field studies and well data in the center part of the basin give a global insight of the  
348 Miocene-Pliocene sedimentary succession and architecture (Dubois and Curnelle 1978;  
349 Clauzon et al., 1989; Couëffe et al., 2004; Besson, 2005; Figs. 4 and 5b). The transgressive  
350 Aquitanian-Burdigalian Lower Marine Molasse Formation consists in tidal facies deposited in  
351 major subsiding environment that pass northward into siliciclastic deposits sourced from the  
352 inner Alps domain (Couëffe et al., 2004). The Langhian to Tortonian-lower Messinian  
353 succession is composed of marls, coarse-grained sandstones and limestones alternations of the  
354 Upper Marine Molasse Formation that pass laterally to prograding fluviodeltaic conglomerate  
355 sequences of the Valensole 1 Formation (Beaudouin et al., 1966, 1970; Dubois and Curnelle

356 1978; Mercier, 1979; Aguilar and Clauzon, 1981; Haccard et al., 1989b; Clauzon et al., 1989;  
357 Besson, 2005; Cojan et al., 2013; Fig. 5b). The Valensole 1 Formation comprises Durance  
358 conglomerates rich in siliciclastic clasts westerly sourced by the paleo-Durance river and  
359 Subalpine conglomerates rich in local Mesozoic limestone clasts easterly sourced (Haccard et  
360 al., 1989b). The Valensole 2 Formation mainly consists of marine clay and continental  
361 deposits (conglomerates, sandstones and claystones) of Pliocene to Quaternary age (Clauzon,  
362 1979; Mercier, 1979; Clauzon et al., 1989). Locally, near Oraison (Fig. 3), a Messinian  
363 canyon was mapped by Dubar (1983, 1984). It allows the distinction between the Valensole 1  
364 and Valensole 2 Formations, separated by a major discontinuity, the Messinian Erosional  
365 Surface (Mercier, 1978, 1979; Clauzon, 1979; Dubar, 1983, 1984; Clauzon, 1996). The  
366 Tanaron Formation is the youngest stratigraphic level in the footwall of the Digne Nappe  
367 (under the La Robine half-klippe) in the northern edge of the Valensole foreland basin (Gigot  
368 et al., 1974; Figs. 3 and 5b). The age of the Tanaron Formation is still a matter for debate. It is  
369 composed of mixed massive olistoliths (Triassic gypsum, Callovian-Oxfordian black shales,  
370 upper Jurassic-lower Cretaceous limestones, upper Eocene-Oligocene continental molasses  
371 and Miocene marine molasse) mainly sourced from the collapse of the Barles fold zone  
372 (Gigot et al., 1974). Rare olistoliths of upper Cretaceous carbonates and nummulitic  
373 limestones are interpreted to come from the erosion of the Digne Nappe (Haccard et al.,  
374 1989b). The olistoliths are included in grey-red marls and sandstones. Gigot et al. (1974),  
375 Crumeyrole et al. (1991) and Hippolyte et al. (2011) pointed out that the Tanaron Formation  
376 infills a very large scale erosional feature. At a time where the Valensole conglomerates were  
377 considered as Pliocene, Gigot et al. (1974) assigned a Late Pliocene age to the overlying  
378 Tanaron Formation. The geological map (Haccard et al., 1989a,b) ascribes a Latest Pliocene  
379 age for this formation. However, Gidon and Pairis (1988, 1992) emphasized that the Tanaron  
380 Formation is not dated biostratigraphically. The mapping of Messinian-Zanclean paleo-

381 valleys around Digne revealed that a Zanclean erosional surface has truncated the Tanaron  
382 Formation at La Bonnette and constrains the age of this formation as older than the Late  
383 Pliocene (Hippolyte et al., 2011). Furthermore, these authors suggested that if the erosional  
384 surface at the base of the Tanaron Formation was the Messinian Erosional Surface related to  
385 the desiccation of the Mediterranean basin at 5.6 Ma (Clauzon et al., 1996; Bache et al., 2012;  
386 Roveri et al., 2014) the age of the Tanaron Formation would be Late Miocene to Early  
387 Pliocene (Hippolyte et al. 2011).

388 **3.6. Décollement levels**

389 Inherited Variscan metamorphic foliation and upper Carboniferous-Permian extensional  
390 faults controlled décollement in the basement as observed in the Cap Sicié and Maures  
391 massifs and also suggested by subsurface data under the Provence cover (Tempier, 1987;  
392 Roure and Colletta, 1996; Cushing et al., 2008; Espurt et al., 2019b). The Paleozoic  
393 framework was intermittently reactivated during the Mesozoic rifting and during the  
394 Provençal and Alpine shortening episodes. The basal Muschelkalk and Keuper units are  
395 interpreted as main regional decollement levels of the sedimentary cover above the Paleozoic-  
396 Triassic (Buntsandstein) basement (Bathiard and Lambert, 1968; Caron, 1979; Gidon, 1982;  
397 Gidon and Pairis, 1992; Fig. 4). This middle-upper Triassic evaporitic-carbonate package  
398 shows major thickness variations related to local depocenters during rifting or tectonic  
399 duplication and disharmonic deformations during the compressive stages (Goguel, 1939;  
400 Bathiard and Lambert, 1968; Gigot et al., 1974; Toutin-Morin et al., 1993, 1994; Baudemont,  
401 1985; Espurt et al., 2019b). Middle Jurassic black shales, upper Jurassic-Berriasian limestones  
402 and Oligocene-Miocene sequences (Fig. 4) promote disharmonic deformations with internal  
403 folding and shearing particularly in the Barles and Vélodrome structures (Gidon and Pairis,  
404 1992).

405 **4. Cross-sectional structural architecture**

406 To illustrate the structural architecture of the Provençal and Subalpine thrust wedges, we  
407 constructed a 150 km-long crustal-scale cross-section from the Mediterranean coastal zone to  
408 the south to the Digne-Barles region to the north (Figs. 3 and 6). The cross-section trends  
409 N175°E in the coastal basement units and the Beausset basin, then N002°E across the Sainte-  
410 Baume Nappe and Aurélien Mount thrust, and finally N024°E across the northern Provençal  
411 thrusts, Valensole basin up to the Digne Nappe. This section was constructed according to  
412 thrust tectonics concepts (e.g., Dahlstrom, 1969; Hossack, 1979; Elliot, 1983; Suppe, 1985).  
413 The section is localized in a zone only weakly affected by the Oligocene rifting (Bestani et al.,  
414 2016). We used existing 1:50,000 geological maps of French Geological Survey (BRGM) and  
415 new surface structural data from several fieldworks. We also used existing cross-sectional  
416 data of Kilian (1892), Goguel (1939, 1944), Morabito (1967), Gigot et al. (1974), Debemas,  
417 1974; Dubois and Curnelle (1978), Combes (1984), Haccard et al., 1989b; Gidon and Pairis  
418 (1992), Hippolyte and Dumont (2000), Guyonnet-Benaize et al. (2015), Bestani et al. (2015,  
419 2016) and Célini et al. (2020). Thrust geometries at depth and basement geometry have been  
420 constrained using exploration wells and geophysical data. We used nine major exploration  
421 wells (from south to north: Gréoux (G3, G2, G1, G4, S1, S4), Les Mées (LM1), and Mirabeau  
422 (M1, M2)) some of them (G1, S1, LM1, M2) reaching the Paleozoic substratum (Fig. 3). We  
423 interpreted two seismic reflection profiles, VL85-P and 75DV-2, that cover the central-  
424 southern part of the Valensole basin over a distance of ~28 km. These profiles have been  
425 reprocessed by Agence de l'Eau Rhône Méditerranée Corse and available for this study (Fig.  
426 3). A time-depth conversion of seismic profiles was performed using the MOVE software and  
427 seismic velocities of sedimentary intervals provided by BRGM. Finally, fault location at  
428 depth is interpreted by some present day deep-located earthquakes (Cushing et al., 2008).

429 In the southern part of the Provençal zone, the cross-section trace located between the Cap  
430 Sicié and the Aurélien Mount thrust follows the section of Bestani et al. (2015) (Figs. 3 and

431 6). This section has been updated from previous version in terms of displacement magnitude  
432 of the thin-skinned thrust sheets and basement deformations based on new structural  
433 interpretations and new geological mapping (Laville et al., 2018). Because the section trace is  
434 located lateral to the Cap Sicié peninsula (~10 km to the east), its thrust geometry has been  
435 projected onto the section. To the north of the Aurélien Mount thrust, the cross-section has  
436 been fully constructed for this study and is presented for the first time (Fig. 3). The proposed  
437 balanced cross-section is one possible construction, but it is the most realistic solution  
438 consistent with the available surface and subsurface structural data presented in this work.

439 The construction, balancing and restoration of the cross-section were performed with the  
440 MOVE structural modeling software following thrust tectonic concepts and flexural-slip  
441 algorithm assuming constant bed length and thickness (Dahlstrom, 1969; Boyer and Elliott,  
442 1982; Suppe, 1983; Suppe and Medwedeff, 1990). For the middle Jurassic black shales, and  
443 Oligocene-Miocene sequences, in zone where these ductile units promote strong internal  
444 deformations (Barles folds and Vélodrome), we assumed an area balance approach (e.g.,  
445 Mitra and Namson, 1989; Mitra, 2002; Butler, 2013; Butler et al., 2020). For the ductile  
446 middle-upper Triassic evaporitic-carbonate units which may move in three dimensions (and  
447 their volumes can change as a result of dissolution, fluid migration and surface erosion during  
448 successive stages deformation and diapirism), we also achieved as much as possible an area  
449 balance approach. For deep crustal level, we also assumed an area balancing approach. The  
450 orientation of the cross-section is orthogonal to the trend of the structures of both orogenic  
451 systems (see section 6). No major strike-slip fault system is crossed except in the Huveaune  
452 zone (Fig. 3; Guillemot et al., 1973; Philip, 2018).

453 **4.1. The Provençal zone**

454 **4.1.1. Surface structure**

455        The surface structure of the Provençal zone is described from south to north, i.e., from the  
456        inner coastal basement units (preserved from the Ligurian-Provençal rifting) and thrust sheet  
457        domain, to outer thrust systems of High Var (Fig. 6a,b).

458        The Cap Sicié peninsula is formed by two imbricate thrusts. The upper N-verging Cap  
459        Sicié thrust is composed of Variscan phyllites and quartzites covered by N-dipping lower-  
460        middle Triassic strata to the north (Fig. 7a-c). The Cap Sicié thrust is folded by the lower  
461        Saint-Mandrier thrust leading to the formation of the Saint-Mandrier half-window (Zürcher,  
462        1893; Haug, 1925; Tempier, 1987), made of lower-middle Triassic and Permian strata at the  
463        surface (Figs. 6b and 7a,c,d) and Variscan phyllites and quartzites at depth.

464        North of the Cap Sicié basement imbricate, the sedimentary cover of the Provençal zone is  
465        detached northward above ductile middle-upper Triassic layers and associated Triassic highs  
466        (Gouvenet, 1963; Bathiard and Lambert, 1968; Tempier, 1987; Bestani et al., 2016; Espurt et  
467        al., 2019b). The Bandol cover thrust including the Bandol syncline is transported at the front  
468        of the Cap Sicié thrust. The Bandol thrust is emplaced above the Saint-Cyr Triassic high  
469        where lower Santonian carbonates unconformably overlain middle Triassic limestones  
470        (Philip, 1967; Philip et al., 1985, 1987; Espurt et al., 2019b; Fig. 8). Klippen of Triassic rocks  
471        of the Bandol thrust rest on upper Santonian and lower Campanian (Valdonnian-Fuvelian  
472        facies) strata of the Beausset syncline (Bertrand, 1887; Gouvenet, 1963) (Fig. 3). The Sainte-  
473        Baume Nappe transported northward the Beausset syncline (Fig. 9; Guieu, 1968; Bestani et  
474        al., 2015; Philip et al., 2018; Philip, 2019). Its hanging wall ramp consists in upper Triassic to  
475        lower Cretaceous strata dipping 10°-15° southward, deformed by out-of-sequence thrusts  
476        (Fig. 9c; Bestani et al., 2015). Its footwall is constituted by the tight Plan d'Aups syncline  
477        cored by lower Campanian strata (Fuvelian facies), Pic des Corbeaux anticline, and broad La  
478        Lare anticline mantled by upper Jurassic limestones. Small klippen of Jurassic and Barremian  
479        rocks in the Huveaune zone (Saint-Zacharie and Nans basins) indicate the northward advance

480 of the Sainte-Baume Nappe (Figs. 3 and 6b; Guieu, 1968). The substratum of the Huveaune  
481 zone is constituted by middle-upper Triassic rocks and relatively thin Jurassic sequences  
482 which are unconformably covered by upper Cretaceous (Valdonnian-Fuvelian and Begudian-  
483 Rognacian facies) and Oligocene strata (Fig. 3; Philip, 2018, 2019). The Aurélien Mount  
484 thrust transported northward Jurassic limestones above the Arc syncline (Figs. 6b and 10;  
485 Aubouin and Chorowicz, 1967; Guieu, 1968; Popoff, 1973). The hanging wall ramp of the  
486 Aurélien Mount thrust shows Jurassic strata dipping 12° southward. The Sainte-Baume Nappe  
487 and Aurélien Mount thrust, and southern limb of the Arc syncline are cut by NE-trending  
488 normal faults (Bestani et al., 2016). This normal faulting is contemporaneous with opening of  
489 the Aubagne, Peypin, Saint-Zacharie and Nans extensional basin framework during the  
490 Oligocene (Figs. 3 and 6b; Nury, 1988; Hippolyte et al., 1993).

491 The surface and well data show that the Arc basin is an asymmetrical syncline  
492 characterized by a N-thinning sedimentary wedge in first lower Santonian rudist carbonates,  
493 then upper Santonian-lower Campanian (Valdonnian-Fuvelian) to middle Campanian-  
494 Maastrichtian (Begudian-Rognacian) continental syn-orogenic facies (from ~1.1 km-thick to  
495 the south, to less than 250 m-thick to the north; Fig. 6b). The core of the syncline is  
496 constituted by ~200 m-thick flat Danian to Ypresian strata that form the Cengle plateau (Figs.  
497 3 and 11a). Along the section, the Arc syncline is transported northward above the Pourrières  
498 thrust constituted by 12° S-dipping Jurassic-lower Cretaceous strata (Fig. 11a). The Pallières  
499 thrust system transports northward the Ollières syncline cored by upper Santonian-Campanian  
500 (Valdonnian-Fuvelian-Begudian) continental facies strata. (Fig. 6b). The Pallières thrust  
501 system is composed by two units. The upper unit corresponds to a ~5° S-dipping homoclinal  
502 made of upper Jurassic-lower Cretaceous limestones. The lower unit involves upper Jurassic  
503 limestones unconformably covered by Danian Microcodium breccias (Fig. 11c). The Pallières  
504 thrust system overthrusts northward the E-trending Rians syncline filled by more than 700 m-

505 thick Danian to Ypresian syn-orogenic package including massive alluvial fan deposits (Fig.  
506 11c; Tempier, 1963; Mennessier, 1970; Angelier, 1971; Angelier and Aubouin, 1976; Philip  
507 et al., 2017). The Pourrières and Pallières thrusts form the eastern continuation of the bi-  
508 verging Sainte-Victoire Mountain thrust system, while to the east they branch into the Barjols  
509 Triassic zone (Figs. 3 and 11a,b). The N-verging Vinon thrust includes the Mont-Major  
510 anticline locally thrusting southward the northern flank on the Rians syncline and Triassic  
511 evaporite-cored anticline of Valavés (Figs. 3 and 6b; Mennessier, 1970). Northward, the  
512 Vinon thrust dips 12° to the south and emplaces upper Jurassic limestones on Paleocene strata  
513 of the Saint-Julien syncline (Fig. 12a). The geometry of the N-verging Les Maurras thrust is  
514 revealed by the well G2 and by intensively sheared Oxfordian marly limestones as observed  
515 in the field (Fig. 12b). The Les Maurras thrust is unconformably covered by poorly deformed  
516 red sandstones and thick breccias layers, and Pliocene conglomerates of the Valensole  
517 Formation. Eastward, the footwall of the Les Maurras thrust is constituted by the La Mourotte  
518 syncline filled by Paleocene and Ypresian strata (Fig. 3; Mennessier, 1970; Angelier and  
519 Aubouin, 1976). Finally, the N-verging Gréoux thrust emplaced lower Jurassic rocks over  
520 lower Cretaceous limestones and Paleocene strata of the Esparron-de-Verdon syncline (Fig.  
521 12c). This thrust dips ~10° southward at surface and increases at depth at ~33° southward as  
522 revealed by the exploration wells G1 and G2 (Morabito, 1967). The thrust systems of northern  
523 Provençal zone are later cut by NW-trending normal faults (e.g., Ginasservis fault) which are  
524 associated with the development of La Combe, Bourdas, Plan d'Auron basins filled by  
525 Oligocene sediments (Fig. 3; Angelier and Aubouin, 1976; Philip et al., 2017).

526 The southern Provençal zone shows locally inherited Mesozoic halokinetic structures  
527 associated with normal faults previously described by Bestani et al. (2015) and Espurt et al.  
528 (2019b) as the Saint-Cyr and Huveaune Triassic highs. The northern Provençal zone connects  
529 eastward with the large Triassic depression of Barjols including halokinetic structures (Fig.

530 3). Along the cross-section, upper Jurassic-lower Cretaceous strata of the Pourrières thrust  
531 depict growth wedge geometry and faulting, suggesting that this thrust could be superimposed  
532 on an early SW-dipping normal fault zone with halokinetic movement of Triassic evaporites  
533 at depth (Figs. 3 and 6b). Similarly, well data show strong thickness variations in upper  
534 Jurassic carbonates into the Les Maurras thrust (Fig. 12d), suggesting early halokinesis.

535 **4.1.2. Deep structure**

536 Cross-section construction suggests that the Provençal zone is characterized by a  
537 heterogenous geometry of the basement-cover interface resulting from basement inheritance  
538 and basement-involved shortening. The basement of Provençal zone shows two styles of  
539 deformation along the cross-section (Fig. 6b). Southward, low-angle basement thrusts (Cap  
540 Sicié and Saint-Mandrier thrusts, and deeper thrust under the Sainte-Baume Nappe) propagate  
541 through the Variscan metamorphic foliation or inherited shear zones (Espurt et al., 2019b).  
542 The extensional geometry of the upper Carboniferous-Permian basins at depth is well  
543 preserved as imaged by E- and N-trending seismic profiles, for instance, in the Luc basin at  
544 the northwestern flank of the Maures massif (Fig. 13; Baudemont, 1985). The basins mainly  
545 correspond to half-grabens filled by more than 1 km-thick upper Carboniferous-Permian  
546 strata and associated with WNW- to NNW-dipping normal faults. These faults inherited from  
547 the rifting of Pangea can have been locally reactivated during the Mesozoic rifting events  
548 (Toutin-Morin et al., 1993, 1994; Espurt et al., 2019b). During the Provençal shortening, the  
549 extensional features were cut and transported passively above N-verging basement thrusts  
550 (Bathiard and Lambert, 1968; Baudemont, 1985; Tempier, 1987; Espurt et al., 2019b). The  
551 shortening of the basement thrusts fed the slip of cover thrusts of the southern Provençal zone  
552 (Bandol, Sainte-Baume and Aurélien Mount). In the northern Provençal domain, field and  
553 geophysical data, and cross-section constructions (Biberon, 1988; Roure and Colletta, 1996;  
554 Espurt et al., 2012, 2019) allow to infer the geometry and depth of the basement cover

555 interface. These data also suggest a heterogenous distribution of the upper Carboniferous-  
556 Permian to Triassic depocenters. The base of the Arc syncline is inferred at ~2.2 km bsl and  
557 the base of the Rians syncline at ~1.7 km below sea level (bsl). At the boundary between the  
558 Provençal zone and Valensole basin (footwall of the Gréoux thrust), the basement depth is  
559 located at ~1.4 km bsl. Surface data and cross-section construction suggest that the Paleozoic  
560 basement is located at a shallow depth (~800 m bsl) under the Valavès Triassic anticline.  
561 Contrary to the south, the basement structure of northern part of Provençal zone is interpreted  
562 as half-grabens delimited by major NE-dipping faults (Fig. 6b). These basement thrusts are  
563 interpreted as short-cut thrusts propagating through inherited upper Carboniferous-Permian to  
564 Triassic half-grabens (Espurt et al., 2012; 2019b). In this zone, shallow-depth earthquakes are  
565 observed (e.g., Valavés anticline; Figs. 3 and 6a). They could be tectonically connected with  
566 deeper events occurring along basement faults as suggested by cross-section construction  
567 (Cushing et al., 2008).

568 **4.2. The Subalpine zone: Digne Nappe, Barles fold system and Valensole foreland basin**

569 **4.2.1. Surface structure**

570 The Digne Nappe, Barles fold system and northern edge of the Valensole basin are well  
571 exposed in a N-S section along the Bès valley (Figs. 3 and 14). The stratigraphy and the main  
572 tectonic structures along this valley have been described for a long time by geologists (e.g.,  
573 Goguel, 1939, 1944; Debèlmas et al., 1970, 1974; Lemoine, 1972; Gigot et al., 1974; Gidon,  
574 1982, 1989; Debèlmas et al., 1983; Gidon and Pairis, 1986, 1988, 1992; Haccard et al.,  
575 1989b). This area around the Barles village became famous for fieldworks with students  
576 coming from national and international universities. More recent studies discussed the timing  
577 of deformation (Fournier et al., 2008; Hippolyte et al., 2011) and tried to decipher Jurassic  
578 salt tectonics through an overprint of Cenozoic contractional tectonics (Graham et al., 2012;

579 Célini et al., 2020). The surface structure of the Subalpine zone is described from north to  
580 south, i.e., from the inner Digne-Barles units to Valensole foreland basin.

581 The Digne Nappe involves a thick (up to 4.5 km) Jurassic-Cretaceous pelagic succession  
582 initially deposited in the Digne basin, and covered by Eocene-Oligocene strata northeastward  
583 (Fig. 4; Goguel, 1944; Rousset et al., 1983). The paleo-temperature (~100 °C) recorded by  
584 Oligocene-Miocene rocks in the footwall of the Digne Nappe indicates that the thickness of  
585 the Digne Nappe was about 2.9 km above the Barles tectonic half-window (Schwartz et al.,  
586 2017a,b; Figs 6c and 14). The Digne Nappe involves locally basement tectonic slices (Fig.  
587 15) and internal folding (Guimard, 1990). It is regionally detached SW-ward above a thick  
588 Triassic evaporitic-carbonate layer and overthrusts the Barles fold system and the  
589 northeastern edge of the Valensole foreland basin (Figs. 6c and 14). North of Digne, its  
590 frontal part is constituted by the syncline-shaped La Robine half-klippe which overlies the  
591 upper Miocene-lower Pliocene sequences of the Thoard syncline. Northward, the hanging-  
592 wall of the Digne Nappe displays a large antiform, leading to the formation of the erosional  
593 Barles half-window (Figs. 6c and 14). Along the cross-section, the Digne Nappe roots north  
594 of the Verdaches anticline in thin layer of middle-upper Triassic strata. The E-trending  
595 asymmetric Verdaches anticline is underlined by middle Triassic limestones and basal  
596 Triassic sandstones which unconformably overlain upper Carboniferous coal and sandstone  
597 beds (Figs. 6c and 15; Haccard et al., 1989b; Guimard, 1990). The northern backlimb dips 10°  
598 northward while the southern forelimb dips 25° southward. The structure of the Barles  
599 antiform corresponds to very tight anticlines (La Petite Cloche, La Grande Cloche and La  
600 Maurière anticlines along the cross-section) mantled by upper Jurassic-lower Cretaceous  
601 limestones and cored by Callovian-Oxfordian black shales (Fig. 14). The anticlines are  
602 bounded by synclines cored by uppermost Eocene-Oligocene strata that unconformably  
603 overlain Mesozoic sequences (Fig. 16; Lemoine, 1972; Gidon, 1982; Haccard et al., 1989a).

604 Cross-section construction suggests that the Barles fold system is detached southward above  
605 middle-upper Triassic strata (Fig. 6c). The La Petite Cloche thrust transports southward the  
606 Les Sauvans syncline filled by thick Callovian-Oxfordian black shales (Fig. 6c). Its vertical to  
607 overturned northern limb is the Barre de Chine armed by ~200 m-thick lower Jurassic  
608 limestones overlain by a huge volume of Triassic shales, cargneules and gypsum of the Barles  
609 diapir (Arnaud et al., 1976; Haccard et al., 1989a; Gidon and Pairis, 1992; Graham et al.,  
610 2012). Although the Barles fold zone and Digne Nappe recorded strong contractional  
611 deformation, field data show structural evidence of pre-existing halokinetic structures and  
612 normal faulting (Gidon, 1982). For instance, the minibasin structures in La Robine half-klippe  
613 and of the Les Sauvans syncline-Barre de Chine flap are interpreted as resulting from  
614 halokinetic motion of Triassic evaporites during the Jurassic-Early Cretaceous times (Graham  
615 et al., 2012; Célini et al., 2020).

616 South of the Barles anticlines, the three-dimensional Vélodrome syncline develops,  
617 involving mainly Miocene rocks (Marine Molasse and Valensole 1 Formations)  
618 unconformably covered by the olistolithic Tanaron Formation (Fig. 14). This complex  
619 structure exhibits important contractional growth strata along syncline limbs with fold-  
620 accommodation faults including out-of-syncline thrusts and disharmonic folding (Goguel,  
621 1939; Gigot et al., 1974; Pairis and Gidon, 1987; Gidon, 1989; Gidon and Pairis, 1992).  
622 Recently, it has been speculated that the three-dimensional structure of the Vélodrome may  
623 correspond to a Miocene minibasin that sank into a hypothetical Oligocene salt layer (Célini  
624 et al., 2020; Célini, 2020). The Vélodrome structure corresponds to the northern limb of the  
625 Thoard syncline. The thickness of the Miocene-Pliocene syn-tectonic deposits increases  
626 southward, from 1 km in the Vélodrome to more than 3.3 km in the core of the Thoard  
627 syncline (Figs. 6c and 17). This syncline is transported southward onto the Aiglun and  
628 Mirabeau-Mallemoisson S-verging fault-propagation folds armed by Miocene conglomerate

629 beds and probably detached in Triassic strata. The northern Aiglun anticline displays a  
630 backlimb dipping 35-40° northward and a forelimb dipping 70° southward (Fig. 18a). The  
631 southern Mirabeau-Mallemoisson anticline has a 40° N-dipping backlimb and a vertical  
632 forelimb (Fig. 18b). Well data indicate that this later is associated with a thrust dipping 38°  
633 northward. Well data also reveal that a sub-thrust develops in the footwall block. South of the  
634 Bléone river (Fig. 3), Miocene strata are deformed by the Quaternary Lambruissier fold-  
635 propagation fault (Hippolyte and Dumont, 2000) probably detached in the upper Triassic  
636 strata. It is characterized by a 10-15° N-dipping backlimb and a 80° S-dipping forelimb. The  
637 displacement on Lambruissier thrust decreases rapidly westward, explaining why it is not  
638 visible in map view as well as in subsurface data near Les Mées borehole (Figs. 3 and 19).  
639 Southward, the Valensole foreland basin is filled by upper Miocene conglomerates of the  
640 Valensole 1 Formation topped by the Valensole 2 Pliocene Formation whose surface forms  
641 the slightly S-dipping Puimichel plateau (Fig. 18c). In the southern edge of the Valensole  
642 basin, upper Miocene-Pliocene rocks lie unconformably on lower Cretaceous strata.

#### 643 **4.2.2. Deep structure**

644 In the southern part of the Valensole basin, reprocessed seismic reflection profiles and well  
645 data have been used to interpret the geometry of hidden thrust systems under the Miocene-  
646 Pliocene sedimentary infill (Fig. 19). The seismic profile 75DV-2 confirms that the Miocene  
647 strata are unconformably deposited on top of a deep basement high, the Les Mées high,  
648 underlined by folded Mesozoic strata with a thin (less than 30 m-thick) Triassic succession  
649 (Dubois et Curnelle, 1978). The uplift of the Les Mées high is controlled by a N-dipping  
650 basement ramp proved by subsurface data (Dubois and Curnelle, 1978). The basement ramp  
651 branches upward into the Triassic strata then splits into two S-verging branches deforming  
652 Miocene-Pliocene deposits under the Asse river as observed on the seismic profile VL85-P.  
653 These hidden compressional structures are interpreted as Provençal folds and thrusts (Dubois

654 and Curnelle, 1978), slightly reactivated during the Alpine compression (Hippolyte and  
655 Dumont, 2000; Godard et al., 2020).

656 Like the Provençal zone, cross-section construction and subsurface data illustrates that the  
657 Subalpine zone (including the Valensole foreland basin) is characterized by a heterogenous  
658 geometry of the basement-cover interface resulting mainly from basement-involved  
659 shortening. Northward, the Carboniferous and lower Triassic teguments of the Verdaches  
660 anticline were uplifted, as a result of reverse motions on a reactivated upper Carboniferous  
661 normal fault (Fig. 15). However, the structural culmination of the Verdaches anticline is  
662 associated with a deeper basement thrust wedge propagating under the Valensole foreland  
663 basin in the Triassic evaporites as initially proposed by Goguel (1944) and Gigot et al. (1974).  
664 Southward, cross-section construction suggests that the depth of basement is located at ~4.2  
665 km bsl under the axis of the Thoard syncline (Fig. 6c) which is consistent with previous cross-  
666 section constructions in this zone (Combes, 1984; Graham et al., 2012). Its depth decreases  
667 progressively toward the south, at ~2.2 km bsl under the Mirabeau-Mallemoisson anticline  
668 and at ~1 km bsl in the Les Mées basement thrust. Southward, the depth of basement-cover  
669 interface goes down at ~2.5 km bsl, then decreases gradually toward the south (Figs. 6c and  
670 19).

671 **5. Restoration of the Mesozoic extensional basin framework**

672 The balanced cross-section has been restored just before the Provençal compression  
673 considering the top of upper Santonian marine strata as a regional flat template from the  
674 South Provence basin domain (preserved from the Beausset syncline to the southern edge of  
675 Arc syncline) to the Vocontian domain to the north (Digne Nappe). This template connects  
676 with the subaerial erosional flat surface of the Durance high, which was used to unfold the  
677 Mesozoic-Jurassic sedimentary cover in the northern Provençal belt, the Valensole high and  
678 the Barles zone (Figs. 4 and 20a).

679 The pre-shortening restoration illustrates the initial extensional framework with a large  
680 uplift zone (Durance high and Valensole high) in the center of the section, which led to the  
681 separation of the Beausset basin (as part of the South Provence basin) to the south and the  
682 Digne basin (as part of the Vocontian basin) to the north (Fig. 20a). The southern Beausset  
683 rift-related structures and the southern edge of the Durance high have preferentially  
684 accommodated the Provençal shortening along the Bandol thrust, Sainte-Baume Nappe and  
685 Aurélien Mount thrust whereas the northern Digne rift-related structures have preferentially  
686 accommodated the Alpine shortening of the Digne Nappe. Restoration of the Beausset basin  
687 geometry is well determined by rift sequences preserved from erosion in the hanging-wall and  
688 footwall of the Sainte-Baume Nappe (Fig. 20a). In contrast, cross-section restoration suggests  
689 that a large part of the frontal Digne Nappe has been eroded (Fig. 20a). This eroded part  
690 might correspond to the adjacent halokinetic Turriers basin located to the west and  
691 transported ahead of the Digne Nappe along the studied cross-section (Gidon, 1982; Célini et  
692 al., 2020, 2021). The restoration suggests that the Digne basin was initially located at ~8 km  
693 to the north from the Barre de Chine and Barles diapir (Fig. 20a; Gigot et al., 1974).

694 In agreement with the structural data of Baudemont et al. (1985) and Espurt et al. (2019b),  
695 cross-section restoration suggests that the basement incorporates a set of ~E- to ENE-trending  
696 ~N-dipping normal faults associated with Permian half-graben systems (Fig. 20a). These  
697 basement faults are reactivated intermittently during the Tethyan, Vocontian and South  
698 Provence extensional episodes (Espurt et al., 2019b). They played a first order control on the  
699 subsidence of the Beausset and Digne basins and thick syn-rift Jurassic-middle Cretaceous  
700 sedimentary infilling (~2.4 km-thick in the Beausset basin and ~4.5 km-thick in the Digne  
701 basin). This strong sediment load in the Beausset and Digne depocenters could have induced  
702 the evacuation of the ductile Triassic evaporitic-carbonate layers from under the subsiding  
703 zones toward local halokinetic features. This early halokinesis drives early folding of the

704 sedimentary pile including large subsiding synclines to narrow minibasins structures  
705 characterized with growth wedges, normal faulting, and gravitational instabilities together  
706 with local salt domes and diapirs initiated from basement faults (e.g., Saint-Cyr, Huveaune,  
707 High Var and Barles halokinetic areas; Graham et al., 2012; Bestani et al., 2015; Espurt et al.,  
708 2019b; Célini et al., 2020; Fig. 20a).

709 The southern edge of the Beausset basin show major E-W thickness and facies changes in  
710 the Jurassic-middle-upper Cretaceous succession that depict depocenters and structural highs  
711 with minor normal faulting (Philip, 1967, 1970; Philip et al., 1987; Espurt et al., 2019b). For  
712 instance, the western Saint-Cyr Triassic high located in the footwall of the Bandol thrust, was  
713 probably controlled by a N-dipping basement fault together with Triassic salt movement at  
714 depth. Similar geometry has been used to restore the structures located in the footwall blocks  
715 of the future Sainte-Baume Nappe and Aurélien Mount thrust (e.g., Huveaune Triassic high;  
716 Guillemot et al., 1973; Bestani et al., 2015; Philip, 2019). In the Durance high, the halokinetic  
717 activity during Late Jurassic-Early Cretaceous is more discrete with small sediment trapping  
718 and normal faulting (e.g., future Pourrières and Les Maurras thrusts). Its result is the  
719 formation of Triassic domes and long-wavelength syncline depocenters where the Jurassic-  
720 Cretaceous platform shows successions with thickness changes (Fig. 20a; Espurt et al.,  
721 2019b).

722 The pre-shortening restoration also suggests that fold structures observed in the footwall  
723 (Barles diapir and Barre de Chine flap, Les Sauvans minibasin and Barles folds) and hanging-  
724 wall (La Robine) of the Digne Nappe have been initiated by early halokinetic deformations  
725 through the Jurassic and maybe until the Early Cretaceous (Fig. 20a; Graham et al., 2012;  
726 Célini et al., 2020, 2021).

727 **6. Tracking superimposed compressions using syn-orogenic sedimentation**  
728 **and fault slip data**

729 Deciphering the timing of deformations and shortening directions in the superimposed  
730 Provençal and Subalpine thrust wedges are fundamental for produce a robust sequential  
731 restoration model. The low-temperature thermochronology data available in the study area are  
732 in the Oligocene-Miocene footwall rocks of the Digne Nappe, upper Cretaceous Arc basin  
733 and Paleozoic basement of Maures and Tanneron-Estérel massifs (Jakni, 2000; Bestani, 2015;  
734 Schwartz et al., 2017a). In the Maures massif, Oligocene-Miocene cooling ages are mainly  
735 related to a reheating of the Paleozoic basement during the back-arc rifting of the Ligurian-  
736 Provençal basin associated with Miocene volcanism (Jakni, 2000; Bestani, 2015). The cooling  
737 ages in sedimentary cover are interpreted as detrital or partially reset ages by small reburial  
738 below the Mesozoic-Cenozoic sedimentary cover or tectonic covering. In the Subalpine zone  
739 thermal modeling of low-temperature thermochronological data suggested a cooling of the  
740 Barles half-window at ~6 Ma (Schwartz et al., 2017a).

741 To constrain the timing of the thrusting, we used syn-orogenic basin infill and growth  
742 strata (Suppe et al., 1992). The syn-orogenic deposits are either related to the Provençal or  
743 Subalpine compression. They are described by previous studies (e.g., Gigot et al., 1974;  
744 Dubois and Curnelle, 1978; Maillart et al., 1987; Haccard et al., 1989a; Espurt et al., 2012) or  
745 highlighted in this work. The analysis of the temporal and spatial distribution of these  
746 deposits was used to determine the growth and/or reactivation of contractional structures  
747 along our section and the progressive advance of the thrust wedges toward the forelands (Fig.  
748 21). In Provençal zone, there is no evidence of growth strata in Neogene deposits. However,  
749 numerous examples of deformed Oligocene and Miocene-Pliocene strata testify to the  
750 presence of Alpine contractional reactivation of pre-existing Provençal thrusts and Ligurian-  
751 Provençal extensional structures (e.g., Hippolyte et al., 1993).

Fault slip data were used to determine regional stress regimes and the thrust transport directions (Angelier, 1984, 1991). Variations in stress regimes through geological times can be stratigraphically dated by reconstructing paleo-stresses at different stratigraphic levels (Hippolyte et al., 1993). Furthermore, the fault slip analysis in growth strata deposits can provide a direct dating of paleo-stresses (Hippolyte et al., 1992). Paleo-stress studies have already been done in the Provençal zone in the Oligocene basins, the Arc syncline and the Sainte-Victoire Mountain by Combes (1984), Gaviglio (1985), Lacombe et al. (1992), Hippolyte et al. (1993), Guignard et al. (2005), and Espurt et al. (2012), and in the Subalpine zone of Digne-Barles by Combes (1984), Fournier et al. (2008) and Hippolyte et al. (2012). In this study, fault slip data were collected in zone with single deformation phase and far from oblique structures or ramps producing local rotations and stress deviations (Lacombe, 2012) as observed locally in the Sainte Victoire Mountain (Espurt et al., 2012). We measured striated fault surfaces along the cross-section at twenty three new sites and computed paleo-stresses using the Angelier method (INVD method, Angelier, 1990). We added to our data five previously published fault sites along our cross-section that were analyzed with the same method in the southern flank of Sainte-Victoire Mountain (Espurt et al., 2012), in the Valensole basin (Hippolyte and Dumont, 2000), and in the Digne area (Hippolyte et al., 2012). The trends of the computed shortening directions (maximum horizontal stress axes  $\sigma_1$ ) are presented in Fig. 21 and all computed data and diagrams in Table 1 and Fig. 22.

## 6.1. Record of the Provençal shortening

The map of Fig. 21a shows the Provençal compressional structures and associated upper Cretaceous to Eocene syn-orogenic basins. In the southernmost part of the Provençal zone, the transition from marine to continental deposits in the Latest Santonian of the Beausset syncline could be related to basement stacking in the inner part of the orogen (Philip, 1970; Philip et al., 1987; Tempier, 1987). The growth of the Sainte-Baume Nappe is recorded by

777 somewhat later Maastrichtian breccias (Rognacian facies) preserved in the folded footwall  
778 block (Fig. 9b; Aubouin and Chorowicz, 1967; Corroy and Philip, 1964; Guieu, 1968; Philip  
779 et al., 2018). Northward, Rognacian facies strata lie unconformably on middle-upper Triassic  
780 rocks and record the uplift of the Huveaune antiform during the Late Cretaceous (Bestani et  
781 al., 2015; Philip, 2018, 2019). Syn-tectonic deposits are not preserved along the Aurélien  
782 Mount thrust. Because it overthrusts Maastrichtian (Rognacian facies) strata of the Arc  
783 syncline (Fig. 10a), we can infer that this thrusting might have occurred during the Latest  
784 Cretaceous like the neighboring Sainte-Baume and Etoile Nappes and then later during the  
785 Paleocene (Fig. 3; Aubouin and Chorowicz, 1967; Guieu, 1968; Popoff, 1973). The initial  
786 growth of the Pourrières thrust is attested by a major pinch out of the continental upper  
787 Cretaceous sequences with intercalated breccia beds in middle Campanian strata (Begudian  
788 facies) (Durand and Mennessier, 1964; Popoff, 1973). A later activity can be also inferred for  
789 the Pourrières thrust as this thrust connects laterally to the S-verging Sainte-Victoire  
790 Mountain thrust with Paleocene growth strata (Espurt et al., 2012; Fig. 11a,b). The Paleocene  
791 growth of the Pallières, Vinon, Les Mauras and Gréoux thrust systems is clearly recorded by  
792 alluvial fan systems of microcodium breccias with local growth strata infilling the Rians,  
793 Saint-Julien, La Mourotte and Esparron-de-Verdon synclines (Figs. 4, 11c and 12; Angelier,  
794 1971; Philip et al., 2017). These thrusts and basins have recorded ongoing deformation maybe  
795 until the Early Eocene (Angelier and Aubouin, 1976; Philip et al., 2017).

796 In the Valensole basin, subsurface data indicate that the Les Méés and Mirabeau-  
797 Mallemoisson structures overprint Provençal thrusts which have been eroded and sealed by  
798 basal Miocene strata (Fig. 19; Dubois and Curnelle, 1978; Gigot et al., 1981a). We can  
799 speculate a similar pre-structuration of the neighboring Lambruissier and Aiglun structures.  
800 Farther to the north evidence of Provençal deformation is also found in the Barles area (Fig.  
801 3). In the Barles tectonic half-window, all E-trending compressional folds have been eroded

802 and unconformably covered by the Basal Breccia Formation with growth stratal architectures  
803 (Lemoine, 1972; Maillart et al., 1987; Haccard et al., 1989a,b). For instance, onlaps and fan  
804 shaped-geometry of the breccia beds can be observed in the northern limb of the Feissal  
805 syncline west of Barles (Fig. 16b). Although the age of these deposits remains poorly  
806 constrained (Latest Eocene-Early Oligocene) this occurrence of growth stratal wedging with  
807 reverse faulting provides evidence for compressional syn-tectonic sedimentation in the  
808 northernmost parts of the Provençal belt in Late Eocene times (Priabonian?). Interestingly,  
809 well dated evidence for late Provençal shortening is found farther west in the E-trending  
810 Eygalayes syncline of the Baronnies area (Fig. 3). Here, Montenat et al. (2005) described  
811 Lutetian to Bartonian lacustrine and conglomerate deposits with growth stratal geometries  
812 which recorded the initial folding of Eygalayes syncline during Middle-Late Eocene before its  
813 reactivation during the Alpine compression.

814 To determine the trend of the compressional stress in the Provençal thrust wedge, we  
815 measured fault-slip data at eleven sites into syn-tectonic conglomerates or growth strata  
816 described above, and in Jurassic-Cretaceous units of clearly define Provençal thrusts (Fig.  
817 21a). Our paleo-stress computation shows evidence for a regional ~NNE-trending  
818 compression as previously shown by Gaviglio (1985), Lacombe et al. (1992) and Espurt et al.  
819 (2012) in the Sainte-Victoire Mountain-Arc syncline area. Syn-depositional tilting and  
820 faulting of the Danian growth strata in the Sainte-Victoire Mountain as well as in the Rians  
821 basin (Figs. 11b, 21a and 22) show that this ~NNE-trending compression occurred at least  
822 during the Danian (Espurt et al., 2012). In the Barles area, paleo-stress studies by Fournier et  
823 al. (2008) and Hippolyte et al. (2012) show a complex polyphase history with structures with  
824 different axial trends and ages interfering. Syn-depositional faulting in the Basal Breccia  
825 Formation growth strata in the slightly deformed ~E-trending Feissal syncline indicates a ~N-  
826 trending shortening (Fig. 16b). This trend is consistent with of the compression characterized

827 by Fournier et al. (2008) in the folded Mesozoic limestones of the Barles canyon. Thus, we  
828 can infer that the ~NNE-trending Provençal compression propagated northward to the  
829 outermost part of the belt in Late Eocene times (Fig. 21a) as previously suggested by  
830 Montenat et al. (2005) for the Baronnies area.

831 **6.2. Record of the Alpine shortening**

832 The map of Fig. 21b shows the Alpine compressional structures and associated syn-  
833 orogenic basins. In the Barles area, folding was recorded immediately after the Provençal  
834 compression by growth stratal geometries in the Oligocene continental Red Molasse  
835 Formation, then in the Grey Molasse Formation south of La Maurière anticline (Maillart et  
836 al., 1987). This Oligocene deformation is consistent with growth stratal geometries in the  
837 Esparron syncline as described by Gidon (1997) and Célini et al. (2021) more to the north  
838 (Fig. 3). The growth of the La Maurière anticline (and probably also other inner folds) was  
839 then recorded by Aquitanian-Burdigalian Lower Marine Molasse Formation, then Langhian,  
840 Serravallian and Tortonian-lower Messinian conglomerates with growth stratal architecture in  
841 the Vélodrome structure (Fig. 14; Gigot et al., 1974; Pairis and Gidon, 1987; Gidon, 1989;  
842 Gidon and Pairis, 1992). West of La Robine half-klippe along the Duyes valley, growth strata  
843 in upper Miocene subalpine conglomerates are identified in second order fold of the Thoard  
844 syncline (Figs. 3 and 17; Haccard et al., 1989b). The upper Miocene-lower Pliocene  
845 olistolithic Tanaron Formation which unconformably lies above folded Oligocene-upper  
846 Miocene rocks, recorded the final growth of the Barles fold system before the emplacement of  
847 the Digne Nappe (Gigot et al., 1974; Pairis and Gidon, 1987; Hippolyte et al., 2011; Fig. 14).

848 Based on thermal modeling of low-temperature thermochronological data from lower  
849 Miocene rocks of the Vélodrome structure, Schwartz et al. (2017a) proposed that the thrusting  
850 of the Digne Nappe started before the cooling of its footwall at ~6 Ma. They proposed that the  
851 modeled upper Miocene cooling and exhumation was controlled by regional basement

852 tectonic thickening under the Valensole foreland basin. However, almost all of samples of the  
853 Barles half-window have Late Pliocene or younger minimum apatite (U-Th)/He cooling ages  
854 (Schwartz et al., 2017b) which is consistent with the proposed Late Miocene-Early Pliocene  
855 age of the Tanaron Formation in the footwall of the Digne Nappe (Hippolyte et al., 2011).  
856 Southward, the Aiglun, Mirabeau-Mallemoisson, Lambruissier, Les Mées and Asse structures  
857 deform upper Miocene conglomerates of the Valensole 1 Formation (Fig. 18; Haccard et al.,  
858 1989a). No growth strata that could support a syn-sedimentary shortening of these folds, was  
859 found on the field and subsurface. This suggest that the growth of these folds occurred after  
860 Late Miocene times (Hippolyte and Dumont, 2000; Godard et al., 2020).

861 Although Provençal and Oligocene structures are often unconformably covered and sealed  
862 by Miocene-Pliocene sequences in the Provençal zone, numerous evidence of contractional  
863 deformations are observed. South of the Valensole foreland basin, the Gréoux, Les Maurras  
864 and Vinon thrusts are unconformably covered by Miocene-Pliocene conglomerates of the  
865 Valensole 1-2 Formations. Along the fault traces, these conglomerates show striated and  
866 sheared pebbles (Figs. 21b, 22 and 23a), suggesting small reverse-reactivation of the inherited  
867 thrusts. The eastern edge of the Vinon thrust, the Rians syncline and Pallières thrust are also  
868 unconformably overlain by Oligocene conglomerate beds of the La Combe half-graben (Fig.  
869 3; Angelier and Aubouin, 1976). The conglomerate beds are also tilted and cut by reverse  
870 faults (Fig. 23b). This evidence of Alpine shortening is consistent with perched Miocene  
871 strata on the Mont-Major and Pallières thrusts; similar strata are located ~100 m lower on the  
872 Valavés anticline to the north (Fig. 3; Angelier and Aubouin, 1976). South of the Aurélien  
873 Mount thrust, Miocene conglomerates, sandstones and shales are folded and faulted, and  
874 unconformably overlie Campanian shales (Begudian facies; Fig. 23c) or middle Triassic  
875 Muschelkalk limestones (Espurt et al., 2019b). To the south, in the Signes and Méounes  
876 grabens, that belong in the Sainte-Baume Nappe, Oligocene-Miocene strata are locally

877 exposed (Nury and Rousset, 1986). At the northern edge of Signes graben, vertical to  
878 overturned Oligocene-Miocene conglomerates unconformably overlie Campanian-  
879 Maastrichtian continental strata (Begudian-Rognacian facies; Répin, 1922) (Fig. 24a). These  
880 field data reveal Alpine contractional deformation in this zone. Evidence of Alpine shortening  
881 are also observed in the Oligocene basins of Saint-Zacharie, Peypin, Destrousse, Aubagne and  
882 Marseille (Fig. 3). The Oligocene strata infilling these basins are generally affected by normal  
883 faults (Hippolyte et al., 1991), but they are also later folded (Guieu, 1968; Weydert and Nury,  
884 1978; Dupire, 1985) and faulted by strike-slip and reverse faults (Hippolyte et al., 1993). For  
885 example, the surface cross-section of Fig. 24b shows that the Peypin basin is an Oligocene  
886 half-graben bounded to the southwest by the Mauvais Vallon normal fault. This Oligocene  
887 basin develops on the eastern edge of the Etoile-Pierresca nappe system (Fig. 3), which  
888 propagated northward above the Arc syncline during the Provençal compression (Aubouin  
889 and Chorowicz, 1967; Guieu, 1968). The present day syncline shape of the Peypin basin  
890 associated with disharmonic folds and strike-slip faults in the Oligocene strata results from  
891 Alpine shortening. Similar deformed Oligocene (Miocene?) strata are also described  
892 westward in the Etoile Nappe near the Les Maurins trough (Figs. 3 and 23d; Nury and  
893 Raynaud, 1986; Hippolyte et al., 1993; Villeneuve et al., 2018). Alpine shortening is also  
894 found at the southern edges of the Marseille and Aubagne basins (Figs. 3 and 23e). In these  
895 areas, lower Cretaceous limestones of the Carpiagne anticline are interpreted as overthrust on  
896 northward tilted to overturned and faulted Oligocene limestone and conglomerate beds  
897 (Guieu, 1968; Weydert and Nury, 1978; Dupire, 1985; Villeneuve et al., 2018). A last  
898 example of Alpine shortening is recognized in the southernmost Bandol basin along the  
899 Mediterranean coast where Oligocene-Miocene conglomerates (Gouvernet, 1963) dip 20°  
900 toward the south and are cut by numerous small-scale reverse faults (Fig. 23f).

901 To reconstruct the orientation of the Alpine compression along our cross-section in the  
902 Subalpine zone and Provençal zone, we measured striated faults in seventeen sites in  
903 Oligocene, Miocene and Pliocene strata (Fig. 21b). Paleo-stress computation reveals a  
904 widespread ~NE-trending compression from the northern edge of the Valensole foreland  
905 basin to the Aubagne and Marseille basins to the south, and up to the Bandol basin along the  
906 Mediterranean coast. This ~NE-trending compression is contemporaneous with the deposition  
907 of upper Miocene growth strata in the Thoard syncline (Fig. 17) and observed up to Pliocene  
908 strata of the Digne area (Hippolyte et al., 2012). Generally, shortening direction may differ  
909 from stress orientation depending for example on the amount of displacement on strike-slip  
910 faults. It was demonstrated that a SSW transport direction of the Digne Nappe was related to  
911 an about NE-SW trend of compression at thrust front (Hippolyte et al., 2012). The post-  
912 Oligocene NE-SW trend identified in Provence is thus similar to the contemporaneous trend  
913 of compression in the Alps. That locally the Miocene-Pliocene trend of compression was  
914 similar to the upper Cretaceous-Eocene one may result from stress reorientation along  
915 Provençal structures. The distinction between the two stress fields was possible only because  
916 we worked in sites where the deformation can be dated. According to other works around the  
917 study area, this ~NE-trending Alpine compression which propagated southwestward into the  
918 Subalpine zone then, in the whole Provençal zone (Fig. 21b), probably prevailed since the  
919 Middle Miocene (Combes, 1984; Gaviglio, 1985; Villeger and Andrieux, 1987; Ritz, 1992;  
920 Champion et al., 2000; Clauzon et al., 2011).

921 **6.3. Modern compressional stress**

922 Beyond the predominant Miocene-Pliocene NE-trending compression presented above,  
923 modern NE- and NNW-trending compressional stresses have been identified by previous  
924 studies. Active shortening in the study area is revealed by earthquakes ( $M_w < 3.5$ ) distributed  
925 in the sedimentary cover and Paleozoic basement (Nicolas et al., 1990; Ritz, 1992; Baroux et

al., 2001; Cushing et al., 2008). The modern state of stress revealed by earthquake focal mechanisms in the Digne-northern Valensole foreland basin area is consistent with NE-trending shortening (Baroux et al., 2001; Cushing et al., 2008). It would be responsible for the Quaternary deformation in the Digne Nappe east of the Bès fault, as well as at the Lambruissier and Les Mées anticlines of the Puimichel plateau (Collina-Girard and Griboulard, 1990; Hippolyte and Dumont, 2000; Hippolyte et al., 2012; Godard et al., 2020; Fig. 18c). The Provençal zone is also characterized by a modern NNW-trending strike-slip regime along the Middle Durance left lateral strike-slip fault (Ritz, 1992; Baroux et al., 2001; Cushing et al., 2008; Mazzotti et al., 2020). This NNW-trending stress regime is consistent with fault slip data collected in Pliocene rocks along the Middle Durance fault zone (Guignard et al., 2005) or very locally in Oligocene rocks of the Marseille basin (Hippolyte et al., 1993). The origin of the modern shortening in Subalpine and Provençal areas is still debated. Some authors proposed that they could be controlled by the buoyancy forces in the core of the Alps, driving compression in the foreland (Le Pichon et al., 2010; Walpersdorf et al., 2018) with local deviations along pre-existing faults (e.g., Guignard et al., 2005), or related to the modern Africa/Europe convergence (Ritz, 1992; Baroux et al., 2001; Mazzotti et al., 2020).

## 7. Structural evolutionary model of the superimposed Provençal and Subalpine foreland thrust wedges

Based on the above mentioned structural data together with the review of deformation in space and time, we built a sequentially balanced cross-section illustrating the long-term thrust kinematic and shortening budget of superimposed Provençal and Subalpine thrust wedges from Latest Santonian to present day (Fig. 20). The structural evolutionary model presented here allows to discuss the role of crustal-scale rift-related anisotropies on vertical partitioning of the shortening, foreland flexure and syn-orogenic sedimentation. The amounts of

950 calculated shortening/extension are minimum because the footwall and hanging wall cut-offs  
951 of some structures are not clearly determined.

952 **7.1. Cross-section trace and thrust transport directions in the frame of the Provençal and**  
953 **Subalpine compressions**

954 Drawing cross-sections approximately parallel to the slip direction, i.e., parallel to the  
955 thrust transport direction is a prerequisite for cross-section balancing and restorations, and  
956 quantifying shortening (Dahlstrom, 1969; Elliot and Johnson, 1980). However, it appears  
957 relatively difficult to study superimposed orogenic deformations with a single and continuous  
958 section. In this study, we proposed to show and evaluate the role of pre-existing structures on  
959 subsequent deformations on a continuous cross-section with three segments of different trends  
960 (Fig. 3) that respect the structural grain of the main structures and the shortening directions.

961 Thus, the cross-sectional trace chosen for this study integrates with tolerable obliquity the  
962 different shortening directions of the two mountain ranges: the mean direction of compression  
963 trends NNE in the Provençal thrust wedge while it trends NE in the Subalpine thrust wedge  
964 (Fig. 21). Small variations in the direction of compressional are related to strike-slip  
965 structures (e.g., Bès fault, site 14 in Fig. 21b; Hippolyte et al., 2011). The magnetic fabric  
966 geometry also suggests SW-directed tectonic transport in all the Subalpine chains (Aubourg et  
967 al., 1999). These trends are consistent with the trace of the balanced cross-section in the zone  
968 where maximum horizontal shortening is recorded (Fig. 21 and see below). Therefore, our  
969 balanced cross-section that trend ~N to NNE can be sequentially restored to illustrate the  
970 structural evolution of Provençal and Subalpine superimposed foreland thrust wedges. To the  
971 south, the cross-section is somewhat oblique to the Alpine shortening direction, which implies  
972 that the amount of Alpine shortening is probably underestimated in this zone.

973 **7.2. Kinematic restoration of the Provençal thrust wedge**

974       The distribution of the upper Cretaceous foreland deposits permits to restore the first  
975       episode of thrust propagation in the inner part of the Provençal foreland between Latest  
976       Santonian and Maastrichtian (Fig. 20b). The transition from marine to continental deposits  
977       described in the uppermost Santonian strata of the Beausset syncline could be related to inner  
978       basement thrust stacking of the Provençal wedge related to the inversion South Provence  
979       basin and basement thrusting. The emplacement of the Cap Sicié basement thrust fed at least  
980       the slip of the Bandol cover thrust (other inner cover thrusts may have been eroded) above the  
981       Saint-Cyr Triassic high. The activity of these thrusts probably occurred during the  
982       Campanian-Maastrichtian because lower Campanian rocks (Fuvelian facies) are the youngest  
983       strata in the footwall of the Bandol thrust. The initial growth of the Sainte-Baume Nappe and  
984       deformation of Plan d'Aups and Pic des Corbeaux folds are recorded by upper Campanian-  
985       Maastrichtian (Begudian-Rognacian facies) syn-tectonic conglomerates. It is fed by the deep  
986       Saint-Mandrier thrust. The uplift of the Huveaune Triassic high is recorded by strata of  
987       Fuvelian or Rognacian facies unconformably resting on the Triassic basement, although these  
988       strata could have been transported onto the incipient Huveaune Triassic high during the  
989       overthrusting of the Etoile Nappe (Fabre et al., 1975; Philip, 2019). The restoration shows that  
990       the displacement of the deep basement Sainte-Baume thrust sheet was first accommodated by  
991       the Arc syncline and then by the Pourrières frontal ramp in the Middle Campanian-  
992       Maastrichtian. This frontal early growth might also result from the reactivation of basement  
993       faults to the north, similarly to this proposed for the early reactivation of the Sainte-Victoire  
994       Mountain deep basement thrusts (Espurt et al., 2012). Northward, the eroded area of the  
995       Valensole high could be interpreted as a forebulge during the Latest Cretaceous (Fig. 20b).

996       The Paleocene-Eocene period (Fig. 20c) corresponds to the complete emplacement of the  
997       southern basement thrusts and complete tectonic covering of the Sainte-Baume Nappe and  
998       Aurélien Mount thrust. Shortening propagates northward in the cover units (Pourrières,

999 Pallières, Vinon and Gréoux thrusts) as recorded by Paleocene syn-tectonic conglomerates  
1000 and subsiding thrust-top basins (i.e., Arc, Rians, Saint-Julien, La Mourotte, Esparron-de-  
1001 Verdon synclines; Fig. 3). Although a huge volume of Triassic evaporites is suspected under  
1002 the Pallières, Vinon and Gréoux units, the restoration suggests that Provençal thrusting also  
1003 propagated northward at depth level into the basement of the Valensole high. The shortening  
1004 recorded in cover of the outer part of the Provençal wedge was partly fed from the south (e.g.,  
1005 Pourrières and Pallières thrusts) but was also controlled by the inversion of basement  
1006 inherited fault system along S-verging thrusts with inferred shortcut trajectories. Although we  
1007 have no growth strata in subsurface data because of the erosion at the base of the Miocene  
1008 strata (Fig. 19), the initial growth of the Asse-Les Mées basement thrust system may have  
1009 occurred with a similar structural style (S-verging basement wedge) during this stage. The  
1010 growth of the Lambruissier, Mirabeau-Mallemoisson and Aiglun thrusts might also have  
1011 started as small domes during this stage (Dubois and Curneille, 1978). According to field  
1012 data, the restoration also shows the propagation of the deformation front up to the northern  
1013 edge of Valensole high as shown by the reactivation of the halokinetic folds of the Barles area  
1014 during the Late Eocene (Fig. 20c; Lemoine, 1972). Interestingly, the late Provençal shortening  
1015 has been recorded west of Barles area by Lutetian-Bartonian growth strata in the small  
1016 Eygalayes syncline (Montenat et al., 2005; Fig. 3). In addition, structural and stratigraphic  
1017 data in onshore Languedoc region confirm that Provençal shortening was active up to  
1018 Priabonian time (Séranne et al., 2021). An alternative interpretation is that the growth of the  
1019 Barles fold system comes from to the north from the early Alpine belt (Ford et al., 1999).  
1020 However, the N-trending compression reconstructed from growth strata (Fig. 16b), and the E-  
1021 W trend of the folds in this zone are rather consistent with the Provençal compression, the  
1022 Alpine compression being oriented more to the NE (Fig. 21). This outer Provençal shortening

1023 in the northern portion of the Valensole high up to and beyond the Barles zone implies that  
1024 shortening was transmitted at depth through the basement under the Valensole high.

1025 The Provençal thrust wedge accommodated a minimum of 38 km (i.e., 17%) of total  
1026 shortening (Fig. 20c). The main part of this shortening, i.e., 32 km, is accommodated by the  
1027 inversion of the South Provence basin to the south in the Provençal zone, the remaining 6 km  
1028 is accommodated in the Valensole high (Les Mées thrust) and Barles area. The sequential  
1029 restoration (Fig. 20a,b,c) allow to calculate a shortening amount of 8.9 km between Latest  
1030 Santonian and Maastrichtian (i.e.,  $\sim 0.5$  km Ma $^{-1}$ ), and of 29.1 km between Danian and Late  
1031 Eocene (i.e.,  $\sim 0.9$  km Ma $^{-1}$ ).

### 1032 **7.3. Oligocene breakup of the Provençal zone**

1033 South of the Valensole high, most of the structural development in the Oligocene is related  
1034 to the breakup of the Provençal thrust wedge by N-S, NNW-SSE and NE-SW extensional  
1035 fault systems (Fig. 20d; Angelier and Aubouin, 1976; Giannerini, 1978; Nury, 1988;  
1036 Hippolyte et al., 1993). The amount of extension remains small ( $\sim 1.6$  km) in the continental  
1037 Provençal margin and focused south of the cross-section in the Provençal zone (Bestani et al.,  
1038 2016). Most of the normal faults are reactivated thrust ramps, strike-slip faults (Roure et al.,  
1039 1992) or diapiric features (Angelier and Aubouin, 1976; Philip, 2018, 2019), which  
1040 accommodate the E-W opening of the West-European rift, then the NNW-SSE stretching of  
1041 the southern Provence crust due to the Ligurian-Provençal back-arc rifting between Provence  
1042 and Corsica-Sardinia block (Hippolyte et al., 1990, 1991, 1993; Bestani et al., 2016).

### 1043 **7.4. Kinematic restoration of the Subalpine thrust wedge**

1044 Following the Provençal shortening, the early orogenic building of the internal Alpine  
1045 wedge during Late Eocene-Oligocene times has been probably associated with major flexural  
1046 subsidence north of the Barles area (Fig. 20d; Ford et al., 2006; Graham et al., 2012).

1047 According to field data, the cross-section suggests small reactivation (less than 500 m of  
1048 shortening) of the pre-existing halokinetic folds of the Barles area (Maillart et al., 1987;  
1049 Gidon, 1997; Célini et al., 2021). This Oligocene deformation might be interpreted as distal  
1050 shortening in the Oligocene Alpine foreland.

1051 The Late Miocene restored stage (Fig. 20e) shows the southward shift of subsidence into  
1052 the Valensole high that became a large foreland basin. The syn-orogenic Miocene  
1053 sedimentary package of the Valensole foreland basin exhibits a wedge-shaped geometry, with  
1054 a more than 3 km-thick sequence in the depocenter zone and a few hundred meters in the  
1055 south of basin. Southward, the Provençal zone was uplifted without fault reactivation. There,  
1056 thin marine to continental sequences fill paleo-valleys overprinting the paleo-morphology of  
1057 the Provençal thrusts, or cover marine abrasion surfaces (Mennessier, 1959; Cornet, 1965;  
1058 Angelier and Aubouin, 1976; Besson, 2005; Oudet et al., 2010). The Provençal zone may  
1059 represent a flexural forebulge, accompanying the subsidence of the Valensole foredeep  
1060 depozone. This uplift is likely to have also been controlled by the Ligurian-Provençal passive  
1061 margin setting to the south. The initial subsidence of the Valensole basin was first recorded by  
1062 the transgressive Aquitanian-Burdigalian Lower Marine Molasse Formation on Mesozoic  
1063 rocks previously folded and faulted during the Provençal compression. Subsidence continues  
1064 through the Langhian to Tortonian (early Messinian?) with the deposition of the Upper  
1065 Marine Molasse Formation that passes laterally and vertically to prograding fluvio-deltaic  
1066 conglomerates of the Valensole 1 Formation. Synchronous syn-folding sedimentation is  
1067 localized in the northern edge of the Valensole basin where growth strata in clastic sediments  
1068 of the Vélodrome structure record the activity of the La Maurière anticline and other inner  
1069 folds through the Miocene (Pairis and Gidon, 1987). Such deformation and uplift of the  
1070 Barles fold system require the existence of basement thrust wedge under the Barles area.  
1071 Although the ductile behavior of the Triassic detachment undeniably participated to the

1072 growth of the folds in cover, we propose that shortening was mainly controlled by the  
1073 inversion of the deep Verdaches half-graben (named here the Verdaches horse) and the  
1074 formation of an inferred frontal basement thrust (named the Barles horse) that propagated  
1075 southward in the Triassic evaporites under the Thoard syncline. To the south of the Valensole  
1076 basin, no growth strata are found within the upper Miocene conglomerate sequences,  
1077 suggesting no contractional reactivation of the pre-existing Provençal structures.

1078 The comparison between the Late Miocene and present day stages (Fig. 20e,f) allows to  
1079 evaluate the upper Miocene-Pliocene thrusting of the Digne Nappe above the Valensole and  
1080 the southward transfer of the shortening into the Valensole foreland basin and Provençal zone.  
1081 The olistolithic Tanaron Formation in the stratigraphically highest part of the Thoard syncline  
1082 indicates strong erosion of the La Maurière anticline (Pairis and Gidon, 1987). The Digne  
1083 Nappe moved above the Valensole basin mainly after the deposition of the upper Miocene-  
1084 lower Pliocene Tanaron Formation. The present antiformal shape of the Digne Nappe is  
1085 related to renewed basement thrusting under the Barles area, leading to the development of  
1086 the present erosional Barles half-window. In this way, the Digne Nappe was folded later  
1087 probably during the Pliocene by the underlying basement thrust wedge (Schwartz et al.,  
1088 2017a,b). During the Pliocene-Quaternary, shortening of the basement thrust wedge was  
1089 transferred southward through a Triassic décollement in the Valensole basin, leading to the  
1090 complete development of the Aiglun, Mirabeau-Mallemoisson and Lambruissier anticlines.  
1091 This period is also marked by the contractional reactivation of Provençal thrusts in the  
1092 Valensole basin and Provençal zone, and inversion of Oligocene-Miocene basins as far as  
1093 Aubagne, Marseille and Bandol basins along the Mediterranean coast. This outer Alpine  
1094 shortening through the Provençal zone implies that part of the shortening was transmitted at  
1095 depth through the continental crust.

1096 Globally, the kinematic restoration shows that the Subalpine thrust wedge is characterized  
1097 by a first order shortening transfer from hinterland to foreland zones (Fig. 20d,e,f). However,  
1098 the structural evolution of the Subalpine Thoard syncline and Digne Nappe show interaction  
1099 between thrusting and syn-tectonic sedimentation and erosion disturbing here temporally this  
1100 forward thrusting sequence as observed in many natural examples and analog and numerical  
1101 models (e.g., Baby et al., 1995; Bonnet et al., 2008; Uba et al., 2009; Fillon et al., 2013; Erdős  
1102 et al., 2015; Butler, 2020; Wu et al., 2021). The structural inversion in the southern margin of  
1103 the Digne basin can be interpreted as a triangle zone model (McMechan, 1985; Price, 1986;  
1104 Jamison, 1993). The large accumulation (up to 3.3 km-thick) of Miocene syn-tectonic  
1105 sediments at the front of Barles basement triangle zone may have influenced the frictional  
1106 properties (increase of the vertical stress) of the potential Triassic décollement under the  
1107 Thoard syncline (Fig. 14b). We suggest that from Oligocene to Late Miocene this behavior  
1108 may have prevented forward thrust propagation, localizing in a first step the deformation front  
1109 at the northern edge of the Valensole basin in the Thoard-Vélodrome zone (Wu et al., 2021).  
1110 When stresses were too strong and the Barles triangle zone could no longer accommodate the  
1111 shortening by folding in the Thoard-Vélodrome zone, the broad Digne Nappe activated and  
1112 cuts the pre-structured folds of the Barles area (Gidon and Pairis, 1992; Fig. 20e,f),  
1113 characterizing an out-of-sequence kinematics as suggested by Vann et al. (1986). After the  
1114 emplacement of the Digne Nappe, the development of the basement thrust wedge continued  
1115 (folding of the Digne Nappe) and its shortening was transferred southward in the Aiglun,  
1116 Mirabeau-Mallemoisson and Lambruissier cover structures.

1117 The Subalpine thrust wedge accommodated a minimum of ~35 km (i.e., 19%) of total  
1118 shortening between Oligocene and present day (Fig. 20f). The main part of this shortening,  
1119 i.e., 22 km, is accommodated by the Digne Nappe, 10 km in the Barles fold system and  
1120 northern Valensole foreland basin, the rest, i.e., 3 km, is accommodated southward by

1121 reactivated Provençal basement thrusts (south of the Lambruissier anticline). The sequential  
1122 restoration (Fig. 20d,e,f) allows to calculate a shortening amount of 13.8 km between  
1123 Aquitanian and Late Miocene (i.e.,  $\sim$ 0.6 km Ma $^{-1}$  for the Aquitanian-Late Miocene period),  
1124 and of 21.2 km between the Late Miocene and present day (i.e.,  $\sim$ 2.1 km Ma $^{-1}$ ). The  
1125 calculated upper Miocene to present day shortening rate is three times larger than the post-  
1126 Zanclean slip (0.7 km Ma $^{-1}$ ) along the Bès fault deduced from the 2.3 km displacement of a  
1127 dissected post 3.4 Ma infilled drainage network (Hippolyte et al., 2012).

1128 **7.5. Foreland basin development**

1129 The propagation of the Provençal and Subalpine thrust wedges led to tectonic loading and  
1130 foreland basin flexure (DeCelles and Giles, 2001). Both thrust wedges exhibit similar flexure  
1131 angle toward hinterland zones of  $\sim$ 7° (Fig. 20c,f). However, the Provençal and Subalpine  
1132 thrust wedges are characterized by foreland basins with contrasted developments and  
1133 geometries. The Provençal thrust wedge is characterized by distributed basement thrusts along  
1134 the cross-section reworking numerous structures inherited from the Variscan belt and  
1135 Permian-Mesozoic rifts. As previously suggested by Roure and Colletta (1996), the inversion  
1136 of this complex structural framework might have favored the development of several upper  
1137 Cretaceous to Eocene foreland depocenters (Beausset, Arc, Rians, Saint-Julien, La Mourotte,  
1138 Esparron-de-Verdon basins; Fig. 3), incorporated into the thrust wedge (Fig. 20c). In contrast,  
1139 the Subalpine thrust wedge is characterized by the stacking of the thick Digne Nappe and  
1140 Barles basement triangle zone. This duplex induced strong tectonic loading which might have  
1141 controlled the large flexure of the Valensole basin, partly incorporated into the thrust wedge  
1142 (Fig. 20f).

1143 **8. Discussion**

1144 **8.1. Basement inheritance and Triassic décollement level**

1145 Inherited or neo-formed décollement levels have strong influence on the vertical  
1146 partitioning of the shortening in fold-thrust belts (e.g., Torres Carbonell et al., 2017).  
1147 Inherited discontinuities in the Paleozoic basement (inherited faults, shear zones, or  
1148 metamorphic foliations) act as decoupling levels that connect at depth with lower crustal level  
1149 (e.g., Espurt et al., 2008; Lacombe and Bellahsen, 2016; Bellahsen et al., 2016). Salt and  
1150 ductile shale levels are also recognized as major decollement levels in the sedimentary cover.  
1151 The tectonic style of both Provençal and Subalpine foreland thrust wedges consists in mixed  
1152 thick- and thin tectonic styles: deep basement thrust wedges kinematically linked with  
1153 shallow thrust wedges detached in middle-upper Triassic evaporites. The basal Muschelkalk  
1154 and Keuper units constitute major decollement levels in the sedimentary cover (Caron, 1979;  
1155 Gidon, 1982; Baudemont, 1985; Tempier, 1987; Gidon and Pairis, 1992; Gidon, 1997). The  
1156 structural data and cross-section restorations reveal that the shortening propagated through  
1157 heterogenous basement frameworks involving the reactivation of pre-existing structures  
1158 related to Permian and Mesozoic rift events (Bathiard and Lambert, 1968). The thinner crust  
1159 of the former Mesozoic rift basins (i.e., the Beausset and Digne basins) associated with  
1160 ductile lower crust might have favored the inversion of basement normal faults and the  
1161 formation of inner thick-skinned thrust wedges during convergence. This style of shortening  
1162 is most likely to occur in a young lithosphere like Europe (Mouthereau et al., 2013;  
1163 Mouthereau et al., 2021). Our kinematic model shows that the Valensole high, separating the  
1164 Beausset and Digne basins, remained a basement block poorly deformed by successive  
1165 Provençal and Alpine orogens (Fig. 20a). If we analyze the distribution of the Triassic  
1166 evaporites in the study area, we observed that these latter have controlled the transfer of the  
1167 thin-skin tectonic displacement into the cover and the geometry of Provençal and Subalpine  
1168 thin-skinned thrust wedges. The Provençal and Subalpine external compressional structures  
1169 developed along the pinchouts of the Triassic evaporites located onto the flanks of the

1170 Valensole high. The near absence of potential Triassic layer overlying the basement of  
1171 Valensole high (Les Mées area) and the relatively thin Mesozoic cover (less than 1 km-thick;  
1172 Figs. 19 and 20) seem to have prevented the propagation of the decollements at shallow level  
1173 into the cover. The restoration suggests that both Provençal and Alpine compressional stresses  
1174 have consequently been transmitted under the basement of the Valensole high (Fig. 20c,f)  
1175 perhaps onto a deep crustal (lower crust?) detachment level (e.g., Lacombe and Moutherau,  
1176 2002; Moutherau et al., 2013, 2014; Lacombe and Bellahsen, 2016; Laborde et al., 2019;  
1177 Moutherau et al., 2021). During the Oligocene-Miocene Ligurian-Provençal back-arc  
1178 extension, the southern Provence crust (Maures massif) was reheated, thinned, and weakened  
1179 (Guieu and Roussel, 1990; Jakni, 2000; Bestani et al., 2016). This may explain the  
1180 involvement of the basement in the shortening related to the Alpine compression as far as the  
1181 Marseille-Bandol zone to the south. Such outer thick-skin deformation related to thermal  
1182 event was already suggested by Jourdon et al. (2014) in the external Castellane area (Fig. 1).  
1183 In the same way, the Provençal shortening has been transmitted under the Valensole high up  
1184 to the weakened zone of the Vocontian rift during the Late Eocene times.

1185 On a larger scale (Fig. 1), the cross-section presented in this study and previously  
1186 published cross-sections constructed across the southwestern Subalpine thrust front (Lickorish  
1187 and Ford, 1998; Laurent et al., 2000; Jourdon et al., 2014; Guyonnet-Benaize et al., 2015;  
1188 Bestani et al., 2016) show that the irregular basement architecture inherited from Paleozoic  
1189 and Mesozoic tectonic stages and the distribution of the Jurassic-Cretaceous basins underlain  
1190 by Triassic evaporites controlled the along-strike geometry of the Subalpine thrust front  
1191 (Roure and Colletta, 1996; Macedo and Marshak, 1999). The Diois-Baronnies-Western  
1192 Provence Arc (Villeger and Andrieux, 1987) and Digne-Castellane Arc (Goguel, 1937)  
1193 coincide with Jurassic-Cretaceous depocenters (more than 5600 m-thick in the western  
1194 Provence, and 1300-2200 m-thick in the Castellane Arc; Ménard, 1979; Laurent et al., 2000;

1195 Guyonnet-Benaize et al., 2015; Bestani et al., 2016) whereas the Valensole high is overlain by  
1196 a thin succession (150-1000 m-thick). We suggest that the shape of the Diois-Baronnies-  
1197 Western Provence Arc (Villeger and Andrieux, 1987) and the Digne-Castellane Arc (Goguel,  
1198 1937) has been preferentially controlled by these paired Jurassic-Cretaceous basins underlain  
1199 by huge volumes of Triassic evaporites. It was well established that the southern units of these  
1200 arcs accommodated Alpine shortening in Miocene. In the Western Provence Arc, the  
1201 Luberon, Costes and Trévaresse thrusts recorded shortening in Middle-Late Miocene as  
1202 revealed by growth strata deposits and uplifted staircase wave-cut platforms (Anglada and  
1203 Colomb, 1967; Champion et al., 2000; Besson, 2005; Clauzon et al., 2011). In the southern  
1204 units of the Castellane Arc, growth strata in the upper Miocene-Pliocene conglomerates of the  
1205 southeastern edge of the Valensole basin, and Eoulx-Brenon, Roque-Escalpon and Aubarède  
1206 synclines more to the east have also recorded the Alpine shortening (Gigot et al., 1976;  
1207 Giannerini et al., 1977; Giannerini, 1978; Dardeau et al., 2010; Fig. 1). In map view, the  
1208 Valensole high can be interpreted as a reentrant between the Diois-Baronnies-Western  
1209 Provence Arc and the Digne-Castellane Arc. The thinning of the Triassic evaporites onto the  
1210 northeastern flank of the Valensole high prevented the large SW-ward propagation of the  
1211 thin-skinned shortening, which was accommodated into the Aiglun, Mirabeau-Mallemoisson  
1212 and Lambruissier anticline, probably recently and partly during the Quaternary for the  
1213 Lambruissier anticline (Hippolyte and Dumont, 2000). The along-strike structural variations  
1214 in the kinematic of the Subalpine thrust systems were accommodated by the development of  
1215 NNE-trending strike-slip systems and oblique structures on lateral ramps on both sides of the  
1216 Valensole foreland basin (e.g., Middle Durance fault zone and Bès fault; Laurent et al., 2000;  
1217 Hippolyte et al., 2012; Guyonnet-Benaize et al., 2015; Fig. 1). Along the study area, the  
1218 transfer of shortening into the basement of Provence induced the small reactivation of

1219 inherited basement faults under the central-southern Valensole basin and Provençal zone,  
1220 causing their uplift during the Pliocene-Quaternary.

1221 Although the shape of the Eocene Provençal frontal thrusts has been strongly modified by  
1222 the Alpine deformation, we also show that the along-strike configuration of the Mesozoic  
1223 basins has controlled the ~NNE-ward propagation of the thin-skinned Provençal thrust front  
1224 (Fig. 1). In the Western Provence Arc, balanced cross-sections of Bestani et al. (2016)  
1225 illustrating the geometry of the Provençal fold-thrust belt at the end of Eocene show that the  
1226 combination of thick sedimentary cover and Triassic evaporitic detachment layers favored the  
1227 propagation of the thin-skinned thrust front up to the Baronnies area north of the Ventoux-  
1228 Lure thrust system (Montenat et al., 2005). Similarly, restored balanced cross-sections of  
1229 Laurent et al. (2000) and Jourdon et al. (2014) suggest that the Provençal cover detached  
1230 easily northward up to the Vocontian basin thanks to the Triassic decollements. During this  
1231 period, the NNE-trending Middle Durance fault zone and probably the Barjols Triassic zone  
1232 (Figs. 1 and 3) accommodated the along-strike kinematic of the Provençal thrust systems  
1233 (Bestani et al., 2016).

1234 **8.2. Accommodation of the shortening by halokinetic structures**

1235 During shortening, the pre-existing halokinetic structures were generally reactivated,  
1236 localizing preferentially the shortening in the cover. The initial geometry of these pre-existing  
1237 halokinetic structures can be strongly modified during the contractional deformations as  
1238 documented, for instance, in the Pyrenees (Saura et al., 2016; Labaume and Teixell, 2020;  
1239 Burrel and Teixell, 2021), in Provence (Angelier and Aubouin, 1976; Espurt et al., 2019b), in  
1240 the Alps (Dardeau et al., 1990; Granado et al., 2018; Célini et al., 2020, 2021), in the Zagros  
1241 (Callot et al., 2007, 2012), and in the eastern Carpathians (Tămaş et al., 2021). Shortening  
1242 induces the lateral and vertical evacuation of the mobile evaporitic material. Inherited salt  
1243 dome structures constitute weak zones, which can evolve in diapirs with upturning flanks

1244 leading to thrust welding. Minibasins related to sedimentary loading evolve in tight synclines.  
1245 As revealed by the palinspastic restoration of Fig. 20a and previous works in the study area,  
1246 the Provençal and Subalpine thrust wedges incorporate numerous pre-existing halokinetic  
1247 structures that initially developed during Mesozoic rifting stages (e.g., Graham et al., 2012;  
1248 Bestani et al., 2015, 2016; Espurt et al., 2019b; Célini et al., 2020, 2021; Wicker and Ford,  
1249 2021) and locally also during the Oligocene (Angelier and Aubouin, 1976). The Mesozoic  
1250 halokinetic structures associated with variable thickness of Triassic evaporites and  
1251 sedimentary cover undeniably generated anisotropic behavior in deformation during  
1252 shortening. In the following, we discuss the role and evolution of some of these pre-existing  
1253 halokinetic features in the Provençal and Subalpine thrust wedges.

1254 Halokinesis and its relationship with basement faulting has been previously analyzed and  
1255 quantified by Espurt et al. (2019b) in eastern Provençal zone where a succession of early  
1256 halokinetic folds have been later deformed by the Provençal and Alpine compressions. This  
1257 work has provided new ideas leading to the reinterpretation of some structures located further  
1258 west along the cross-section studied in this paper. For instance, the emplacement of the  
1259 Bandol thrust was controlled by the Saint-Cyr Triassic high developed earlier at least up to  
1260 the Early Santonian (Philip, 1967; Philip et al., 1987). The initial geometry of the dome has  
1261 been squeezed and probably decapitated by the Bandol thrust. Shortening may have also  
1262 driven salt migration and the northward expulsion of the Saint-Cyr Triassic evaporites onto  
1263 the floor of the Beausset syncline (Fig. 8). The dip of the northern limb of the dome, made of  
1264 lower Santonian limestone beds, has been enhanced during Provençal shortening and sheared  
1265 by low-angle reverse faulting. Although we have no direct evidence of early halokinetic  
1266 motion in the footwall block of the Sainte-Baume Nappe, we inferred that its emplacement  
1267 might have been initiated on an early halokinetic structures above a N-dipping basement  
1268 normal fault. However, we interpret the present day tight geometry of the Plan d'Aups

1269 syncline as mostly resulting from the emplacement of the far-travelled Sainte-Baume Nappe  
1270 and contractional shear into its footwall block (e.g., Bertagne tectonic slice; Fig. 9b). A  
1271 tectonic model implying an early growth (Jurassic?) of diapiric structures can be proposed for  
1272 the Huveaune Triassic high (Bestani et al., 2015; Philip, 2018; 2019). This high is interpreted  
1273 as an early dome controlled by a huge volume of Triassic evaporites overlying a basement  
1274 fault (Guillemot et al., 1973). The restoration suggests that the dome has been strongly  
1275 squeezed by Provençal shortening. As suggested by analog models in Callot et al. (2007), the  
1276 initial shape of the dome controlled the propagation of the hanging-wall flat of the Aurélien  
1277 Mount thrust through southern limb of the former dome. Surface exposure of the halokinetic  
1278 structures after the Provençal compression might explain why some of them (e.g., the  
1279 Huveaune or Barjols Triassic zones; Fig. 3), constituted by ductile material, have been easily  
1280 reactivated during the Oligocene extension and Alpine compression (Angelier and Aubouin,  
1281 1976; Philip, 2018, 2019; Espurt et al., 2019b).

1282 North of the Arc syncline, field data and cross-section restoration suggest that thrust  
1283 systems are superimposed on Jurassic-lower Cretaceous salt domes and large synclines with  
1284 local normal faults (Fig. 20a,b,c). Folding of the Rians syncline may have initiated during the  
1285 Jurassic. However, its present tight geometry could rather result from the combined effects of  
1286 halokinetic processes and thrusting (Cojan, 1993). We suggest that syn-tectonic sedimentary  
1287 loading of the Paleocene-Eocene Rians syncline has favored its sinking into the thick ductile  
1288 Triassic evaporitic-carbonate layer (Fig. 20c) as previously shown in the Sivas basin in  
1289 Turkey by Kergaravat et al. (2016).

1290 In the Subalpine zone, cross-section restoration and field data also confirm that halokinetic  
1291 features located in the hanging-wall and footwall of the Digne Nappe have localized and  
1292 accommodated Alpine shortening. As suggested by the restored stage (Fig. 20a), the Digne  
1293 Nappe involves frontal halokinetic structures (lateral continuation of the Turriers unit (now

1294 eroded) and La Robine; Célini et al., 2020). These structures are not only passively  
1295 transported within the nappe but recorded major internal contractional deformation. The  
1296 Barles diapiric structure is interpreted as a major halokinetic structure that localized the  
1297 leading edge of the Digne Nappe (Fig. 20a; Graham et al., 2012). Beneath this thrust, and in  
1298 contrast to the cross-sections of Graham et al. (2012) and Célini et al. (2020), the Barles fold  
1299 system is not interpreted as an allochthonous unit transported above inferred deep cover sub-  
1300 thrust. Although we have no subsurface data at Barles to highlight the thrust system geometry  
1301 at depth, our construction favors a simple detachment fold interpretation as previously  
1302 proposed by Goguel (1944) (Fig. 14b). The La Grande Cloche and La Maurière anticlines are  
1303 detached from the underlying basement along Triassic evaporites. We agree that in places,  
1304 folding has been initiated during Mesozoic rifting as a result of motion of the Triassic  
1305 evaporites together with normal faulting as observed immediately north of the La Grande  
1306 Cloche anticline in the Les Sauvans minibasin and Barles diapir. These pre-existing folds  
1307 naturally localized contractional deformation during shortening. The present squeezed  
1308 geometry of the detachment folds at Barles and complete overturning of the Barre de Chine  
1309 flap were likely favored by ductile behavior of Triassic evaporites, but also by compaction of  
1310 the ductile Callovian-Oxfordian shales in fold cores (Fig. 14c). Thus, the present day  
1311 squeezed geometry of the Barles folds has been likely enhanced by shortening and the  
1312 emplacement of the overlying Digne Nappe. Recently, Célini et al. (2020) interpreted the  
1313 Neogene Vélodrome syncline as a mini-basin structure and the contact between the La  
1314 Maurière anticline and the Vélodrome as a salt weld. These interpretations require a salt or  
1315 allochthonous salt sheet Oligocene in age but the Oligocene strata exposed near Esclangon are  
1316 fluvial deposits without any evidence of salt level.

1317 To sum up, Mesozoic halokinetic structures belonging in the South Provence and  
1318 Vocontian extensional basins were rejuvenated and squeezed by Provençal and Alpine

1319 compressions. These structures localize preferentially the shortening and a significant amount  
1320 of shortening might have been also accommodated by internal deformation within evaporitic  
1321 layers. It appears therefore important to perform microstructural analysis into the evaporitic  
1322 layers of salt-core structures to better constrain the amount of internal deformation  
1323 accommodated within these structures during subsequent shortening (Malavieille and Ritz,  
1324 1989; Rowan et al., 2019; Tămaş et al., 2021).

## 1325 **9. Conclusion**

1326 In this study, available surface and subsurface data together with the construction of a 150  
1327 km-long sequentially restored balanced cross-section were combined to provide a regional  
1328 overview of geology, structural evolution and quantification of crustal shortening budget of  
1329 the superimposed Provençal and Subalpine fold-thrust belts in Central Provence region.  
1330 Along the studied cross-section, the multistage growth of the fold-thrust belt systems has been  
1331 remarkably recorded by well-preserved syn-orogenic deposits, growth strata and kinematic  
1332 indicators of thrusting in the foreland basins. The major points arising from this study case are  
1333 as follow:

1334 - The Provençal and Subalpine thrust wedges are characterized by a mixed thick- and thin-  
1335 skinned tectonic style including basement thrusts propagating through inherited basement  
1336 discontinuities (Variscan structures and normal faults delimiting upper Carboniferous-  
1337 Permian basins, Mesozoic Tethyan, Vocontian and South Provence basins, and Oligocene  
1338 basins) and cover thrusts detached in the middle-upper Triassic evaporites. The palinspastic  
1339 restoration of the thrust wedges to Late Santonian shows a large uplift zone in the center of  
1340 the study area (Durance high and Valensole high), which led to the separation of the Beausset  
1341 basin (as part of the South Provence basin) to the south and the Digne basin (as part of the  
1342 Vocontian basin) to the north. These extensional basins reactivated ~N-dipping normal faults  
1343 related to upper Carboniferous-Permian basins.

1344 - The Provençal shortening propagated NNE-ward from the inverted Beausset basin up to  
1345 the Barles area during Latest Santonian-Campanian to Late Eocene (i.e., ~50 m.y.). The  
1346 Subalpine shortening propagated SW-ward from the inverted Digne basin up to the  
1347 Mediterranean coast during Oligocene-Aquitanian to present (i.e., ~30 m.y.). In Provence, the  
1348 Provençal and Alpine episodes of shortening are clearly separated by the Oligocene rifting  
1349 events including the West-European rift followed by the back-arc rift of the Ligurian-  
1350 Provençal basin destroying the inner Provence crystalline thrust wedge. In the studied area,  
1351 NNW-SSE extension was mainly accommodated by crustal thinning and upper crustal ENE-  
1352 trending normal faults together with major phases of erosion and sedimentation. In contrast,  
1353 the recognition of upper Eocene, Oligocene and Miocene growth strata in the Subalpine zone  
1354 of Barles might suggest a continuum of contractional deformation.

1355 - The amount of horizontal crustal shortening, derived from sequential restoration, is  
1356 relatively similar in both thrust wedges: 38 km (17%) in the Provençal thrust wedge and 35  
1357 km (19%) in the Subalpine thrust wedge.

1358 - By distributing the deformation through numerous inherited Permian-Mesozoic basement  
1359 structures, the Provençal thrust wedge might have favored the development of confined  
1360 foreland basins, as the Arc and Rians basins. In contrast, the vertical stacking of the thick  
1361 Digne Nappe and Barles basement triangle zone in the Subalpine thrust wedge might have  
1362 controlled the large flexure of the Valensole foreland basin.

1363 - The sequential restoration suggests that the shortening has been mainly controlled by the  
1364 inversion of the South Provence basin-Durance high (Provençal shortening) to the south, by  
1365 the inversion of the Vocontian basin (Alpine shortening) to the north, and by other factors as  
1366 the pinch out of the Triassic décollement level onto the Valensole high and early halokinetic  
1367 structures. At the scale of our cross-section, we show that syn-tectonic sedimentation has  
1368 small and localized impact on thrusts kinematics (i.e., Digne Nappe).

1369 - This study highlights that the development of pre-shortening extensional basins and long-  
1370 term structural evolution of the Provençal and Subalpine fold-thrust belts have been  
1371 controlled by inherited crustal structures. These crustal heterogeneities have greatly  
1372 influenced the propagation of the contractional deformation and foreland basin development  
1373 in space and time.

1374 **Acknowledgments**

1375 Financial support for fieldworks in the frame of the Phd thesis of Jocelyn Balansa came  
1376 from the BRGM-RGF (French Geological Survey-Référentiel Géologique de la France) Alpes  
1377 et bassins périphériques program. We thank the Agence de l'Eau Rhône Méditerranée Corse  
1378 for providing seismic profiles in the Valensole basin. This paper is also part of the Karst-  
1379 Huveaune project (2018-2022) funded by Agence de l'Eau Rhône Méditerranée Corse,  
1380 Région Sud-Provence Alpes Côte d'Azur, Conseil Départemental des Bouches-du-Rhône,  
1381 Aix-Marseille Provence Métropole, BRGM, Aix-Marseille Université. We thank Stéphane  
1382 Marc, Eglantine Husson and Marie Genevier from BRGM for seismic profile interpretation,  
1383 and Myette Guiomar from the Réserve naturelle géologique de Haute-Provence for field  
1384 assistance. We also thank Pierre Henry, Michel Corsini, Gérard Giannerini and David  
1385 Baudemont for useful discussions. The MOVE Software Suite was donated by Petroleum  
1386 Experts Limited. Finally, we acknowledge Eldert Advokaat and an anonymous reviewer for  
1387 the constructive comments and suggestions which greatly helped to improve the original  
1388 manuscript.

1389 **Data Availability**

1390 Datasets related to this article can be consulted by contacting J. Balansa (balansa@cerege.fr)

1391 **References**

- 1392 Advokaat, E. L., van Hinsbergen, D. J., Maffione, M., Langereis, C. G., Vissers, R. L.,  
 1393 Cherchi, A., Schroeder, R., Columbu, S., 2014. Eocene rotation of Sardinia, and the  
 1394 paleogeography of the western Mediterranean region. *Earth and Planetary Science Letters*,  
 1395 401, 183-195, <https://doi.org/10.1016/j.epsl.2014.06.012>.
- 1396 Aguilar, J.-P., Clauzon, G., 1981. Découverte de trois nouveaux gisements à Rongeurs d'âge  
 1397 miocène en Provence nord-orientale. Implications géodynamiques et paléogéographiques.  
 1398 *C. R. Acad. Sci. Paris*, 292, II, 909-912.
- 1399 Alvarez-Marron, J., Rodriguez-Fernandez, R., Heredia, N., Busquets, P., Colombo, F.,  
 1400 Brown, D., 2006. Neogene structures overprinting Palaeozoic thrust systems in the Andean  
 1401 Precordillera at 30° S latitude. *Journal of the Geological Society, London*, 163, pp. 949-  
 1402 964, doi:10.1144/0016-76492005-142.
- 1403 Angelier, J., 1971. La partie septentrionale de la bande triasique de Barjols (Var). Paris, PhD  
 1404 thesis.
- 1405 Angelier, J., 1984. Tectonic analysis of fault slip data sets. *Journal of Geophysical Research*,  
 1406 Vol. 89, No. B7, 5835-5848.
- 1407 Angelier, J., 1990. Inversion of field data in fault tectonics to obtain the regional stress. III-a  
 1408 new rapid direct inversion method by analytical means. *Geophysical Journal International*,  
 1409 103, 363-376.
- 1410 Angelier, J., 1991. Inversion directe et recherche 4-D : comparaison physique et  
 1411 mathématique de deux modes de détermination des tenseurs des paléocontraintes en  
 1412 tectonique de failles. *C. R. Acad. Sci. Paris*, 312, II, 1213-1218.
- 1413 Angelier, J., Aubouin, J., 1976. Contribution à l'étude géologique des bandes triasiques  
 1414 provençales : de Barjols (Var) au bas Verdon. *Bull. B.R.G.M.*, 2, 1, no. 3, 187-217.
- 1415 Anglada, R., Colomb, E., 1967. Precisions tectoniques sur le flanc sud de l'anticlinal du  
 1416 Grand-Luberon (Vaucluse). *Bulletin de la Société Géologique de France*; S7-IX (4): 596-  
 1417 599, doi-org.insu.bib.cnrs.fr/10.2113/gssgbull.S7-IX.4.596.
- 1418 Angrand, P., Moutherieu, F., 2021. Evolution of the Alpine orogenic belts in the Western  
 1419 Mediterranean region as resolved by the kinematics of the Europe-Africa diffuse plate  
 1420 boundary. *Bulletin de la Société Géologique de France - Earth Sci Bulletin*.  
<https://doi.org/10.1051/bsgf/2021031>.
- 1422 Arlhac, P., Catzigras, F., Colomb, E., Gervais, J., Gouvernet, C., Gueirard, S., Lambert, C.,  
 1423 Mercier, H., Nury, D., Rousset, C., Tempier, C., Viencent, H., Weydert, P., 1970. Carte  
 1424 géol. France (1/50000), feuille PERTUIS (995). Orléans: Bureau de recherches  
 1425 géologiques et minières.
- 1426 Arnaud, H., Debemas, J., Flandrin, J., Gidon, M., Kerckhove, C., 1976. Remarques et  
 1427 réflexions à propos de l'attribution au Néogène d'une partie des cargneules et des gypses  
 1428 alpins. *Bull. Soc. géol. Fr.*, 7, XVIII, No. 4, 973-979, doi:10.2113/gssgbull.S7-  
 1429 XVIII.4.973.
- 1430 Aubouin, J., Mennessier, G., 1962. Essai sur la structure de la Provence. In Durand-Delga M.  
 1431 (Coord.) : Livre à la Mémoire du Professeur Paul Fallot, Mémoire hors-série de la Société  
 1432 géologique de France, II, p. 45-98, pl. I.
- 1433 Aubouin, J., Chorowicz, J., 1967. Le chevauchement sud-provençal : de l'Etoile à la Sainte-  
 1434 Baume. *Bull. Soc. géol. Fr.*, 9, 600-608.

- 1435 Aubourg, C., Rochette, P., Stéphan, J.-F., Popoff, M., Chabert-Pelline, C., 1999. The  
1436 magnetic fabric of weakly deformed Late Jurassic shales from the southern subalpines  
1437 chains (French Alps): evidence for SW-directed tectonic transport direction.  
1438 *Tectonophysics*, 307, 15-31
- 1439 Baby, P., Colletta, B., Zubietta, D., 1995. Etude géométrique et expérimentale d'un bassin  
1440 transporté : exemple du synclinorium de l'Alto Beni (Andes centrales). *Bull. Soc. géol. Fr.*,  
1441 t. 166, no 6, pp. 797-811.
- 1442 Bache, F., Olivet, J. L., Gorini, C., Aslanian, D., Labails, C., Rabineau, M., 2010. Evolution  
1443 of rifted continental margins: the case of the Gulf of Lions (Western Mediterranean Basin).  
1444 *Earth and Planetary Science Letters*, 292(3-4), 345-356.
- 1445 Bache, F., Popescu, S.-M., Rabineau, M., Gorini, C., Suc, J.-P., Clauzon, G., Olivet, J.-L.,  
1446 Rubino, J.-L., Melinte-Dobrinescu, M.C., Estrada, F., Londeix, L., Armijo, R., Meyer, B.,  
1447 Jolivet, L., Jouannic, G., Leroux, E., Aslanian, D., Dos Reis, A.T., Mocochain, L.,  
1448 Dumurdžanov, N., Zagorchev, I., Lesić, V., Tomić, D., Çağatay, M.N., Brun, J.-P.,  
1449 Sokoutis, D., Csato, I., Ucarkus, G., Çakir, Z., 2012. A two-step process for the reflooding  
1450 of the Mediterranean after the Messinian Salinity Crisis. *Basin Research*, 24, 125–153.
- 1451 Baroux, E., Béthoux, N., Bellier, O., 2001. Analyses of the stress field in southeastern France  
1452 from earthquake focal mechanisms. *Geophys. J. Int.*, 145, 336–348.
- 1453 Bathiard, M., Lambert, C., 1968. Rapports entre la tectonique de socle et la tectonique de  
1454 couverture sur la bordure ouest des Maures. *Bull. Soc. géol. Fr.*, 7, X, 428-435.
- 1455 Baubron, J.C., 1984. Volcanisme du Sud-Est de la France. In *Synthèse géologique du Sud-Est*  
1456 de la France, Mém. BRGM, n° 125, p. 514-517.
- 1457 Baudemont, D., 1985. Relations socle-couverture en Provence orientale. Evolution  
1458 tectonosédimentaire permienne du bassin du Luc (Var). Université Louis Pasteur,  
1459 Strasbourg, PhD thesis.
- 1460 Baudrimont, F., Dubois, P., 1977. Un bassin mésogénien du domaine péri-alpin : le sud-est de  
1461 la France. *Bull. Centres Rech. Explor. Elf-Aquitaine*, 1, 261–308.
- 1462 Beauchamp, W., Allmendinger, R.W., Barazangi, M., Demnati, A., El Alji, M., Dahmani, M.,  
1463 1999. Inversion tectonics and the evolution of the High Atlas Mountains, Morocco, based  
1464 on a geological-geophysical transect. *Tectonics* 18, 2, 163-184.
- 1465 Beaudouin, B., Cavelier, C., Haccard, D., Lanteaume, M., Perrin, M., 1966. A propos de l'âge  
1466 des molasses de Tanaron (Basses-Alpes) ; la redécouverte du gisement de Cérithe et ses  
1467 conséquences structurales. *Bull. Soc. géol. Fr.*, 7, VIII, 458-460.
- 1468 Beaudouin, B., Gigot, P., Haccard, D., 1970. Flysch et molasse, approche sédimentologique.  
1469 *Bull. Soc. géol. Fr.*, 7, XII, No. 4, 664-672.
- 1470 Bellahsen, N., Sebrier, M., Siame, L., 2016. Crustal shortening at the Sierra Pie de Palo  
1471 (Sierras Pampeanas, Argentina): near-surface basement folding and thrusting. *Geol. Mag.*,  
1472 153, (5/6), 992-1012, doi:10.1017/S0016756816000467.
- 1473 Bellahsen, N., Jolivet, L., Lacombe, O., Bellanger, M., Boutoux, A., Garcia, S., Mouthereau,  
1474 F., Pourhiet, L.L., Gumiaux, C., 2012. Mechanisms of margin inversion in the external  
1475 Western Alps: Implications for crustal rheology. *Tectonophysics* 560, 62-83.  
1476 <https://doi.org/10.1016/j.tecto.2012.06.022>.
- 1477 Bergerat, F., 1987. Stress fields in the European platform at the time of Africa-Eurasia  
1478 collision. *Tectonics* 6, 99-132, doi:10.1029/TC006i002p00099.

- 1479 Bertrand, M., 1887. Ilot triasique du Beausset (Var). Analogie avec le bassin houiller franco-  
1480 belge et avec les Alpes de Glaris. Bull. Soc. géol. Fr., 3, XV, 667-702.
- 1481 Bertrand, M., 1888. Nouvelles études sur la chaîne de la Sainte-Baume. Allure sinueuse des  
1482 plis de la Provence. Bull. Soc. géol. Fr., 3, XVI, 748-778.
- 1483 Besson, D., 2005. Architecture du bassin rhodano-provençal miocène (Alpes, SE France).  
1484 Relations entre déformation, physiographie et sédimentation dans un bassin molassique  
1485 d'avant-pays. Mines ParisTech, Paris, France, PhD thesis.
- 1486 Bestani, L., 2015. Géométrie et cinématique de l'avant-pays provençal : modélisation par  
1487 coupes équilibrées dans une zone à tectonique polyphasée. Aix-Marseille Université, PhD  
1488 thesis, [https://agse-geologues.fr/documents/docs\\_sciences/theses/2014\\_L.Bestani-CoupesEqu.Prov.18-12-2014.pdf](https://agse-geologues.fr/documents/docs_sciences/theses/2014_L.Bestani-CoupesEqu.Prov.18-12-2014.pdf).
- 1489
- 1490 Bestani, L., Espurt, N., Lamarche, J., Floquet, M., Philip, J., Bellier, O., Hollender, F., 2015.  
1491 Structural style and evolution of the Pyrenean-Provence thrust belt, SE France. Bull. Soc.  
1492 géol. Fr., 2015, 186, 3-19, doi:10.2113/gssgbull.186.4-5.223.
- 1493 Bestani, L., Espurt, N., Lamarche, J., Bellier, O., Hollender, F., 2016. Reconstruction of the  
1494 Provence Chain evolution, southeastern France. Tectonics, 35,  
1495 doi:10.1002/2016TC004115.
- 1496 Béthoux, N., Tric, E., Chery, J., Beslier, M.-O., 2008. Why is the Ligurian Basin  
1497 (Mediterranean Sea) seismogenic? Thermomechanical modeling of a reactivated passive  
1498 margin. Tectonics, vol. 27, TC5011, doi:10.1029/2007TC002232.
- 1499 Biberon, B., 1988. Mécanismes et évolution des chevauchements à vergences opposées.  
1500 Exemple des structures de la Sainte-Victoire (Provence). Université Joseph Fourier,  
1501 Grenoble, France, PhD thesis.
- 1502 Blanc, J.-J., Caron, J.-P., Choquet, C., Gouvernet, C., Guieu, G., Mennessier, G., Nahon, D.,  
1503 Philip, J., Rouire, J., Tempier, C., 1974. Carte géol. France (1/50000), feuille CUERS  
1504 (1045). Orléans: Bureau de recherches géologiques et minières.
- 1505 Blanc, J.-J., Gouvernet, C., Philip, J., Tempier, C., Froget, C., Muschotti, E., 1977. Carte géol.  
1506 France (1/50000), feuille LA CIOTAT (1063). Orléans: Bureau de recherche géologiques  
1507 et minières.
- 1508 Blanc, J.-J., Weydert, P., Masse, J.-P., Roux, M., de Peyronnet, P., 1973. Carte géol. France  
1509 (1/50000), feuille SAULT-DE-VAUCLUSE (942). Orléans: Bureau de recherches  
1510 géologiques et minières.
- 1511 Bonnet, C., Malavieille, J., Mosar, J., 2008. Surface processes versus kinematics of thrust  
1512 belts: impact on rates of erosion, sedimentation, and exhumation – Insights. In: analogue  
1513 models. Bull. Soc. géol. Fr., 179(3), 297-314, doi:10.2113/gssgbull.179.3.297.
- 1514 Bordet, P., Chamley, H., Blanc, J.-J., Jeudy de Grissac, A., 1976. Carte géol. France  
1515 (1/50000), feuille HYERES-PORQUEROLLES (1065). Orléans: Bureau de recherches  
1516 géologiques et minières.
- 1517 Boyer, S.E., Elliott, E., 1982. Thrust Systems. The American Association of Petroleum  
1518 Geologists Bulletin, 66, No. 9, 1196-1230.
- 1519 Branquet, Y., Cheillett, A., Cobbold, P.R., Baby, P., Laumonier, B., Giuliani, G., 2002.  
1520 Andean deformation and rift inversion, eastern edge of Cordillera Oriental (Guateque-  
1521 Medina area), Colombia. J. South Am. Earth Sci., 15, 391–407, doi:10.1016/S0895-  
1522 9811(02)00063-9.

- 1523 Bréhéret, J.-G., 1995. L'Aptien et l'Albien de la fosse Vocontienne (des bordures au bassin) :  
 1524 évolution de la sédimentation et enseignements sur les évènements anoxiques. PhD thesis.  
 1525 Université François Rabelais-Tours, tel-00805488.
- 1526 Brocard, C., Philip, J., 1989. Précisions stratigraphiques sur le Trias de la Provence orientale :  
 1527 conséquences structurales et paléogéographiques. Géologie de la France, 3, 27-32.
- 1528 Burbank, D.W., Vergés, J., 1994. Reconstruction of topography and related depositional  
 1529 systems during active thrusting. Journal of Geophysical Research, 99, No. B10, 20,281-  
 1530 20,297.
- 1531 Burrel, L., Teixell, A., 2021. Contractional salt tectonics and role of pre-existing diapiric  
 1532 structures in the Southern Pyrenean foreland fold-thrust belt (Montsec and Serres  
 1533 Marginals). Journal of the Geological Society, 178, doi:10.1144/jgs2020-085.
- 1534 Butler, R.W.H., 2013. Area balancing as a test of models for the deep structure of mountain  
 1535 belts, with specific reference to the Alps. J. Struct. Geol., 52, 2-16.
- 1536 Butler, R.W.H., 2017. Basement-cover tectonics, structural inheritance, and deformation  
 1537 migration in the outer parts of orogenic belts: A view from the western Alps. In Law, R.D.,  
 1538 Thigpen, J.R., Merschat, A.J., and Stowell, H.H. (Eds.), Linkages and Feedbacks in  
 1539 Orogenic Systems: Geological Society of America Memoir 213, p. 55-74,  
 1540 doi:10.1130/2017.1213(03).
- 1541 Butler, R.W.H., 2020. Syn-kinematic strata influence the structural evolution of emergent  
 1542 fold-thrust belts. In : Hammerstein, J.A., Di cuia, R., Cottam, M.A., Zamora, G., Butler,  
 1543 R.W. H. (Eds), Fold and Thrust Belts: Structural Style, Evolution and Exploration.  
 1544 Geological Society, London, Special Publications, 490, 57-78.
- 1545 Butler, R.W.H., Bond, C.E., Cooper, M.A., Watkins, H., 2020. Fold-thrust structures – where  
 1546 have all the buckles gone? in: Bond, Lebit, H.D. (Eds), Folding and Fracturing of Rocks:  
 1547 50 Years of Research since the Seminal Text Book of J. G. Ramsay. Geological Society,  
 1548 London, Special Publications, 487, 21-44, doi:10.1144/SP487.7.
- 1549 Calderon, Y., Baby, P., Hurtado, C., Brusset, S., 2017. Thrust tectonics in the Andean retro-  
 1550 foreland basin of northern Peru: Permian inheritances and petroleum implications. Marine  
 1551 and Petroleum Geology, 82, 238-250, doi:10.1016/j.marpetgeo.2017.02.009.
- 1552 Callot, J.-P., Jahani, S., Letouzey, J., 2007. The role of pre-existing diapirs in fold and thrust  
 1553 belt development. In Lacombe, O., Lavé, J., Roure, F., Vergés J. (Eds.), Thrust belts and  
 1554 foreland basins. Berlin Heidelberg: Springer-Verlag, 309-325.
- 1555 Callot, J.-P., Trocmé, V., Letouzey, J., Albouy, E., Jahani, S., Sherkati, S., 2012. Pre-existing  
 1556 salt structures and the folding of the Zagros Mountains. Geological Society, London,  
 1557 Special Publications, 363(1), 545–561. <https://doi.org/10.1144/SP363.27>.
- 1558 Campredon, R., Giannerini, G., 1982. Le synclinal de Saint-Antonin (arc de Castellane,  
 1559 chaînes subalpines méridionales) Un exemple de bassin soumis à une déformation  
 1560 compressive permanente depuis l'Eocène supérieur. Géologie Alpine, t. 58, 15-20.
- 1561 Cassinis, G., Durand, M., Ronchi, A., 2003. Permian-Triassic continental sequences of  
 1562 northwest Sardinia and south Provence: stratigraphic correlations and palaeogeographical  
 1563 implications. Bolletino della Società Geologica Italiana, Volume speciale, 2, 119-129.
- 1564 Catzigras, F., Colomb, E., Durand, J.-P., Guieu, G., Rousset, C., Tempier, C., 1969. Carte  
 1565 géol. France (1/50000), feuille AIX-EN-PROVENCE (1021). Orléans: Bureau de  
 1566 recherches géologiques et minières.

- 1567 Caron, J.P., 1970. Episodes volcaniques et volcano-détritiques dans le Trias moyen de la  
 1568 partie méridionale de l'arc de Barjols (Var). In: Comptes rendus de l'Académie des  
 1569 Sciences, Paris. vol. 270. pp. 1223-1226 D.
- 1570 Caron, J.-P., 1979. Trias au sud de l'Argens (Var). In: Rouire et al., Notice géologique de la  
 1571 feuille Brignoles à 1/50.000, 6-7.
- 1572 Célini, N., 2020. Le rôle des évaporites dans l'évolution tectonique du front alpin : cas de la  
 1573 Nappe de Digne. Université de Pau et des Pays de l'Adour, Pau, France, PhD thesis.
- 1574 Célini, N., Callot, J.-P., Ringenbach, J.-C., Graham, R., 2020. Jurassic Salt Tectonics in the  
 1575 SW Sub-Alpine Fold-and-Thrust Belt. *Tectonics*, 39, e2020TC006107,  
 1576 doi:10.1029/2020TC006107.
- 1577 Célini, N., Callot, J.-P., Ringenbach, J.-C., Graham, R., 2021. Anatomy and evolution of the  
 1578 Astoin diapiric complex, sub-Alpine fold-and-thrust belt (France). *BSGF - Earth Sciences*  
 1579 Bulletin, Vol: 200052, doi:10.1051/bsgf/2021018.
- 1580 Champion, C., Choukroune, P., Clauzon, G., 2000. La déformation post-Miocène en Provence  
 1581 occidentale. *Geodinamica Acta*, 13, 67-85.
- 1582 Chardon, D., Hermitte, D., Nguyen, F., Bellier, O., 2005. First paleoseismological constraints  
 1583 on the strongest earthquake in France (Provence) in the twentieth century. *Geology*, v. 33,  
 1584 no. 11, 901-904, doi:10.1130/G21713.1.
- 1585 Clauzon, G., 1978. The Messinian Var canyon (Provence, southern France): Paleogeographic  
 1586 implication. In: Cita, M.B., Ryan, B.F. (Eds), *Messinian erosional surfaces in the*  
 1587 *Mediterranean marine geology*. Mar. Geol., 27, (3/4), 203-222.
- 1588 Clauzon, G., 1979. Le canyon messinien de la Durance (Provence, France): une preuve  
 1589 paléogéographique de bassin profond de dessiccation. *Palaeogeography,*  
 1590 *Palaeoclimatology, Palaeoecology*, 29, 15-40.
- 1591 Clauzon, G., 1996. Limites de séquence et évolution géodynamique. *Géomorphologie* : relief,  
 1592 processus, environnement, 1, 3-22.
- 1593 Clauzon, G., 1982. Le canyon messinien du Rhône: une preuve décisive du « dessicated deep-  
 1594 basin model » [Hsü, Cita et Ryan, 1973]. *Bull. Soc. géol. Fr.*, 7, XXIV, 597-610.
- 1595 Clauzon, G., Aguilar, J.-P., Michaux, J., 1989. Relation temps-sédimentation dans le Néogène  
 1596 méditerranéen français. *Bull. Soc. géol. France*, 8, V, No. 2, 361-372.
- 1597 Coadou, A., Beaudoin, B., Mouterde, R., 1971. Variations lithologiques et corrélations  
 1598 stratigraphiques dans le Lias moyen et supérieur de Barles et du Plateau de Chine (Alpes  
 1599 de Haute-Provence). *Bull. Soc. géol. Fr.*, 7, 5-12.
- 1600 Clauzon, G., Fleury, T. J., Bellier, O., Molliex, S., Mocochain, L., Aguilar, J. P., 2011.  
 1601 Morphostructural evolution of the Luberon since the Miocene (SE France), *Bull. Soc. géol.*  
 1602 *Fr.*, 182, 95-110, doi:10.2113/gssgbull.182.2.95.
- 1603 Cojan, I., 1989. Discontinuités majeures en milieu continental. Proposition de corrélation avec  
 1604 des événements globaux (Bassin de Provence, S. France, Passage Crétacé/Tertiaire). *C. R.*  
 1605 *Acad. Sci. Paris*, 309, II, 1013-1018.
- 1606 Cojan, I., 1993. Alternating fluvial and lacustrine sedimentation: tectonic and climatic  
 1607 controls (Provence Basin, S., France, Upper Cretaceous/Palaeocene). *Spec. Publs Int. Ass.*  
 1608 *Sediment.*, 17, 425-438.

- 1609 Cojan, I., Renard, M., Emmanuel, L., 2003. Palaeoenvironmental reconstruction of dinosaur  
1610 nesting sites based on a geochemical approach of eggshells and associated palaeosols  
1611 (Maastrichtian, Provence basin, France). – *Palaeogeogr., Palaeoclimatol., Palaeoecol.*, 191,  
1612 111-138.
- 1613 Cojan, I., Bialkowski, A., Gillot, T., Renard, M., 2013. Paleo-environnement and paleoclimate  
1614 reconstruction for the early to middle Miocene from stable isotopes in pedogenic  
1615 carbonates (Digne-Valensole basin, southeastern France). *Bull. Soc. géol. France*, 184, No.  
1616 6, 583-599.
- 1617 Collina-Girard, J., Griboulard, R., 1990. The deep-structure of the Valensole Plateau (French  
1618 Alps). Contribution of network valley and topographic analysis. *Géologie  
1619 méditerranéenne*, 17, 153–171.
- 1620 Combès, P., 1984. La tectonique récente de la Provence occidentale microtectonique,  
1621 caractéristiques dynamiques et cinématiques : méthodologie de zonation tectonique et  
1622 relations avec la séismicité. Université Louis Pasteur, Strasbourg, France, PhD thesis.
- 1623 Cornet, C., 1961. Le delta vindobonien du bas-pays de Saint-Maximin et de Ginasservis  
1624 (Var). *Bull. Soc. géol. Fr.*, 7, III, 424-431, doi:10.2113/gssgbull.S7-III.5.424.
- 1625 Cornet, C., 1965. Evolution tectonique et morphologique de la Provence depuis l'Oligocène.  
1626 *Mém. Soc. Géol. France, nouv. sér.*, XLIV, No. 103, Paris, PhD thesis.
- 1627 Corroy, G., 1957. La Montagne Sainte-Victoire. *Bulletin du Service de la Carte géologique de  
la France*, LV, 251, 1-46.
- 1629 Corroy, G., Philip, J., 1964. Le brachyanticlinal des pics des Corbeaux dans le massif de la  
1630 Sainte-Baume (Var). *Bull. Soc. géol. Fr.*, 7, VI, 560-563.
- 1631 Corsini, M., Bosse, V., Féraud, G., Demoux, A., Crèvola, G., 2010. Exhumation processes  
1632 during post-collisional stage in the Variscan belt revealed by detailed  $^{40}\text{Ar}/^{39}\text{Ar}$  study  
1633 (Tanneron Massif, SE France). *Int J Earth Sci (Geol Rundsch)* (2010) 99:327–341,  
1634 doi:10.1007/s00531-008-0397-x
- 1635 Couëffé, R., Tessier, B., Gigot, P., Beaudouin, B., 2004. Tidal rhythmites as possible  
1636 indicators of very rapid subsidence in a foreland basin: an example from the Miocene  
1637 marine molasse formation of the Digne foreland basin, SE France. *Journal of sedimentary  
1638 research*, 74, No. 6, 746–759, doi:10.1306/040904740746.
- 1639 Coulon, C., 1967. Le volcanisme tertiaire de la région toulonnaise (Var). *Bull. Soc. Géol.  
France* 7, 691-700.
- 1641 Coward, M.P., 1996. Balancing sections through inverted basins, in: Buchanan, E.G.,  
1642 Nieuwland, D.A. (Eds), *Modern Developments in Structural Interpretation, Validation and  
1643 Modelling*. Geological Society Special Publication No. 99, pp. 51-77.
- 1644 Crèvola, G., Pupin, J.-P., 1994. Crystalline Provence: structure and Variscan evolution, in:  
1645 Keppie J.D. (ed.), *Pre-Mesozoic Geology in France and Related Areas*, Springer Verlag,  
1646 Berlin, 426-441. *C. R. Geoscience*, 341, 214-223.
- 1647 Crumeyrolle, P., Rubino, J.-L., Clauzon, G., 1991. Miocene depositional sequences within a  
1648 tectonically controlled transgressive-regressive cycle. *Spec. Publs. Int. Ass. Sediment.*, 12,  
1649 373-390.
- 1650 Cushing, E.M., Bellier, O., Nechtschein, S., Sébrier, M., Lomax., Volant, P., Dervin, P.,  
1651 Guignard, P., Bove, L., 2008. A multidisciplinary study of a slow-slipping fault for seismic

- 1652 hazard assessment: the example of the Middle Durance Fault (SE France). Geophys. J. Int.,  
1653 doi:10.1111/j.1365-246X.2007.03683.x.
- 1654 Dahlstrom, C.D.A., 1969. Balanced cross-sections. Can. J. Earth Sci., 6(4), 743-757.
- 1655 Dardeau, G., 1988. Tethyan evolution and Alpine reactivation of Jurassic extensional  
1656 structures in the French “Alpes maritimes”. Bull. Soc. géol. Fr., 4, 651-657.
- 1657 Dardeau, G., de Graciansky, P.-C., 1990. Halocinèse et rifting téthysien dans les Alpes-  
1658 Maritimes (France). Bulletin des Centres de Recherches Exploration-Production Elf-  
1659 Aquitaine, 14(2), 443-464.
- 1660 Dardeau, G., Dubar, M., Toutin-Morin, N., Courme, M.-D., Crévola, G., Mangan, Ch., 2010.  
1661 Notice explicative, Carte géol. France (1/50 000), feuille Grasse-Cannes (999). Orléans,  
1662 BRGM, 194 p. Carte géologique par Dardeau G., Dubar M., Toutin-Morin N., Courme M.-  
1663 D., Crévola G., Mangan Ch.
- 1664 Debemas J., 1974. Les chaines plissées du cycle alpin et leur avant-pays. Géologie de la  
1665 France, volume II, doin éditeurs, Paris. 2, 293 p.
- 1666 Debemas J., Arnaud, H., Caron, C., Gidon, M., Kerckhove, Cl., Lemoine, M., Vialon, P.,  
1667 1970. Guides géologiques régionaux: Alpes (Savoie et Dauphiné). France, Masson (Ed),  
1668 214 p.
- 1669 Debemas J., Arnaud, H., Gidon, M., Kerckhove, Cl., Giraud, P., Lemoine, M., Menot, J.P.,  
1670 Monjuvent, G., Vialon, P., 1983. Guides géologiques régionaux: Alpes du Dauphiné.  
1671 France, Masson (Ed), 198 p.
- 1672 DeCelles, P.G., Giles, P.C., 2001. Rates of shortening, propagation, underthrusting, and  
1673 flexural wave migration in continental orogenic systems. Geology. 29, 135-138.
- 1674 Delfaud, J., Toutin-Morin, N., Morin, R., 1989. Un cône alluvial en bordure d'un bassin  
1675 intramontagneux : La formation permienne du Rocher de Roquebrune (Bassin du Bas-  
1676 Argens, Provence orientale). C. R. Acad. Sci. Paris, II, 309, 1811-1817.
- 1677 Dorkel, A., Grégoire, J.-Y., Belleville, J.-M., Pachoud, A., Savornin, J., Destombes, J.-P.,  
1678 Roch, E., de Peyronnet, P., Demarcq, G., 1966. Carte géol. France (1/50000), feuille  
1679 REILLANE (968). Orléans: Bureau de recherches géologiques et minières.
- 1680 Dubar, M., 1983. Reconnaissance de la discontinuité de ravinement messinienne dans le  
1681 bassin de Riez-Valensole ; implications stratigraphiques. C. R. Acad. Sci. Paris, II, 885-  
1682 887.
- 1683 Dubar, M., 1984. Chronologie et signification des dépôts continentaux de Néogène supérieur  
1684 du bassin de Riez-Valensole (Alpes-de-Haute-Provence, France). Bull. Soc. géol. Fr., 7,  
1685 XXVI, No. 5, 971-978.
- 1686 Dubois, P., Curnelle, R., 1978. Résultats apportés par le forage Les Mées no 1 sur le plateau  
1687 de Valensole (Alpes de Haute-Provence). C. R. somm. Soc. géol. Fr., 4, 181-184.
- 1688 Dupire, S., 1985. Étude cartographique au 1/25 000 de la zone sud du bassin de Marseille. Les  
1689 Travertins de Marseille : aperçu géomorphologique et néotectonique. Université de  
1690 Provence, PhD thesis.
- 1691 Durand, J.-P., 1962. Sur le poudingue de la Galante (région d'Aix-en-Provence). C.R. Soc.  
1692 géol. Fr., 4, 109-111.
- 1693 Durand, J.-P., 1980. Les sédiments fuvéliens du synclinal de l'Arc (Provence). Industrie  
1694 Minérale, « Le gisement de charbon du bassin de l'Arc », 62, 13-25.

- 1695 Durand, J.-P., Mennessier, G., 1964. Sur l'existence d'une discordance entre le Bégudo-  
 1696 Rognacien et le Fuvélien à l'extrémité orientale du synclinal de l'Arc en Basse-Provence  
 1697 occidentale. *C. R. Somm. Soc. géol. Fr.*, 253-254.
- 1698 Durand, J.-P., Tempier, C., 1962. Etude tectonique de la zone des brèches du massif de  
 1699 Sainte-Victoire dans la région du Tholonet (Bouches-du-Rhône). *Bull. Soc. géol. Fr.*, 7, IV,  
 1700 97-101.
- 1701 Durand, M., 1993. Un exemple de sédimentation continentale permienne dominée par  
 1702 l'activité de chenaux méandriformes : la Formation de Saint-Mandrier (Bassin de Toulon,  
 1703 Var). *Géologie de la France* (2), 43-55.
- 1704 Echavarria, L., Hernandez, R., Allmendinger, R., Reynolds, J., 2003. Subandean thrust and  
 1705 fold belt of northwestern Argentina: Geometry and timing of the Andean evolution. *AAPG*  
 1706 *Bulletin*, 87, No. 6, 965-985.
- 1707 Ege, H., Sobel, E.R., Scheuber, E., Jacobshagen, V., 2007. Exhumation history of the  
 1708 southern Altiplano plateau (southern Bolivia) constrained by apatite fission track  
 1709 thermochronology. *Tectonics*, 26, TC1004, doi:10.1029/2005TC001869.
- 1710 Elliott, D., 1983. The construction of balanced cross-sections. *J. Struct. Geol.*, 5, No. 2, 101.
- 1711 Elliott, D., Johnson, M.R.W., 1980. The structural evolution of the northern part of the Moine  
 1712 thrust zone. *Royal Soc. Edinburgh Trans. Earth Sci.*, 71, 69-96.
- 1713 Erdős, Z., Huismans, R.S., van der Beek, P., 2015. First-order control of syntectonic  
 1714 sedimentation on crustal-scale structure of mountain belts. *J. Geophys. Res. Solid Earth*,  
 1715 120, 5362–5377, doi:10.1002/2014JB011785.
- 1716 Espurt, N., Brusset, S., Baby, P., Hermoza, W., Bolaños, R., Uyen, D., Déramond, J., 2008.  
 1717 Paleozoic structural controls on shortening transfer in the Subandean foreland thrust  
 1718 system, Ene and southern Ucayali basins, Peru. *Tectonics*, vol. 27, TC3009,  
 1719 doi:10.1029/2007TC002238.
- 1720 Espurt, N., Barbarand, J., Roddaz, M., Brusset, S., Baby, P., Saillard, M., Hermoza, W., 2011.  
 1721 A scenario for late Neogene Andean shortening transfer in the Camisea Subandean zone  
 1722 (Peru, 12° S): Implications for growth of the northern Andean Plateau. *Geological Society*  
 1723 of America Bulletin, 123, pp. 2050-2068, doi:10.1130/B30165.1.
- 1724 Espurt, N., Hippolyte, J.-C., Saillard, M., Bellier, O., 2012. Geometry and kinematic  
 1725 evolution of a long-living foreland structure inferred from field data and cross section  
 1726 balancing, the Sainte-Victoire System, Provence, France. *Tectonics*, vol. 31, TC4021,  
 1727 doi:10.1029/2011TC002988.
- 1728 Espurt, N., Angrand, P., Teixell, A., Labaume, P., Ford, M., de Saint Blanquat, M., Chevrot,  
 1729 S., 2019a. Crustal-scale balanced cross-section and restorations of the Central Pyrenean  
 1730 belt (Nestes-Cinca transect): Highlighting the structural control of Variscan belt and  
 1731 Permian-Mesozoic rift systems on mountain building. *Tectonophysics*, 764, 25-45,  
 1732 doi:10.1016/j.tecto.2019.04.026.
- 1733 Espurt, N., Wattelier, F., Philip, J., Hippolyte, J.-C., Bellier, O., Bestani, L., 2019b. Mesozoic  
 1734 halokinesis and basement inheritance in the eastern Provence fold-thrust belt, SE France.  
 1735 *Tectonophysics*, 766, pp. 60-80, doi:10.1016/j.tecto.2019.04.027.
- 1736 Fabre, J., Guieu, G., Philip, J., Tronchetti, G., 1975. Mise en évidence d'une écaille crétacée  
 1737 superposée au Trias de l'Huveaune, près de Roquevaire (Bouches-du-Rhône).  
 1738 Conséquences structurales. *C. R. Acad. Sci., Paris, (D)*, 281, 11-114.

- 1739 Fabre, P., Lami, A., Pairis, J.L., Gidon, M., 1985. Déformations synsédimentaires paléogènes,  
1740 du Pelvoux au Dévoluy (Alpes externes). *Terra cognita*, vol.5, no 2-3, 243.
- 1741 Fabre-Taxy, S., Philip, J., 1964. La zone du Plan d'Aups dans sa région type, la Sainte-Baume  
1742 (Var). *Bull. Soc. géol. Fr.*, 7, VI, 554-559.
- 1743 Faucher, T., Gidon, M., Pairis, J.L., Mascle, G., 1988. Directions de transport au front de la  
1744 nappe de Digne (chaînes subalpines méridionales). *C. R. Acad. Sci. Paris*, 306, II, 227-230.
- 1745 Fillon, C., Huismans, R.S., van der Beek, P., 2013. Syntectonic sedimentation effects on the  
1746 growth of fold-and-thrust belts. *Geology*, 41, 83–86, doi:10.1130/G33531.1.
- 1747 Flandrin, J., Gottis, M., Viallix, J., Golenko, N., Riche, P., Parant, J., Rebelli, G., Bejanin, J.,  
1748 Issenmann, O., Teisserenc, P., Mollier, M., Cochet, E., 1964. Carte géol. France (1/50000),  
1749 feuille SEDERON (916). Orléans: Bureau de recherches géologiques et minières.
- 1750 Floquet, M., Gari, J., Hennuy, J., Léonide, P., Philip, J., 2005. Sédimentations gravitaires  
1751 carbonatées et silicoclastiques dans un bassin en transtension, séries d'âge cénomanien à  
1752 coniacien moyen du Bassin sud-provençal. Livret guide d'excursion géologique, 10e  
1753 Congrès français de Sédimentologie, 14-15 octobre 2005, Publication ASF, Paris, 52.
- 1754 Floquet, M., Philip, J., Léonide, P., Gari, J., 2006. Sédimentation et géodynamique du Bassin  
1755 Sud-Provençal au Crétacé supérieur. Livret-guide d'excursion géologique, Université de  
1756 Provence, Centre Saint-Charles, Marseille, Ouvrage en dépôt à la SGF Paris.
- 1757 Floquet, M., Leleu, S., Tortosa, T., 2021. Du bassin marin au bassins continentaux sud-  
1758 provençaux durant la Crétacé supérieur et au Paléogène, de -100 à -43 Ma. In: *La Géologie*  
1759 des Bouches-du-Rhône - Roches et paysages remarquables – éditions du BRGM. 447p.,  
1760 chap. 2.5., 69-116.
- 1761 Ford, M., Lickorish, W.H., Kusznir, N.J., 1999. Tertiary foreland sedimentation in the  
1762 Southern Subalpine Chains, SE France: a geodynamic appraisal. *Basin Research*, 11, 315-  
1763 336. doi:10.1046/j.1365-2117.1999.00103.x.
- 1764 Ford, M., Duchêne, S., Gasquet, D., Vanderhaeghe, O., 2006. Two-phase orogenic  
1765 convergence in the external and internal SW Alps. *Journal of the Geological Society*,  
1766 London, 163, 815-826.
- 1767 Fournier, M., Agard, P., Petit, C., 2008. Micro-tectonic constraints on the evolution of the  
1768 Barles half-window (Digne nappe, southern Alps). Implications for the timing of folding in  
1769 the Valensole foreland basin. *Bull. Soc. géol. Fr.*, 179, No. 6, 551-568.
- 1770 Friès, G., 1987. Dynamique du bassin subalpin méridional de l'Aptien au Cénomanien.  
1771 Université Paris VI, Paris, France, 1986, Mém. Sci. Terre ENS Mines Paris 4, PhD thesis.
- 1772 Garcia, G., Vianey-Liaud, M., 2001. Nouvelles données sur les coquilles d'oeufs de  
1773 dinosaures Megaloolithidae du Sud de la France : systématique et variabilité  
1774 intraspécifique. *C. R. Acad. Sci. Paris, Sciences de la Terre et des planètes / Earth and*  
1775 *Planetary Sciences*, 332, 185-191, doi:10.1016/S1251-8050(00)91401-0.
- 1776 Gattacceca, J., Deino, A., Rizzo, R., Jones, D. S., Henry, B., Beaudoin, B., Vadeboin, F.,  
1777 2007. Miocene rotation of Sardinia: New paleomagnetic and geochronological constraints  
1778 and geodynamic implications. *Earth Planet. Sci. Lett.*, 258, 359–377,  
1779 doi:10.1016/j.epsl.2007.02.003.
- 1780 Gaviglio, P., 1985. A fault and stress field analysis in a coal mine (Gardanne, Bouches du  
1781 Rhône, France. *Tectonophysics*, 113, 349-366.

- 1782 Giannerini, G., Gigot, P., Campredon, R., 1977. Le Tertiaire de La Roque-Esclapon (front sud  
 1783 de l'arc de Castellane) : la superposition de deux déformations synsédimentaires oligocène  
 1784 et miocène et des bassins sédimentaires associés. Bull. BRGM, Fr., (2), Section 1, n°3,  
 1785 179-188.
- 1786 Giannerini, G., 1978. Contribution à l'étude géologique de la bordure méridionale de l'arc de  
 1787 Castellane entre Mons et Bargème (Var) : relations entre les déformations tectoniques et la  
 1788 sédimentation au cours du Tertiaire. PhD thesis. Université Nice Sophia Antipolis.
- 1789 Gidon, M., 1982. La reprise de failles anciennes par une tectonique compressive : sa mise en  
 1790 évidence et son rôle dans les chaînes subalpines des Alpes occidentales. Géologie Alpine,  
 1791 58, 53-68.
- 1792 Gidon, M., 1989. La rupture des charnières anticliniales par cisaillement dans les flancs longs  
 1793 des plis : un mode méconnu de formation des chevauchements, observable dans les chaînes  
 1794 subalpines des Alpes occidentales françaises. Géologie alpine, t.65, 65-74.
- 1795 Gidon, M., 1997. Les chaînons subalpins au nord-est de Sisteron et l'histoire tectonique de la  
 1796 nappe de Digne. Géologie Alpine, 73, 23-57.
- 1797 Gidon, M., Arnaud, H., Pairis, J.L., Aprahamian, J., Uselle, J.P., 1970. Les déformations  
 1798 tectoniques superposées du Dévoluy méridional (Hautes-Alpes). Géologie Alpine, t. 46,  
 1799 87-110.
- 1800 Gidon, M., Pairis, J.L., 1976. Le rôle de mouvements tectoniques éocènes dans la genèse des  
 1801 structures de l'extrême NE du Dévoluy et dans celle du chevauchement de Digne.  
 1802 Géologie alpine, t. 52, 73-83.
- 1803 Gidon, M., Pairis, J.L., 1986. La nappe de Digne (Chaînes subalpines méridionales): origine,  
 1804 déplacement et signification régionale. C.R. Acad. Sc. Paris, t.303, Série II, n°10, 981-984
- 1805 Gidon, M., Pairis, J.L., 1988. La structure des environs de Digne (Chaînes subalpines  
 1806 méridionales, Alpes-de-Haute-Provence) : un exemple d'interférence entre l'avancée d'une  
 1807 nappe de charriage épiglyptique et la sédimentation sur son front. C.R. Acad. Sci. Paris,  
 1808 307, II, 1283-1288.
- 1809 Gidon, M., Pairis, J.L., 1992. Relations entre le charriage de la Nappe de Digne et la structure  
 1810 de son autochtone dans la vallée du Bès (Alpes de Haute-Provence, France). Eclogae geol.  
 1811 Helv., Vol.85/2, 327-359.
- 1812 Gidon, M., Pairis, J.L., Arnaud, H., Aprahamian, J., Uselle, J.P., 1970. Les déformations  
 1813 tectoniques superposées du Dévoluy méridional (Hautes-Alpes). Travaux du Laboratoire  
 1814 de Géologie de l'Université de Grenoble, t.46 (1970), 87-110.
- 1815 Gigot, P., Cotillon, P., Haccard, D., Montjuvent, G., Dardeau, G., 2013. Carte géol. France  
 1816 (1/50000), feuille SISTERON (917). Orléans: Bureau de recherches géologiques et  
 1817 minières.
- 1818 Gigot, P., Grandjacquet, C., Haccard, D., 1974. Evolution tectono-sédimentaire de la bordure  
 1819 septentrionale du bassin tertiaire de Digne depuis l'Eocène. Bull. Soc. géol. Fr., 7, XVI,  
 1820 no. 2, 128-139.
- 1821 Gigot, P., Mein, P., Truc, G., 1976. La série continentale du pont d'Aiguines près de  
 1822 Moustiers-Sainte-Marie : un équivalent latéral du Miocène marin du bassin de Digne  
 1823 (Alpes-de-Haute-Provence). Géobios, 9, 795-799.

- 1824 Gigot, P., Thomel, G., Colomb, E., Dubar, M., Durozoy, G., Damiani, L., 1981a. Notice  
 1825 explicative, Carte géol. France (1/50000), feuille FORCALQUIER (943). Orléans : Bureau  
 1826 de recherches géologiques et minières.
- 1827 Gigot, P., Thomel, G., Colomb, E., Dubar, M., Durozoy, G., Damiani, L., 1981b. Carte géol.  
 1828 France (1/50000), feuille FORCALQUIER (943). Orléans : Bureau de recherches  
 1829 géologiques et minières.
- 1830 Godard, V., Hippolyte, J.-C., Cushing, E., Espurt, N., Fleury, J., Bellier, O., Ollivier, V., the  
 1831 ASTER team, 2020. Hillslope denudation and morphologic response across a rock uplift  
 1832 gradient. *Earth Surf. Dynam.*, 8, 221-243, doi:10.5194/esurf-8-221-2020.
- 1833 Goguel, J., Vuillermoz, M., Lanteaume, M., Lemoine, M., 1964. Carte géol. France  
 1834 (1/50000), feuille DIGNE (944). Orléans: Bureau de recherches géologiques et minières.
- 1835 Goguel, J., 1963. L'interprétation de l'arc des Alpes occidentales. *Bulletin de la Société*  
 1836 *Géologique de France*, 7, V.
- 1837 Goguel, J., 1944. La tectonique de fond dans la zone externe des Alpes. *Bulletin de la Société*  
 1838 *Géologique de France*, 5, 14, 201-218, doi:10.2113/gssgbull.S5-XIV.4-6.201.
- 1839 Goguel, J., 1939. Tectonique des chaînes subalpines entre la Bléone et la Durance-Alpes.  
 1840 Bulletin des services de la carte géologique de France, 202(XLI), 1-48.
- 1841 Goguel, J., 1937. Description tectonique de la bordure des Alpes de la Bléone au Var.  
 1842 Université de Paris, PhD thesis.
- 1843 Gouvenet, C., Blanc, J.-J., Philip, J., Caron, J.-P., Coulon, C., Gueirard, S., 1969. Carte géol.  
 1844 France (1/50000), feuille TOULON (1064). Orléans: Bureau de recherches géologiques et  
 1845 minières.
- 1846 Gouvenet, C., 1963. Structure de la région toulonnaise. *Mémoire de la Carte géologique*  
 1847 détaillée de la France, 244 p.
- 1848 Graciansky, P.-C. de, Dardeau, G., Lemoine, M., Tricart, P., 1989. The inverted margin of the  
 1849 French Alps and foreland basin inversion. *Geol. Soc. London, Spec. Publ.*, 44, 87–104,  
 1850 doi:10.1144/GSL.SP.1989.044.01.06.
- 1851 Graciansky, P.-C. de, Lemoine, M., 1988. Early Cretaceous extensional tectonics in the  
 1852 southwestern French Alps : A consequence of North-Atlantic rifting during Tethyan  
 1853 spreading. *Bull. Soc. géol. Fr.*, 8, IV, No. 5, 733-737, doi:10.2113/gssgbull.IV.5.733.
- 1854 Granado, P., Roca, E., Strauss, P., Pelz, K., Muñoz, J.A., 2018. Structural styles in fold-and-  
 1855 thrust belts involving early salt structures: The Northern Calcareous Alps (Austria).  
 1856 *Geology*, 47, 51-54, doi:10.1130/G45281.1.
- 1857 Guieu, G., 1968. Etude tectonique de la région de Marseille. Université d'Aix-Marseille,  
 1858 France, PhD thesis, 604 p.
- 1859 Guieu, G., Roussel, J., 1990. Arguments for the pre-rift uplift and rift propagation in the  
 1860 Ligurian-Provençal basin (Northwestern Mediterranean) in the light of Pyrenean Provençal  
 1861 orogeny. *Tectonics*, 9, No. 5, 1113-1142.
- 1862 Graham, R., Jackson, M., Pilcher, R., Kilsdonk, B., 2012. Allochthonous salt in the sub-  
 1863 Alpine fold-thrust belt of Haute Provence, France. *Geological Society, London, Special*  
 1864 *Publications* 2012, 363, 595-615, doi:10.1144/SP363.30.

- 1865 Guignard, P., Bellier, O., Chardon, O., 2005. Géométrie et cinématique post-oligocène des  
1866 failles d'Aix et de la moyenne Durance (Provence, France). C. R. Geoscience, 337, 375-  
1867 384, doi:10.1016/j.crte.2004.10.009.
- 1868 Guillemot, J., Guy M., Lobjoit, M., 1973. Un système cohérent d'alignements structuraux  
1869 commun aux Alpes et aux Pyrénées mis en évidence par le satellite ERTS 1. C. R. Acad.  
1870 Sci., Paris, 277, 481-484.
- 1871 Guillot, S., Menot, R.-P., 2009. Paleozoic evolution of the External Crystalline Massifs of the  
1872 Western Alps. C. R. Geosci., 341, 253–265.
- 1873 Guiomar, M., 1990. Le Carbonifère des chaînes subalpines de Haute-Provence (France) dans  
1874 son cadre structural. Université de Provence, Marseille, France, PhD thesis.
- 1875 Guyonnet-Benaize, C., Lamarche, J., Hollender, F., Visuer, S., Münch, P., Borgomano, J.,  
1876 2015. Three-dimensional structural modeling of an active fault zone based on complex  
1877 outcrop and subsurface data: The Middle Durance Fault Zone inherited from polyphase  
1878 Meso-Cenozoic tectonics (southeastern France). Tectonics, 34, 265–289,  
1879 doi:10.1002/2014TC003749.
- 1880 Guyonnet-Benaize, C., Lamarche, Masse, J.-P., Villeneuve, M., Viseur, S., 2010. 3D  
1881 structural modelling of small-deformations in poly-phase faults pattern. Application to the  
1882 Mid-Cretaceous Durance uplift, Provence (SE France). Journal of Geodynamics, 50, 81–  
1883 93, doi:10.1016/j.jog.2010.03.003.
- 1884 Haccard, D., Beaudoin, B., Gigot, P., Jorda, M., et al., 1989a. Carte géol. Fr. (1/50 000),  
1885 Feuille LA JAVIE (918). Orléans : Bureau de recherches géologiques et minières.
- 1886 Haccard, D., Beaudoin, B., Gigot, P., Jorda, M., 1989b. Notice explicative, Carte géol. Fr.  
1887 (1/50 000), feuille LA JAVIE (918). Orléans : Bureau de recherches géologiques et  
1888 minières.
- 1889 Haug, E., 1925. Les nappes de charriage de la Basse-Provence. Première partie. La région  
1890 toulonnaise. Mémoire du Service de la Carte géologique détaillée de la France, 304 p.
- 1891 Hennuy, J., 2003. Sédimentation carbonate et silicoclastique sous contrôle tectonique, le  
1892 bassin sud-provençal et sa plate-forme carbonatée du Turonien moyen au Coniacien  
1893 moyen. Evolutions séquentielle, diagénétique, paléogéographique. Université de Provence,  
1894 France, PhD thesis, 194 p.
- 1895 Hernandez, J.I., Hernandez, R.M., Farjat, A.D., Cristallini, E.O., Alvarez,L.A., Dellmans,  
1896 L.M., Costilla, M.R., Alvarez, A.F., Becchio, R., Bordese, S., Arzadun, G., Guibaldo,  
1897 C., Glasmacher, U.A., Tomezzoli, R.N., Stockli, D.F., Fuentes, F., Galvarro, J.S., Rosales,  
1898 A., Dzelalija, F., Haring, C., 2020. Multiple thermochronometers applied to the quantitative  
1899 analysis of compressive systems: The southern sub-Andean fold and thrust belt of Bolivia.  
1900 From source rock to trap, Journal of South American Earth Sciences,  
1901 doi:10.1016/j.jsames.2020.102949.
- 1902 Heermance, R.V., Chen, J., Burbank, D.W., Miao, J., 2008. Temporal constraints and pulsed  
1903 Late Cenozoic deformation during the structural disruption of the active Kashi foreland,  
1904 northwest China. Tectonics, 27, TC6012, doi:10.1029/2007TC002226.
- 1905 Hinsch, R., 2013. Laterally varying structure and kinematics of the Molasse fold and thrust  
1906 belt of the Central Eastern Alps: Implications for exploration. AAPG Bulletin, 97, 1805-  
1907 1831.

- 1908 Hippolyte, J.-C., Angelier, J., Bergerat, F., Nury, D., Raynaud, S., 1990. Evolution tectono-  
 1909 sédiminaire d'un bassin faille: le bassin oligocène de Marseille. C. R. Acad. Sci. Paris,  
 1910 310, 53-58.
- 1911 Hippolyte, J.-C., Nury, D., Angelier, J., Bergerat, F., 1991. Bull. Soc. Géol. Fr., 162, 1083-  
 1912 1094.
- 1913 Hippolyte, J.-C., Angelier, J., Roure, F., 1992. Les permutations de contraintes dans un  
 1914 orogène: exemple des terrains quaternaires du sud de l'Apennin. C. R. Acad. Sci. Paris,  
 1915 315, 89-95.
- 1916 Hippolyte, J.-C., Angelier, J., Nury, D., Bergerat, F., Guieu, G., 1993. Tectonic-stratigraphic  
 1917 record of paleostress time changes in the Oligocene basins of the Provence, southern  
 1918 France. Tectonophysics, 226, 15-35, doi:10.1016/0040-1951(93)90108-V.
- 1919 Hippolyte, J.-C., Dumont, T., 2000. Identification of Quaternary thrusts, folds and faults in a  
 1920 low seismicity area: examples in the Southern Alps (France). Terra Nova, 12, 156-162.
- 1921 Hippolyte, J.-C., Clauzon, G., Suc, J.-P., 2011. Messinian-Zanclean canyons in the Digne  
 1922 nappe (southwestern Alps): tectonic implications. Bull. Soc. géol. Fr., 182, No. 2, 111-132.
- 1923 Hippolyte, J.-C., Bellier, O., Espurt, N., 2012. Quaternary deformation and stress  
 1924 perturbations along the Digne thrust front, Southwestern Alps. C. R. Geoscience, 344,  
 1925 205-213, doi:10.1016/j.crte.2012.03.002.
- 1926 Hossack, J.R., 1979. The use of balanced cross-sections in the calculation of orogenic  
 1927 contraction: A review. J. geol. Soc. London, 136, 705-711.
- 1928 Jamison, W.R., 1993. Mechanical stability of the triangle zone: the backthrust wedge. Journal  
 1929 of geophysical research. 98, B11, 20,015-20,030.
- 1930 Jakni, B., 2000. Thermochronologie par traces de fission des marges conjuguées du bassin  
 1931 liguro-provençal : la Corse et le massif des Maures-Tanneron. Université Joseph Fourier,  
 1932 Grenoble I, France, PhD thesis, <https://tel.archives-ouvertes.fr/tel-00644736/document>.
- 1933 Jolivet, M., Labaume, P., Monié, P., Brunel, M., Arnaud, N., Campani, M., 2007.  
 1934 Thermochronology constraints for the propagation sequence of the south Pyrenean  
 1935 basement thrust system (France-Spain). Tectonics, 26, TC5007,  
 1936 doi:10.1029/2006TC002080.
- 1937 Jourdon, A., Rolland, Y., Petit, C., Bellahsen, N., 2014. Style of Alpine tectonic deformation  
 1938 in the Castellane fold-and-thrust belt (SW Alps, France): Insights from balanced cross-  
 1939 sections. Tectonophysics, 633, 143-155, doi:10.1016/j.tecto.2014.06.1022.
- 1940 Jourdon, A., Pourhiet, L.L., Moutherneau, F., Masini, E., 2019. Role of rift maturity on the  
 1941 architecture and shortening distribution in mountain belts. Earth and Planetary Science  
 1942 Letters 512, 89-99, doi.org/10.1016/j.epsl.2019.01.057.
- 1943 Jourdon, A., Moutherneau, F., Le Pourhiet, L., Callot, J.-P., 2020. Topographic and tectonic  
 1944 evolution of mountain belts controlled by salt thickness and rift architecture. Tectonics, 39,  
 1945 e2019TC005903, doi.org/10.1029/2019TC005903.
- 1946 Kerckhove, C., Antoine, P., 1963. Nouvelles données sur le chevauchement de Rougon - Pont  
 1947 de Soleil (zone subalpine, région de Castellane, Basses-Alpes). C. R. Acad. Sci. Paris, 257,  
 1948 716-718.
- 1949 Kerckhove, C., Roux, M., Mercier, H., 1978. Carte géol. France (1/50000), feuille  
 1950 MOUSTIER-SAINTE-MARIE (970). Orléans: Bureau de recherches géologiques et  
 1951 minières.

- 1952 Kergaravat, C., Ribes, C., Legeay, E., Callot, J.P., Kavak, K.S., Ringenbach, J.C., 2016.  
 1953 Minibasins and salt canopy in foreland fold-and-thrust belts: The central Sivas Basin,  
 1954 Turkey. *Tectonics*, 35, 1342–1366, doi:10.1002/2016TC004186.
- 1955 Kilian, W., 1892. Sur l'existence de phénomènes de recouvrement aux environs de Gréoux  
 1956 (Basses-Alpes) et sur l'âge de ces dislocations. *C. R. Acad. Sci. Paris*, 115, 1024-1026.
- 1957 Kley, J., Monaldi, C.R., 2002. Tectonic inversion in the Santa Barbara System of the central  
 1958 Andean foreland thrust belt, northwestern Argentina. *Tectonics*, vol. 21, 6, 1061,  
 1959 doi:10.1029/2002TC902003, 2002
- 1960 Labaume, P., Meresse, F., Kolivet, M., Teixell, A., Lahfid, A., 2016. Tectonothermal history  
 1961 of an exhumed thrust-sheet-top basin: An example from the south Pyrenean thrust belt.  
 1962 *Tectonics*, 35, 1280-1313, doi:10.1002/2016TC004192.
- 1963 Labaume, P., Teixell, A., 2020. Evolution of salt structures of the Pyrenean rift (Chaînons  
 1964 Béarnais, France): From hyper-extension to tectonic inversion. *Tectonophysics*,  
 1965 doi:10.1016/j.tecto.2020.228451.
- 1966 Laborde, A., Barrier, L., Simoes, M., Li, H., Coudroy, T., Van der Woerd, J., Tapponnier, P.,  
 1967 2019. Cenozoic deformation of the Tarim Basin and surrounding ranges (Xinjiang, China):  
 1968 A regional overview. *Earth-Science Reviews*, 197, 102891,  
 1969 doi.org/10.1016/j.earscirev.2019.102891.
- 1970 Lacombe, O., 2012. Do fault slip data inversions actually yield "paleostresses" that can be  
 1971 compared with contemporary stresses? A critical discussion. *C. R. Geoscience*, 344, 159-  
 1972 173, doi:10.1016/j.crte.2012.01.006.
- 1973 Lacombe, O., Angelier, J., Laurent, P., 1992. Determining paleostress orientations from faults  
 1974 and calcite twins: a case study near the Sainte-Victoire Range (southern France).  
 1975 *Tectonophysics*, 201, 141-156.
- 1976 Lacombe, O., Mouthereau, F., 2002. Basement-involved shortening and deep detachment  
 1977 tectonics in forelands of orogens: Insights from recent collision belts (Taiwan, Western  
 1978 Alps, Pyrenees). *Tectonics*, 21(4), 1030, doi:10.1029/2001TC901018.
- 1979 Lacombe, O., Jolivet, L., 2005. Structural and kinematic relationships between Corsica and  
 1980 the Pyrenees-Provence domain at the time of the Pyrenean orogeny. *Tectonics*, vol. 24,  
 1981 TC1003, doi:10.1029/2004TC001673.
- 1982 Lacombe, O., Bellahsen, N., 2016. Thick-skinned tectonics and basement-involved fold-  
 1983 thrust belts: insights from selected Cenozoic orogens. *Geol. Mag.* 153 (5/6), 763–810,  
 1984 doi:10.1017/S0016756816000078.
- 1985 Lapparent, A.F. de, 1935. Le bassin tertiaire d'Eoulx, près Castellane (Haute-Provence). *C. R.*  
 1986 *Acad. Sci. Paris*, 200, 334-336.
- 1987 Lapparent, A.F. de, 1938. Etudes géologiques dans les régions provençales et alpines entre le  
 1988 Var et la Durance. *Bull. Serv. Carte géol. Fr.*, 40, No. 198, 302 p.
- 1989 Larroque, C., Baize, S., Albaric, J., Jomard, H., Trévisan, J., Godano, M., Cushing, M.,  
 1990 Deschamps, A., Sue, C., Delouis, B., Potin, B., Courboulex, F., Régnier, M., Rivet, D.,  
 1991 2021. Seismotectonics of southeast France: from the Jura mountains to Corsica. *Comptes  
 1992 Rendus. Géoscience*, 1-47, doi:10.5802/crgeos.69.
- 1993 Laurent, O., Stephan, J.-F., Popoff, M., 2000. Modalités de la structuration miocène de la  
 1994 branche sud de l'arc de Castellane (chaînes subalpines méridionales). *Géologie de la  
 1995 France*, 3, 33-65.

- 1996 Laville, P., 1981. La formation bauxitique provençale (France). Séquence des faciès  
 1997 chimiques et paléomorphologie crétacée, *Chron. Rech. Min.*, 461, 51-68.
- 1998 Laville, P., Monteau, R., Villeneuve, M., et al., 2018. Carte géologique Aubagne-Marseille à  
 1999 1/50.000 (1044), 3e éd. BRGM, Orléans. Notice explicative par Villeneuve, M., Floquet,  
 2000 M., Philip, J. et al. (2019).
- 2001 Leleu, S., Ghienne, J.-F., Manatschal, G., 2009. Alluvial fan development and morpho-  
 2002 tectonic evolution in response to contractional fault reactivation (Late Cretaceous-  
 2003 Palaeocene), Provence, France. *Basin Research*, 21, 157–187.
- 2004 Lemoine, M., 1972. Rythme et modalités des plissements superposés dans les chaînes  
 2005 subalpines méridionales des Alpes occidentales françaises. *Geologische Rundschau*, 61(3),  
 2006 975–1010.
- 2007 Lemoine, M., de Graciansky, P.-C., 1988. Histoire d'une marge continentale passive: les  
 2008 Alpes occidentales au Mésozoïque. Introduction. *Bull. Soc. géol. Fr.*, 8, 597–600.
- 2009 Lemoine, M., Graciansky, P.-C. de, Tricart, P., 2000. De l'océan à la chaîne de montagnes :  
 2010 tectonique des plaques dans les Alpes. Editions scientifiques GB, Paris.
- 2011 Léonide, P., Floquet, M., Villier, L., 2007. Interaction of tectonics, eustasy, climate and  
 2012 carbonate production on the sedimentary evolution of an early/middle Jurassic extensional  
 2013 basin (Southern Provence Sub-basin, SE France). *Basin Research*, 19, 125–152,  
 2014 doi:10.1111/j.1365-2117.2007.00316.x.
- 2015 Le Pichon, X., Rangin, C., Hamon, Y., Loget, N., Lin, J.Y., Andreani, L., Flotte, N., 2010.  
 2016 Geodynamics of the France Southeast Basin. *Bull. Soc. géol. Fr.*, 181, 6, 477-501.
- 2017 Li, S., Kusky, T.M., Zhao, G., Liu, X., Zhang, G., Kopp, H., Wang, L., 2010. Two-stage  
 2018 Triassic exhumation of HP-UHP terranes in the western Dabie orogen of China:  
 2019 Constraints from structural geology. *Tectonophysics*, 490, 267-293,  
 2020 doi:10.1016/j.tecto.2010.05.010.
- 2021 Lickorish, W.H., Ford, M., 1998. Sequential restoration of the external Alpine Digne thrust  
 2022 system, SE France, constrained by kinematic data and synorogenic sediments. In: Mascle,  
 2023 A., Puigdefabregas, C., Luterbacher, H.P., Fernandez, M. (Eds), *Cenozoic Foreland Basins*  
 2024 of Western Europe. Geological Society Special Publications, 134, 189-211.
- 2025 Lucaleau, F., Mailhe, D., 1986. Heat flow, heat production and fission track data from the  
 2026 Hercynian basement around the Provençal basin (western Mediterranean). *Tectonophysics*,  
 2027 128, 335-356.
- 2028 Lutaud, L., 1924. Étude tectonique et morphologique de la Provence cristalline. Université de  
 2029 Paris, France, PhD thesis.
- 2030 Lutaud, L., 1957. La tectogenèse et l'évolution structurale de la Provence. *Revue de*  
 2031 *Géographie physique et de Géologie dynamique*, (2), I, (2), 103-112.
- 2032 Macedo, J., Marshak, S., 1999. Controls on the geometry of fold-thrust belt salient. *GSA*  
 2033 *Bulletin*, 111, 1808-1822.
- 2034 Machhour, L., Philip, J., Oudin, J.-L., 1994. Formation of laminite deposits in anaerobic-  
 2035 dysaerobic marine environments. *Marine Geology*, 117, 287-302.
- 2036 Maillart, J., Beaudoin, B., Cojan, I., Joseph, P., Pinoteau, B., 1987. Rôle de la compaction  
 2037 dans la déformation synsédimentaire : exemples dans le Sud-Est de la France. *Ier Congr.*  
 2038 *Français de Sédimentologie*, A.S.F., Paris, Livre des Résumés, p. 253-254.

- 2039 Malavieille, J., Ritz, J.F., 1989. Mylonitic deformation of evaporites in decollements:  
 2040 examples from the southern Alps, France. *Journal of Structural Geology*, 11, 583-590,  
 2041 doi.org/10.1016/0191-8141(89)90089-8.
- 2042 Malavieille, J., Konstantinovskaya, E., 2010. Impact of surface processes on the growth of  
 2043 orogenic wedges: Insights from analog models and case studies. *Geotectonics*, 44, 6, 541-  
 2044 558.
- 2045 Martín-González, F., Fernández-Lozano, J., De Vicente, G., Crespo-Martín, C., Heredia, N.,  
 2046 2021. Role of multiple inherited basement structures on orogen geometry and evolution:  
 2047 Insights from analogue modelling. *Journal of Structural Geology*, 144,  
 2048 doi.org/10.1016/j.jsg.2020.104267.
- 2049 Mascle, G., Arnaud, H., Dardeau, G., Debemas, J., Delpech, P.-Y., Dubois, P., Gidon, M.,  
 2050 Graciansky, P.-C. de, Kerckhove, C., Lemoine, M., 1988.). Salt tectonics, Tethyan rifting  
 2051 and Alpine folding in the French Alps. *Bull. Soc. géol. Fr.*, 5, 747-758.
- 2052 Masse, J.-P., Philip, J., 1976. Paléogéographie et tectonique du Crétacé moyen en Provence :  
 2053 révision du concept d'isthme Durancien. *Revue de géographie physique et de géologie*  
 2054 dynamique, XVIII, 1, 49-66.
- 2055 Masse, J.-P., Villeneuve, M., Leonforte, E., Nizou, J., 2009. Block tilting of the North  
 2056 Provence early Cretaceous carbonate margin: stratigraphic, sedimentologic and tectonic  
 2057 data. *Bull. Soc. géol. Fr.*, 180, No. 2, 105-115, doi:10.2113/gssgbull.180.2.105.
- 2058 Matte, P., 2001. The Variscan collage and orogeny ( $480 \pm 290$  Ma) and the tectonic definition  
 2059 of the Armorica microplate: A review. *Terra Nova*, 13, 122–128.
- 2060 Mazzotti, S., Jomard, H., Masson, F., 2020. Processes and deformation rates generating  
 2061 seismicity in metropolitan France and conterminous Western Europe, BSGF - Earth  
 2062 Sciences Bulletin 2020, 191, 19.
- 2063 McMechan, M.E., 1985. Low-taper triangle zone geometry: An interpretation for the Rocky  
 2064 Mountains foothills, Pine Pass–Peace River, British Columbia. *Bulletin of Canadian*  
 2065 *Petroleum Geology*, 33, 3-38.
- 2066 Meigs, A.J., Burbank, D.W., 1997. Growth of the South Pyrenean orogenic wedge. *Tectonics*,  
 2067 16, No. 2, 239-258.
- 2068 Ménard, G., 1979. Relations entre structures profondes et structures superficielles dans le sud-  
 2069 est de la France. Essai d'utilisation de données géophysiques. Université de Grenoble,  
 2070 France, PhD thesis.
- 2071 Mennessier, G., 1959. Etude tectonique des confins alpino-provençaux entre le Verdon et  
 2072 l'Argens. *Mém. Soc. géol. Fr.*, t. XXXVIII, n° 87.
- 2073 Mennessier, G., 1963. Carte géol. France (1/50000), feuille SALERNES (997). Orléans:  
 2074 Bureau de recherches géologiques et minières.
- 2075 Mennessier, G., Modret, D., 1966. Carte géol. France (1/50000), feuille TAVERNES (996).  
 2076 Orléans: Bureau de recherches géologiques et minières.
- 2077 Mennessier, G., Bordet, P., 1969. Carte éol. France (1/50000), feuille COLLOBRIERES  
 2078 (1046). Orléans: Bureau de recherches géologiques et minières.
- 2079 Mennessier, G., 1970. Étude tectonique des chaînons situés au Sud-Est du confluent du  
 2080 Verdon et de la Durance (Basse-Provence orientale) *Bulletin du BRGM*, 1970, I, n°1, 35-  
 2081 72.

- 2082 Mennessier, G., Modret, D., Aussedat, J.-L., Thiers, R., Caron, J.-P., Durand, J.-P.,  
 2083 Ferrandini, J., Guieu, G., Rousset, C., 1979. Carte géol. France (1/50000), feuille  
 2084 BRIGNOLES (1022). Orléans: Bureau de recherches géologiques et minières.
- 2085 Mercier, H., 1978. Le Néogène et le Pléistocène inférieur duranciens. Université de Grenoble,  
 2086 France, PhD thesis.
- 2087 Mercier, H., 1979. Le Néogène et le Pléistocène inférieur duranciens. Géologie Alpine, t. 55,  
 2088 111-132.
- 2089 Mitra, S., Namson, J., 1989. Equal area balancing. American Journal of Science, 289, 563-  
 2090 599.
- 2091 Mitra, M., 2002. Fold-accommodation faults. Am. Assoc. Pet. Geol. Bull., 86, 671–693.
- 2092 Montenat, C., Barrier, P., Hibsch, C., 2005. Enregistrement des événements pyrénéo-  
 2093 provençaux dans les chaînes subalpines méridionales (Baronnies, France). Géologie de la  
 2094 France, 23-73.
- 2095 Mora, A., Parra, M., Strecker, M.R., Kammer, A., Dimaté, C., Rodriguez, F., 2006. Cenozoic  
 2096 contractional reactivation of Mesozoic extensional structures in the Eastern Cordillera of  
 2097 Colombia. Tectonics, v. 25, TC2010, doi:10.1029/2005TC001854.
- 2098 Morabito, J., 1967. Evolution tectonique des régions du Bas-Verdon. Bull. Soc. géol. Fr. IX,  
 2099 4, 585–592.
- 2100 Morillon, A.-C., 1997. Etude thermo-chronométrique appliquée aux exhumations et contexte  
 2101 orogénique: le Massif des Maures (France) et Les Cordillères Bétiques (Espagne).  
 2102 Université de Nice, France, PhD thesis.
- 2103 Moutherneau, F., Angrand, P., Jourdon, A., Ternois, S., Fillon, C., Calassou, S., Chevrot, S.,  
 2104 Ford, M., Jolivet, L., Manatschal, G., Masini, E., Thinon, I., Vidal, O., Baudin, T., 2021.  
 2105 Cenozoic mountain building and topographic evolution in Western Europe: impact of  
 2106 billions of years of lithosphere evolution and plate kinematics. Bull. Soc. géol. Fr - Earth  
 2107 Sci Bulletin 192, 56. <https://doi.org/10.1051/bsgf/2021040>.
- 2108 Moutherneau, F., Filleaudeau, P.-Y., Vacherat, A., Pik, R., Lacombe, O., Fellin, M.G.,  
 2109 Castelltort, S., Christophoul, F., and Masini, E., 2014. Placing limits to shortening  
 2110 evolution in the Pyrenees: Role of margin architecture and implications for the  
 2111 Iberia/Europe convergence. Tectonics, 33, 2283–2314, doi:10.1002/2014TC003663.
- 2112 Moutherneau, F., Watts, A.B., Burov, E., 2013. Structure of orogenic belts controlled by  
 2113 lithosphere age. Nature Geoscience 6, 785-789. <https://doi.org/10.1038/ngeo1902>.
- 2114 Nicolas, M., Santoire, J.-P., Delpech, P.-Y., 1990. Intraplate seismicity: new seismotectonic  
 2115 data in Western Europe. Tectonophysics, 179, 27-53.
- 2116 Nury, D. 1988. L’Oligocène de Provence méridionale. Documents du BRGM, 163, 411 p.
- 2117 Nury, D., Raynaud, S., 1986. Etude tectono-sédimentaire du fossé oligocène de Marseille,  
 2118 Bouches-du-Rhône. Evolution postérieure. Géologie de la France, 4, 377-397.
- 2119 Nury, D., Rousset, C., 1985. Extension des dépôts oligocènes de la région de Toulon (Var,  
 2120 Sud-Est France). Cadre structural et implications paléogéographiques. Géologie  
 2121 méditerranéenne, XII-XIII, 3-4, 175-184.
- 2122 Nury, D., Villeneuve, M., Arlhac, P., Gärtner, A., Linnemann, U., Châteauneuf, J.-J.,  
 2123 Riveline, J., Hippolyte, J.-C., 2016. New insights on the Marseille-Aubagne Oligocene  
 2124 basins (France). Boletín Geológico y Minero, 127 (2/3), 483-498.

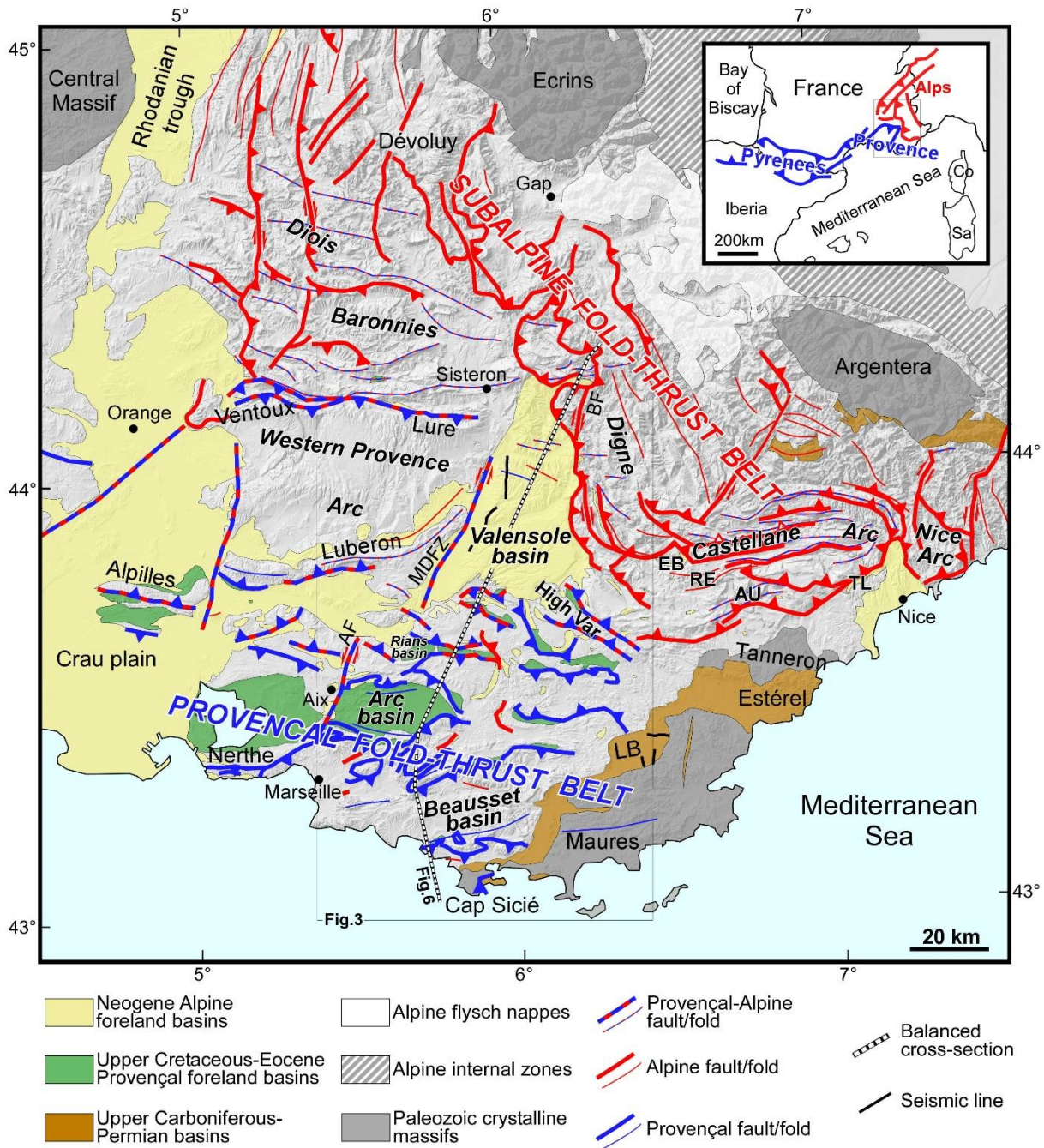
- 2125 Onézime, J., Faure, M., Crévola, G., 1999. Etude pétro-struccturale du complexe granitique  
 2126 Rouet – Plan-de-la-Tour (massifs des Maures et du Tanneron occidental, Var). C. R. Acad.  
 2127 Sci. Paris, 328, 773-779.
- 2128 Oudet, J., Münch, P., Borgomano, J., Quillevere, F., Melinte-Dobrinescu, M.-C., Demory, F.,  
 2129 Viseur, S., Cornée, J.-J., 2010. Land and Sea study of the Northeastern Golfe du Lion  
 2130 rifted margin: the Oligocene-Miocene of southern Provence (Nerthe area, SE France). Bull.  
 2131 Soc. géol. Fr., 181, 591-607.
- 2132 Pairis, J.L., Gidon, M., 1987. Le détritisme néogène et ses relations avec la tectonique, à  
 2133 l'extrême NE du bassin de Valensole (Alpes externes méridionales). Géologie alpine,  
 2134 Mém. H.S. no. 13, 417-426.
- 2135 Parra, M., Mora, A., Lopez, C., Rojas, L.E., Horton, B.K., 2012. Detecting earliest shortening  
 2136 and deformation advance in thrust belt hinterlands: Example from the Colombian Andes.  
 2137 Geology, 40, no. 2, pp. 175-178, doi:10.1130/G32519.1.
- 2138 Philip, J., 1967. Modalités et importance de la transgression du Sénonien inférieur dans la  
 2139 région de Saint-Cyr-sur-Mer (Var). C. R. Acad. Sci. Paris, D, 265, 1883-1886.
- 2140 Philip, J., 1970. Les formations calcaires à rudistes du Crétacé supérieur provençal et  
 2141 rhodanien. Université d'Aix-Marseille, Marseille, France, PhD thesis, 438 p.
- 2142 Philip, J., 2012. L'exploration géologique de la Provence: deux siècles et demi de débats et de  
 2143 controverses, Paris: Presses des Mines, Collection Histoire Sciences et sociétés. 366 p.
- 2144 Philip, J., 2018. La bande triasique de l'Huveaune, in Villeneuve, M., et al., Mémoire  
 2145 explicatif, Carte géol. France (1/50.000), feuille Aubagne Marseille, 3ème édition (1044),  
 2146 p. 148-156.
- 2147 Philip, J. 2019. La bande triasique de l'Huveaune, in Villeneuve, M., Floquet, M., Philip, J. et  
 2148 al., Notice explicative de la carte géologique Aubagne-Marseille à 1/50.000 (1044), 3e éd.  
 2149 BRGM, Orléans, 72-76.
- 2150 Philip, J., Allemann, J., 1982. Comparaison entre les plates-formes du Crétacé supérieur de  
 2151 Provence et de Sardaigne. Cretaceous Research, 3, 35-45.
- 2152 Philip, J., Bercovici, C., Machhour, L., Masse, P.J.L. 1985. La tectonique crétacée de la  
 2153 région toulonnaise. Réunion Extraordinaire de la Société Géologique de France du 2 au 7  
 2154 septembre à Marseille. Première journée. Documents du BRGM, 94, 1-22.
- 2155 Philip, J., Masse, P.J.-L., Machhour, L., 1987. L'évolution paléogéographique et structurale  
 2156 du front de chevauchement nord-toulonnais (Basse-Provence occidentale, France). Bull.  
 2157 Soc. géol. Fr., 8, III, No. 3, 541-550.
- 2158 Philip, J., Vianey-Liaud, M., Martin-Closas, C., Tabuce, R., Léonide, P., Margerel, J.-P.,  
 2159 Noël, J., 2017. Stratigraphy of the Haut Var Paleogene continental series (Northeastern  
 2160 Provence, France): New insight on the age of the ‘Sables bleutés du Haut Var’ Formation.  
 2161 Geobios, 50, 319–339, doi:10.1016/j.geobios.2017.06.002.
- 2162 Philip, J., Argyriadis, I., Bestani, L., 2018. Le massif de la Sainte-Baume, in Villeneuve et al.,  
 2163 Mémoire explicatif, Carte géol. France (1/50.000), feuille Aubagne-Marseille, 3e édition  
 2164 (1044), 133-148.
- 2165 Popoff, M., 1973. La bande triasique de Barjols (Var) : la bordure sud-occidentale. Université  
 2166 Paris VI, Paris, France, PhD thesis, 160 p.

- 2167 Price, R.A., 1986. The southeastern Canadian Cordillera: thrust faulting, tectonic wedging,  
2168 and delamination of the lithosphere. *J. Struct. Geol.*, 8, 3/4, 239-254, doi:10.1016/0191-  
2169 8141(86)90046-5.
- 2170 Rat, J., Mouthereau, F., Brichau, S., Crémades, A., Balvay, M., Ganne, J., Lahfid, A.,  
2171 Gautheron, C., 2019. Tectonothermal Evolution of the Cameros Basin: Implications for  
2172 Tectonics of North Iberia. *Tectonics*, 38, doi:10.1029/2018TC005294.
- 2173 Répelin, J. (1922). Monographie géologique du massif de la Sainte-Baume. *Annales de la*  
2174 *Faculté des Sciences de Marseille*, XXV (I), 85 p.
- 2175 Ritz, J.-F., 1992. Recent tectonics and seismotectonics in the southern Alps: stress analysis,  
2176 *Quaternaire*, 3, 111–124, doi:10.3406/quate.1992.1980.
- 2177 Rolland, Y., Corsini, M., Demoux, A., 2009. Metamorphic and structural evolution of the  
2178 Maures-Tanneron massif (SE Variscan chain): evidence of doming along a transpressional  
2179 margin. *Bull. Soc. géol. Fr.*, 180, 217-230.
- 2180 Romagny, A., Jolivet, L., Menant, A., Bessière, E., Maillard, A., Canva, A., Gorini, C.,  
2181 Augier, R., 2020. Detailed tectonic reconstructions of the Western Mediterranean region  
2182 for the last 35 Ma, insights on driving mechanisms. *BSGF-Earth Sciences Bulletin*, 191,  
2183 37, doi.org/10.1051/bsgf/2020040.
- 2184 Roure, F., Brun, J.P., Colletta, B., Van Den Driessche, J., 1992. Geometry and kinematics of  
2185 extensional structures in the Alpine foreland of southeastern France. *J. Struct. Geol.*, 14,  
2186 503-519.
- 2187 Roure, F., Colletta, B., 1996. Cenozoic inversion structures in the foreland of the Pyrenees  
2188 and Alps, in: Ziegler, P. A., Horvath, F. (Eds), *Peri-Tethys Memoir 2: Structure and*  
2189 *Prospects of Alpine Basins and Forelands*. *Mém. Mus. natn. Hist. nat.*, 170, 173-209.
- 2190 Rousset, C., Kerckhove, C., Bambier, A., 1983. Notice explicative, *Carte géol. Fr.* (1/50,000),  
2191 feuille SEYNE (894). Orléans : Bureau de recherches géologiques et minières.
- 2192 Roux, M., 1968. Étude géologique du massif des Cadières de Brandis à l'ouest de Castellane.  
2193 *Géologie Alpine*, t. 44, 339-352.
- 2194 Roux, M., 1970. Le synclinal de Taulanne (Basses-Alpes) et les conséquences du  
2195 chevauchement de Castellane sur sa bordure nord-est. *Géologie Alpine*, t. 46, 177-188.
- 2196 Roveri, M., Flecker, R., Krijgsman, W., Lofi, J., Lugli, S., Manzi, V., Sierro, F.J., Bertini, A.,  
2197 Camerlenghi, A., De Lange, G., Govers, R., 2014. The Messinian salinity crisis: past and  
2198 future of a great challenge for marine sciences. *Marine Geology*, 352, 25-58,  
2199 doi:10.1016/j.margeo.2014.02.002.
- 2200 Rowan, M.G., Urai, J.L., Fiduk, J.C., Kukla, P.A., 2019. Deformation of intrasalt competent  
2201 layers in different modes of salt tectonics. *Solid Earth*, 10, 987-1013, doi.org/10.5194/se-  
2202 10-987-2019.
- 2203 Saura, E., Ardèvol i Oró, L., Teixell, A., Vergés, J., 2016. Rising and falling diapirs, shifting  
2204 depocenters, and flap overturning in the Cretaceous Sopeira Brine migration, rifting and  
2205 thrusting in the Pyrenees and Sant Gervàs subbasins (Ribagorça Basin, southern Pyrenees).  
2206 *Tectonics*, 35, 638-662, doi:10.1002/2015TC004001.
- 2207 Schneider, J., Corsini, M., Reverso-Peila, A., Lardeaux, J.-M., 2014. Thermal and mechanical  
2208 evolution of an orogenic wedge during Variscan collision: an example in the Maures-  
2209 Tanneron Massif (SE France). In: Schulmann, K., Martínez Catalán, J.R., Lardeaux, J.-M.,  
2210 Janousek, V., Oggiano, G., (Eds), *The Variscan Orogeny: Extent, Timescale and the*

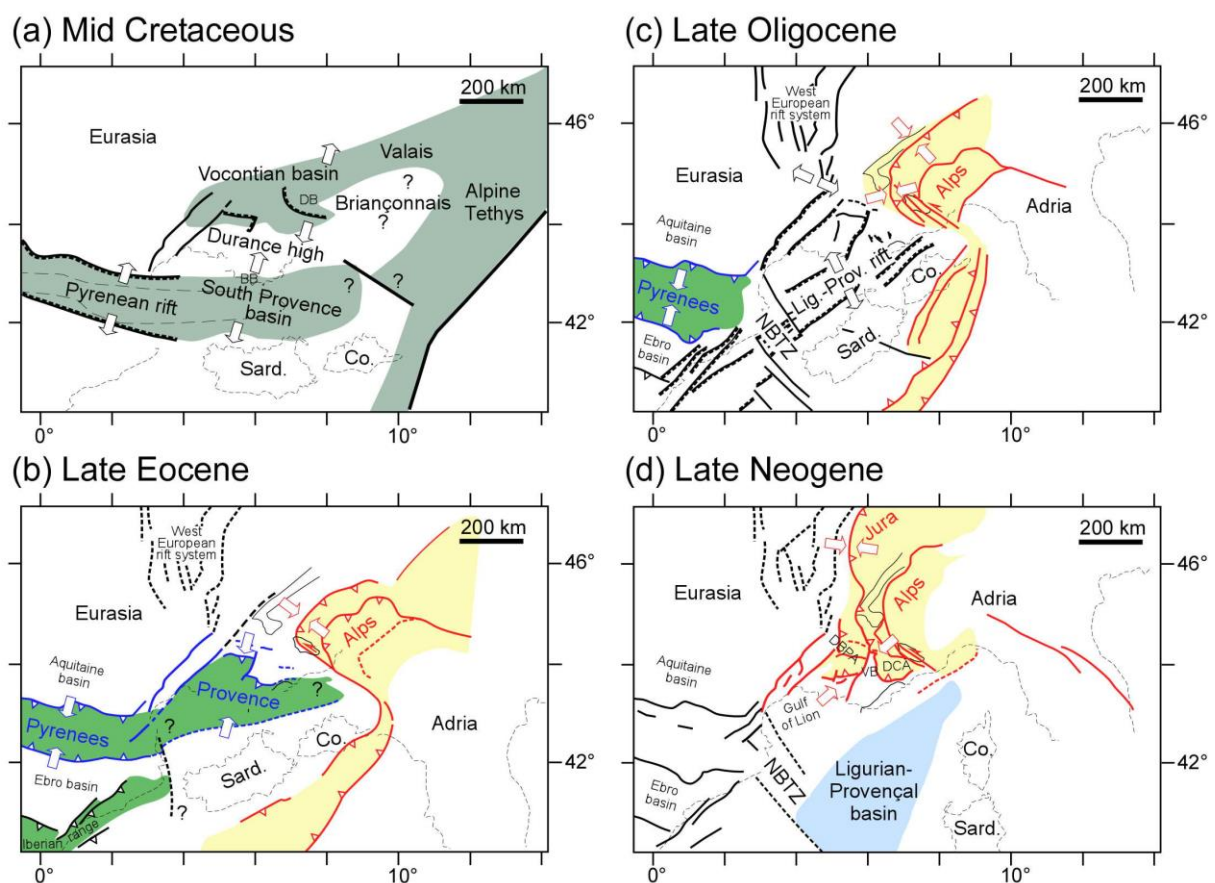
- 2211 Formation of the European Crust. Geological Society, London, Special Publications, 405,  
2212 doi:10.1144/SP405.4.
- 2213 Schreiber, D., Giannerini, G., Lardeaux, J.-M., 2011. The Southeast France basin during Late  
2214 Cretaceous times: The spatiotemporal link between Pyrenean collision and Alpine  
2215 subduction. *Geodinamica Acta*, 24/1, 23-27, doi:10.3166/ga.24.23-37.
- 2216 Schwartz, S., Gautheron, C., Audin, L., Dumont, T., Nomade, J., Barbarand, J., Pinna-Jamme,  
2217 R., van der Beek, P., 2017a. Foreland exhumation controlled by crustal thickening in the  
2218 Western Alps. *Geology*, 45, No. 2, 139-142, doi:10.1130/G38561.1.
- 2219 Schwartz, S. et al., 2017b. Supplemental material: Foreland exhumation controlled by crustal  
2220 thickening in the Western Alps. Geological Society of America. Journal contribution.  
2221 <https://doi.org/10.1130/2017035>
- 2222 Séranne, M., Couëffé, R., Husson, E., Baral, C., Villard, J., 2021. The transition from  
2223 Pyrenean shortening to Gulf of Lion rifting in Languedoc (South France)-A tectonic-  
2224 sedimentation analysis. *BSGF-Earth Sciences Bulletin*, 192, 27,  
2225 doi.org/10.1051/bsgf/2021017.
- 2226 Siddans, A.W.B., 1979. Arcuate fold and thrust patterns in the Subalpine Chains of Southeast  
2227 France. *Journal of Structural Geology*, 1, 2, 117-126.
- 2228 Simonetti, M., Carosi, R., Montomoli, C., Corsini, M., Petroccia, A., Cottle, J.M., Iaccorino,  
2229 S., 2020. Timing and kinematics of flow in a transpressive dextral shear zone, Maures  
2230 Massif (Southern France). *Int J Earth Sci (Geol Rundsch)*, 109, 2261-2285,  
2231 doi.org/10.1007/s00531-020-01898-6.
- 2232 Souquet, P., Delvolvéd, J.-J., Brusset, S., 2003. Identification of an underfilled foreland basin  
2233 system in the Upper Devonian of the Central Pyrenees: implications for the Hercynian  
2234 orogeny. *Int. J. Earth Sci.*, 92, 316-337, doi:10.1007/s00531-003-0334-y.
- 2235 Spitz, R., Bauville, A., Epard, J.-L., Kaus, B.J.P., Popov, A.A., Schmalholz, S.M., 2020.  
2236 Control of 3-D tectonic inheritance on fold-and-thrust belts: insights from 3-D numerical  
2237 models and application to the Helvetic nappe system, *Solid Earth*, 11, 999–1026,  
2238 doi.org/10.5194/se-11-999-2020.
- 2239 Suppe, J., 1983. Geometry and kinematics of fault-bend folding. *American Journal of  
2240 Science*, 283, 684–721.
- 2241 Suppe, J., 1985. Principles of structural geology. Prentice-Hall, Inc., Englewood Cliffs, New  
2242 Jersey.
- 2243 Suppe, J., Chou, G.T., Hook, S.C., 1992. Rates of folding and faulting determined from  
2244 growth strata. In McClay, K.R. (Ed), *Thrust tectonics*. Springer-Science+Business Media,  
2245 B.V.
- 2246 Suppe, J., Medwedeff, D.A., 1990. Geometry and kinematics of fault-propagation folding.  
2247 *Eclogae geol. Helv.* 83/3, 409-454.
- 2248 Tămaş, D.M., Tămaş, A., Barabasch, J., Rowan, M.G., Schleider, Z., Krézsek, C., Urai, J.L.,  
2249 2021. Low-angle shear within the exposed Mânzăleşti diapir, Romania: Salt decapitation in  
2250 the Eastern Carpathians fold-and-thrust belt. *Tectonics*, 40, e2021TC006850,  
2251 doi:10.1029/2021TC006850.
- 2252 Tavani, S., Storti, F., Lacombe, O., Corradetti, A., Muñoz, J.A., Mazzoli, S., 2015. A review  
2253 of deformation pattern templates in foreland basin systems and fold-and-thrust belts:

- 2254 Implications for the state of stress in the frontal regions of thrust wedges., Earth-Science  
2255 Reviews, 141, 82-104, doi.org/10.1016/j.earscirev.2014.11.013.
- 2256 Tavani, S., Bertok, C., Granado, P., Piana, F., Salas, R., Vigna, B., Muñoz, J.A., 2018. The  
2257 Iberia-Eurasia plate boundary east of the Pyrenees. Earth-Science Reviews, 187, 314-337,  
2258 doi:10.1016/j.earscirev.2018.10.008.
- 2259 Tempier, C., 1963. Étude tectonique du double pli des Pallières à l'Est de Rians (Var).  
2260 Travaux du Laboratoire de Géologie de la Faculté des Sciences de l'Université d'Aix-  
2261 Marseille, VII, p. 159-173.
- 2262 Tempier, C., 1987. Modèle nouveau de mise en place des structures provençales, Bull. Soc.  
2263 géol. Fr., 8, 533-540.
- 2264 Thomas, W.A., Bayona, G., 2002. Palinspastic restoration of the Anniston transverse zone in  
2265 the Appalachian thrust belt, Alabama. J. Struct. Geol., 24, 797-826.
- 2266 Torres Carbonell, P.J., Cao, S.J., Dimieri, L.V., 2017. Spatial and temporal characterization of  
2267 progressive deformation during orogenic growth: Example from the Fuegian Andes,  
2268 southern Argentina. J. Struct. Geol., 99, 1-19, doi:10.1016/j.jsg.2017.04.003.
- 2269 Touraine, F., 1967. Les rapports de l'Oligocène avec les structures N-S du Nord-Varois. Bull.  
2270 Soc. géol. Fr., 7, IX, 530-536.
- 2271 Toutin-Morin, N., Bonijoly, D., Brocard, C., Dardeau, G., Dubar, M., 1993. Enregistrement  
2272 sédimentaire de l'évolution post-hercynienne, en bordure des Maures et du Tanneron, du  
2273 Carbonifère supérieur à l'Actuel. Géologie de la France, No. 2, 3-22.
- 2274 Toutin-Morin, N., Bonijoly, D., Brocard, C., Broutin, J., Crévola, G., Dardeau, G., Dubar, M.,  
2275 Féraud, J., Giraud, J.D., Godefroy, P., Laville, P., Meinesz, A., 1994. Carte géologique de  
2276 la France à 1/50.000. Fréjus- Cannes 2e édition. Notice explicative. vol. 187.
- 2277 Uba, C.E., Kley, J., Strecker, M.R., and Schmitt, A.K., 2009. Unsteady evolution of the  
2278 Bolivian Subandean thrust belt: The role of enhanced erosion and clastic wedge  
2279 progradation: Earth and Planetary Science Letters. 281, 134–146,  
2280 doi:10.1016/j.epsl.2009.02.010.
- 2281 Unalan, G., 1970. Etude géologique de la bordure ouest de l'arc de Castellane (Alpes de Haute  
2282 Provence-Var). Minéralogie. Université de Grenoble, France, PhD thesis.
- 2283 van Hinsbergen, D.J.J., Vissers, R.L., Spakman, W., 2014. Origin and consequences of  
2284 western Mediterranean subduction, rollback, and slab segmentation. Tectonics, 33(4), 393-  
2285 419.
- 2286 van Hinsbergen, D.J.J. van, Torsvik, T.H., Schmid, S.M., Małenco, L.C., Maffione, M.,  
2287 Vissers, R.L.M., Gürer, D., Spakman, W., 2020. Orogenic architecture of the  
2288 Mediterranean region and kinematic reconstruction of its tectonic evolution since the  
2289 Triassic. Gondwana Res 81, 79-229, <https://doi.org/10.1016/j.gr.2019.07.009>.
- 2290 Vann, I.R., Graham, R.H., Hayward, A.B., 1986. The structure of mountain fronts. J. Struct.  
2291 Geol., 8, 215-227, doi:10.1016/0191-8141(86)90044-1.
- 2292 Vergés, J., Munoz, J.A., 1990. Thrust sequences in the Southern Central Pyrenees. Bull. Soc.  
2293 Géol. Fr., 8, VI, No. 2, 265-271, doi:10.2113/gssgbull.VI.2.265.
- 2294 Vergés, J., Ramos, V.A., Meigs, A., Cristallini, E., Bettini, F.H., Cortés, J.M., 2007. Crustal  
2295 wedging triggering recent deformation in the Andean thrust front between 31°S and 33°S:  
2296 Sierras Pampeanas-Precordillera interaction. J. Geophys. Res., 112, B03S15,  
2297 doi:10.1029/2006JB004287.

- 2298 Villeger, M., Andrieux, J., 1987. Phases tectoniques post-éocènes et structuration polyphasée  
2299 du panneau de couverture nord provençal (Alpes externes méridionales). Bull. Soc. géol.  
2300 Fr., 8, t. III, no. 1, 147-156.
- 2301 Villeneuve, M., Nury, D., Arlhac, P., Gärtner, A., Linnemann, U., 2018. Les bassins  
2302 oligocènes, in Villeneuve et al., Mémoire explicatif, Carte géol. France (1/50.000), feuille  
2303 Aubagne-Marseille, 3e édition (1044), 179-199.
- 2304 Walpersdorf, A., Pinget, L., Vernant, P., Sue, C., Deprez, A., the RENAG team, 2018. Does  
2305 long-term GPS in the Western Alps finally confirm earthquake mechanisms? Tectonics,  
2306 37, doi:10.1029/2018TC005054.
- 2307 Westphal, M., Durand, J.-P., 1990. Magnétostratigraphie des séries continentales fluvio-  
2308 lacustres du Crétacé supérieur dans le synclinal de l'Arc (région d'Aix-en-Provence,  
2309 France). Bull. Soc. géol. Fr., 8, VI, No. 4, 609-620.
- 2310 Weydert, P., Nury, F., 1978. Données nouvelles sur la stratigraphie et la tectonique de la zone  
2311 méridionale du bassin de Marseille. C. R. Acad. Sci. Paris, 287, 591-594.
- 2312 Wicker, V., Ford, M., 2021. Assessment of the tectonic role of the Triassic evaporites in 1 the  
2313 north Toulon fold-thrust belt. BSGF-Earth Sci. Bull., 192, 51.
- 2314 Wu, Z., Yin, H., Li, C., Yang, X., Wang, L., Wang, F., Dong, S., Jia, D., 2021. Influence of  
2315 regional erosion and sedimentary loading on fault activities in active fold-thrust belts:  
2316 Insights from discrete element simulation and the southern and central Longmen Shan  
2317 fold-thrust belt. Front. Earth Sci. 9:659682, 10.3389/feart.2021.659682.
- 2318 Zapata, T.R., Allmendinger, R.W., 1996. Growth stratal records of instantaneous and  
2319 progressive limb rotation in the Precordillera thrust belt and Bernejo basin.  
2320 Argentina. Tectonics, 15, No. 5, 1065-1083.
- 2321 Zubietta-Rossetti, D., Huyghe, P., Mascle, G., Mugnier, J.L., Baby, P., 1993. The influence of  
2322 the pre-Devonian on the front of the Andean Belt, central Bolivia. C.R.Acad.Sc.Paris,  
2323 Série II, 316, 951-957.
- 2324 Zürcher, P., 1891. Les zones de plissements de Salernes et d'Aups. Bull. Soc. géol. Fr., 3,  
2325 XIX, 1178-1201.
- 2326 Zürcher, P., 1893. Note sur les phénomènes de recouvrement des environs de Toulon. Bull.  
2327 Soc. géol. Fr., 3, XXI, 65-77.
- 2328

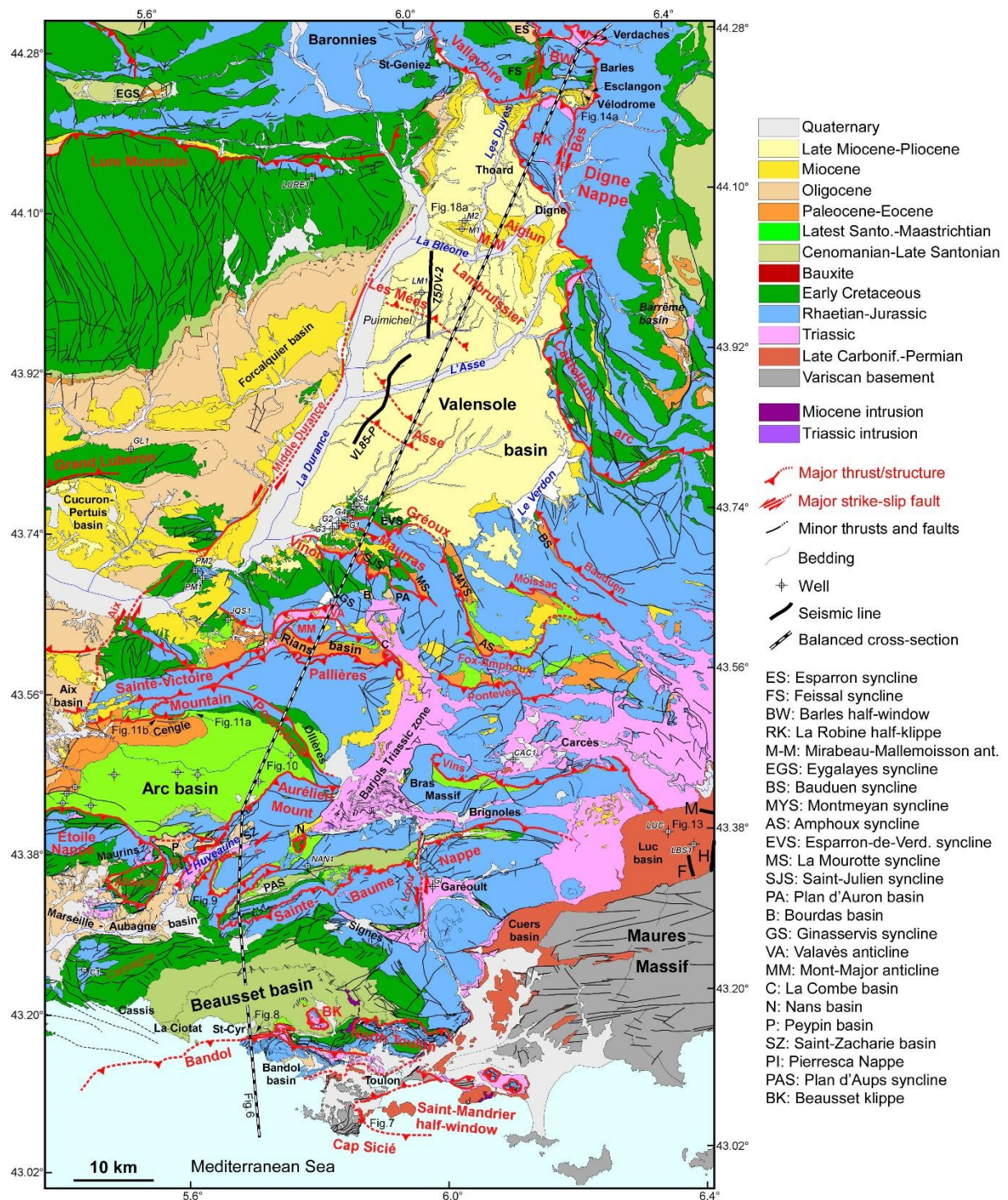


2336 (2012), Bestani et al. (2016), Villeneuve et al. (2018) and Espurt et al. (2019b), and from this  
 2337 study. Thin black square indicates location of the geological map of Fig. 3. Dashed thick  
 2338 black and white line shows the trace of the balanced and restored cross-section of Fig. 6  
 2339 across the upper Cretaceous Beausset and upper Cretaceous-Eocene Arc and Rians foreland  
 2340 basins and Neogene Valensole foreland basin. MDFZ: Middle Durance fault zone. AF: Aix  
 2341 fault. BF: Bès fault. LB: Luc basin. Locations of Miocene-Pliocene syn-orogenic basins of  
 2342 Eoulx-Brenon (EB), Roque-Esclapon (RE), Aubarède (AU) and Tourette-sur-Loup (TL) in  
 2343 the Castellane Arc are also shown.



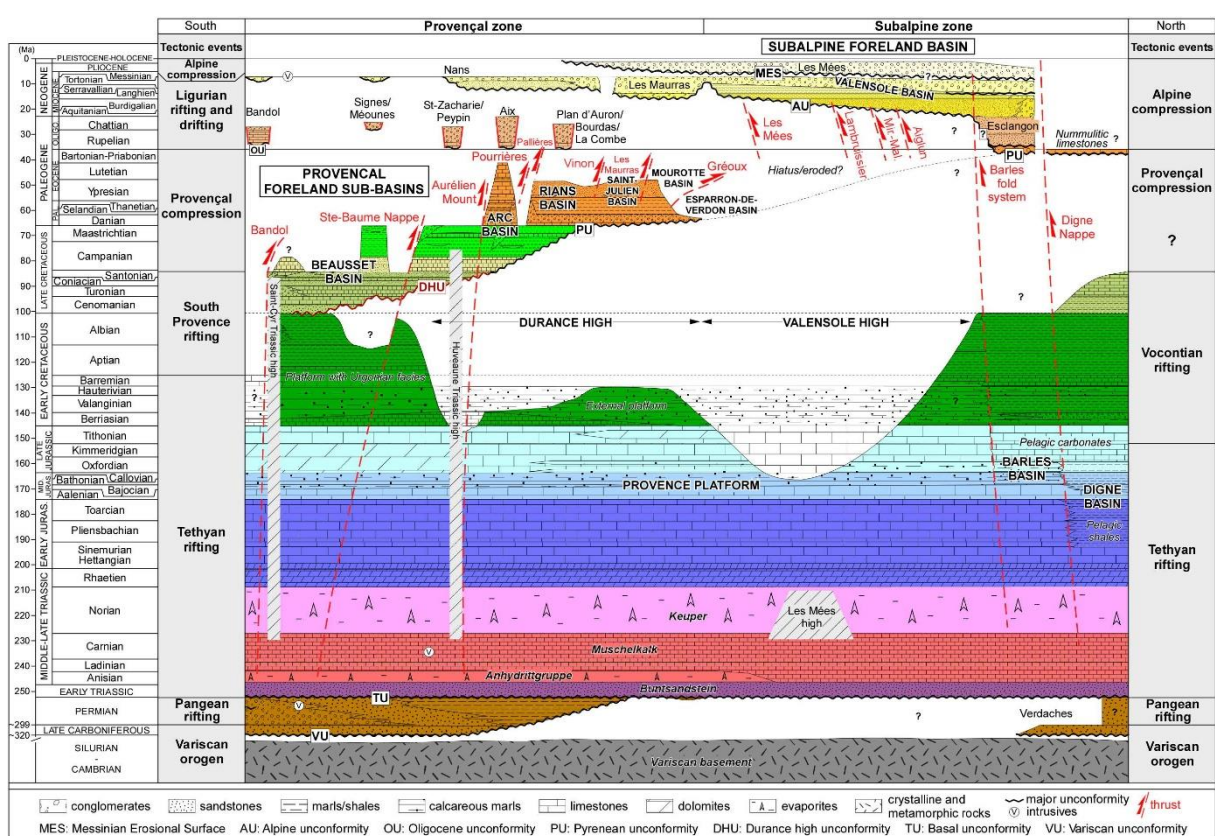
2344  
 2345 **Fig. 2.** Geological map of the central Provençal and southwestern Subalpine zones. This is a  
 2346 compilation of existing geological maps of BRGM (1/50000) of Mennessier (1963), Goguel  
 2347 (1964), Flandrin et al. (1964), Dorkel et al. (1966), Mennessier and Modret (1966), Catzigras  
 2348 et al. (1969), Mennessier and Bordet (1969), Gouvernet et al. (1969), Arlhac et al. (1970),

2349 Blanc et al. (1973), Blanc et al. (1974), Bordet et al. (1976), Blanc et al. (1977), Mennessier et  
 2350 al. (1979), Gigot et al. (1981b), Rousset et al. (1983), Haccard et al. (1989a), Gigot et al.  
 2351 (2013) and Laville et al. (2018), our field observations and subsurface data. Thick dashed  
 2352 black and white line shows the trace of the balanced and restored cross-section of Fig. 6.



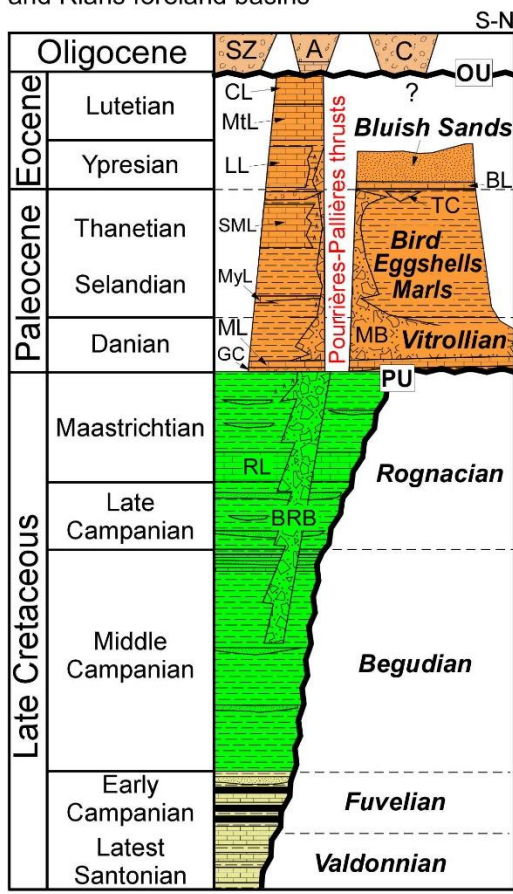
2353

2354 **Fig. 3.** Geological map of the central Provençal and Subalpine zones. This is a compilation of  
 2355 existing geological maps of BRGM (1:50,000) of Goguel (1966), Rouire et al. (1969a,b),  
 2356 Rouire et al. (1970), Rouire et al. (1974), Rouire et al. (1977), Rouire et al. (1979), Rouire et  
 2357 al. (1981), De Graciansky et al. (1981), Gigot et al. (1981b), Haccard et al. (1989a), Rousset  
 2358 et al. (1983), Gigot et al. (2013) and Laville et al. (2018), our field observations and  
 2359 subsurface data. Thick dashed black and white line shows the trace of the balanced and  
 2360 restored cross-section of Fig. 6.

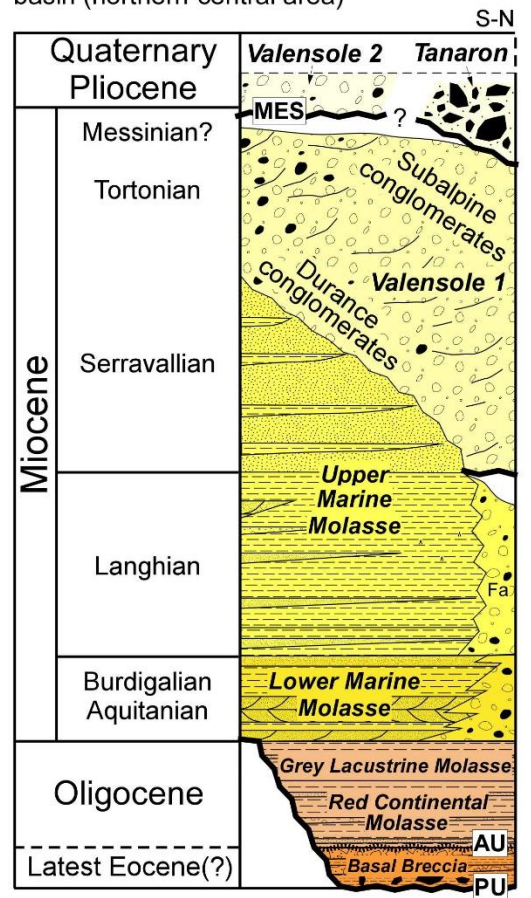


2361 **Fig. 4.** Synthetic stratigraphic chart along the studied cross-section across the Provençal zone  
 2362 and southwestern Subalpine zone. Locations of the Oligocene-Miocene Bandol,  
 2363 Signes/Méounes, Saint-Zacharie/Peypin, Nans, Aix, Plan d'Auron/Bourdas/La Combe basins  
 2364 are shown in Fig. 3. See details in text for references.  
 2365

(a) Upper Cretaceous-Eocene infill of the Arc and Rians foreland basins



(b) Cenozoic infill of the Valensole foreland basin (northern-central area)



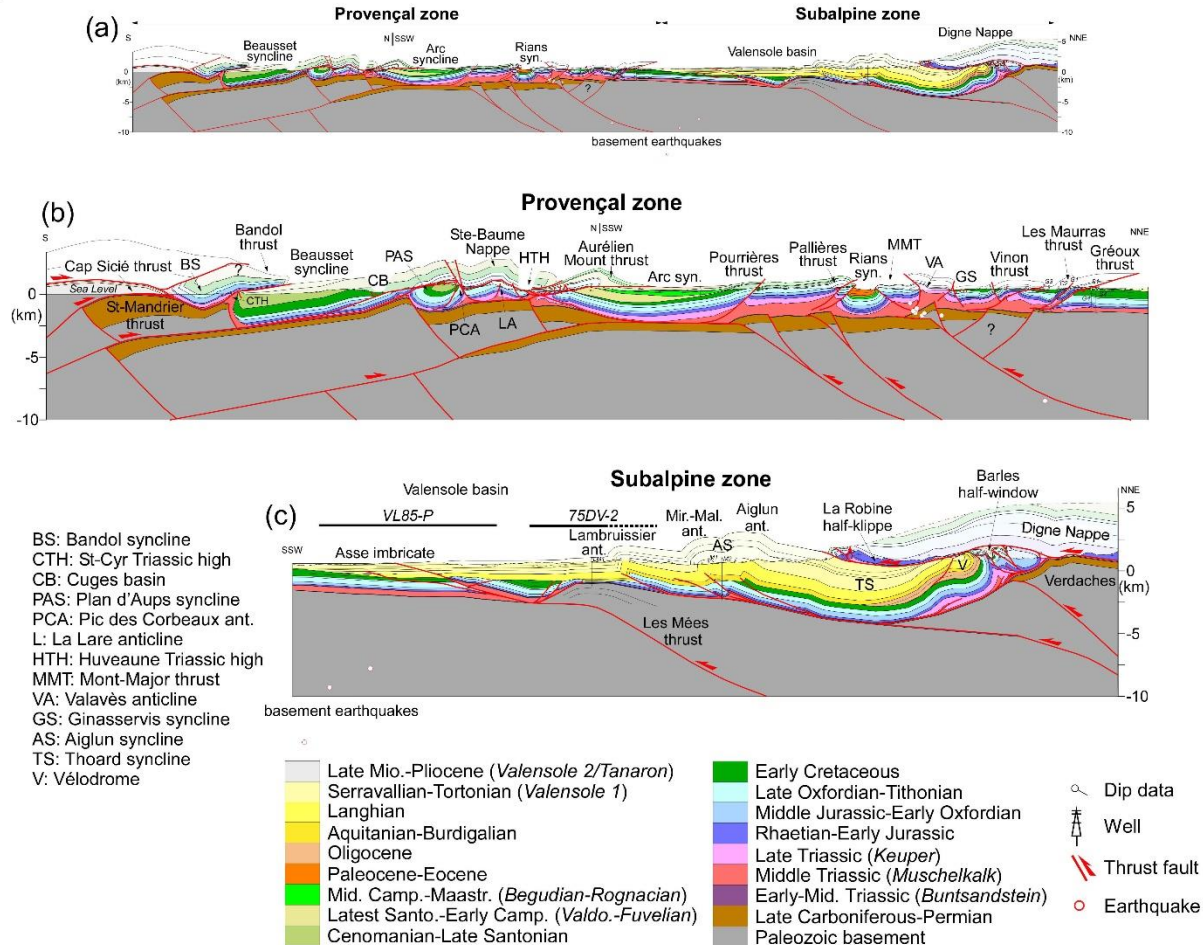
MES: Messinian Erosional Unconformity  
AU: Alpine unconformity  
OU: Oligocene unconformity  
PU: Pyrenean unconformity  
SZ: Saint-Zacharie basin  
A: Aix basin  
C: La Combe basin

CL: Cuques limestones  
Mtl: Montaigut limestones  
LL: Langesse limestones  
TC: Touars conglomerates  
BL: Bithynies limestones  
SML: Saint-Marc limestones  
MyL: Meyreuil limestones

MB: Microcodium breccias  
ML: Microcodium limestones  
GC: Galante conglomerates  
RL: Rousset limestones  
BRB: Begudian-Rognacian breccias  
Fa: Facibelle

2366

2367 **Fig. 5.** Details of the syn-orogenic sedimentary successions of the (a) upper Cretaceous-  
2368 Eocene infill of the Arc and Rians foreland basins and (b) Cenozoic infill of the Valensole  
2369 foreland basin. Locations of the Oligocene Saint-Zacharie, Aix and La Combe basins are  
2370 shown in Fig. 3. See details in text for references.



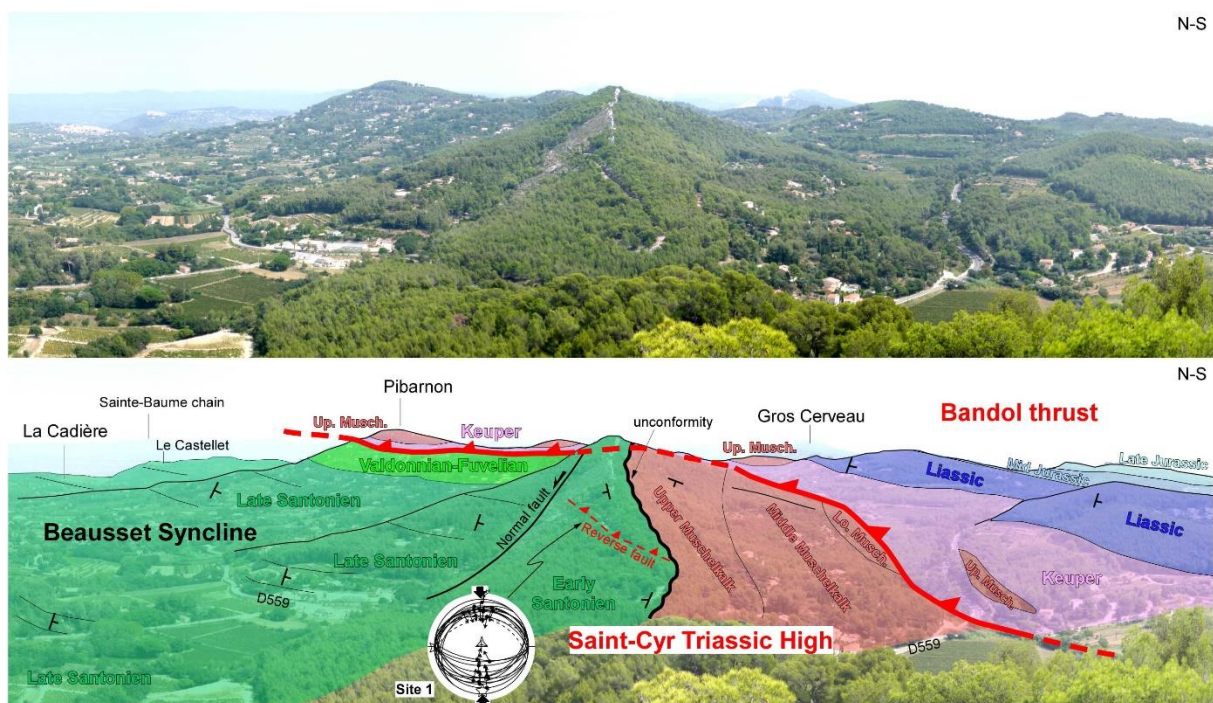
2371

2372 **Fig. 6.** (a) Cross-sectional geometry of the Provençal and southwestern Subalpine foreland  
 2373 thrust wedges. Details of the (b) Provençal zone and (c) Subalpine zone. For location of  
 2374 section trace, see Fig. 3. Location of seismic profiles VL85-P and 75DV-2 (Fig. 19) are  
 2375 shown. Note that transparency has been applied to the eroded structures.



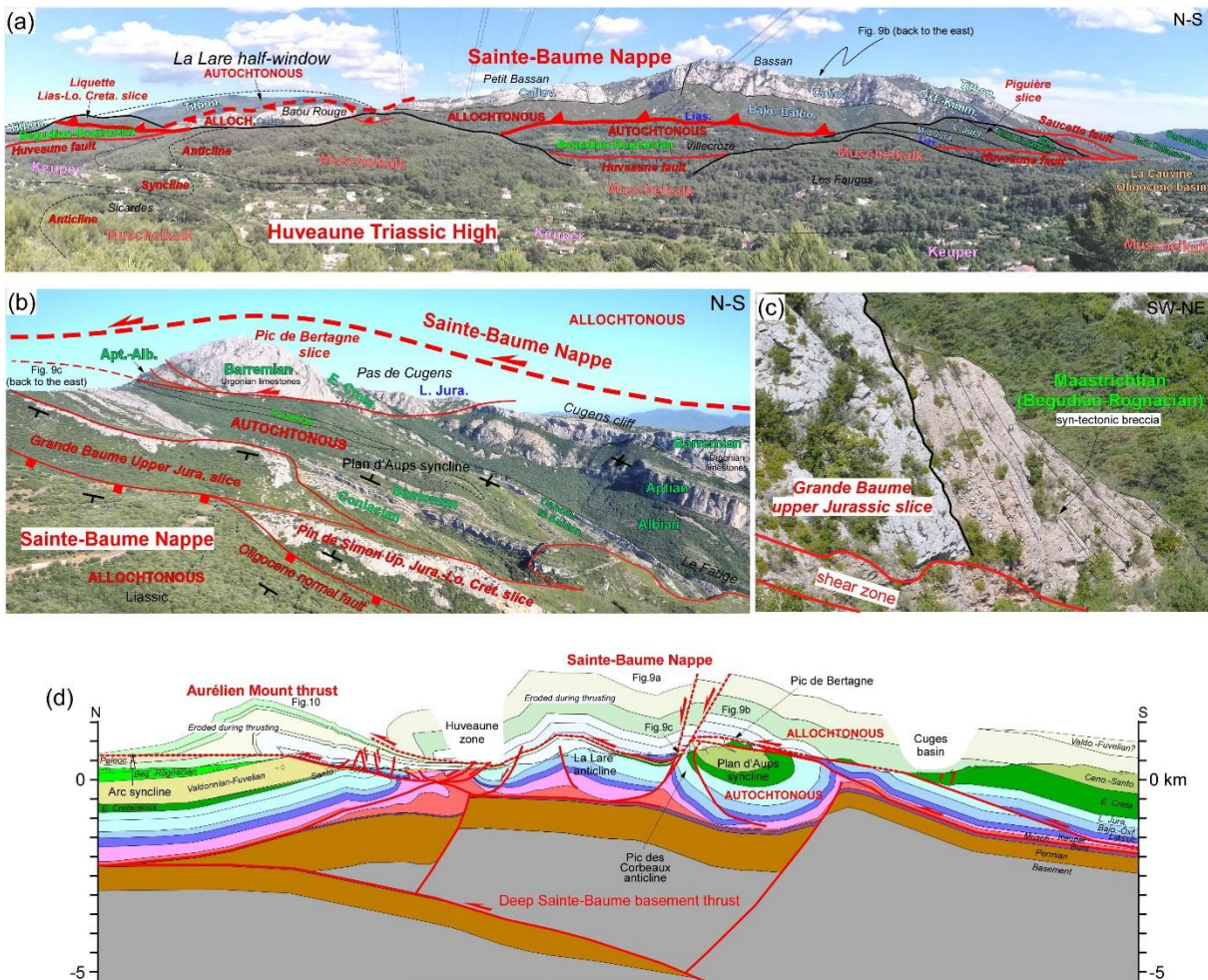
2376

2377 **Fig. 7.** (a) Panoramic view of the Saint-Mandrier half-window and folded N-verging Cap  
 2378 Sicié basement thrust (view looking westward;  $43.070431^\circ$ ,  $5.907101^\circ$ ). For location, see also  
 2379 Fig. 3. (b) Permian strata in the southern limb of the Saint-Mandrier anticline ( $43.067175^\circ$ ,  
 2380  $5.913673^\circ$ ). (c) North-dipping lower-middle Triassic (Buntsandstein) conglomerates and  
 2381 sandstones at the front of the Cap Sicié thrust ( $43.112546^\circ$ ,  $5.792338^\circ$ ). (d) Stratigraphic  
 2382 contact between lower-middle Triassic sandstones (Buntsandstein) and middle Triassic  
 2383 carbonates (Muschelkalk) at the northern front of the Cap Sicié thrust ( $43.113050^\circ$ ,  
 2384  $5.791026^\circ$ ).



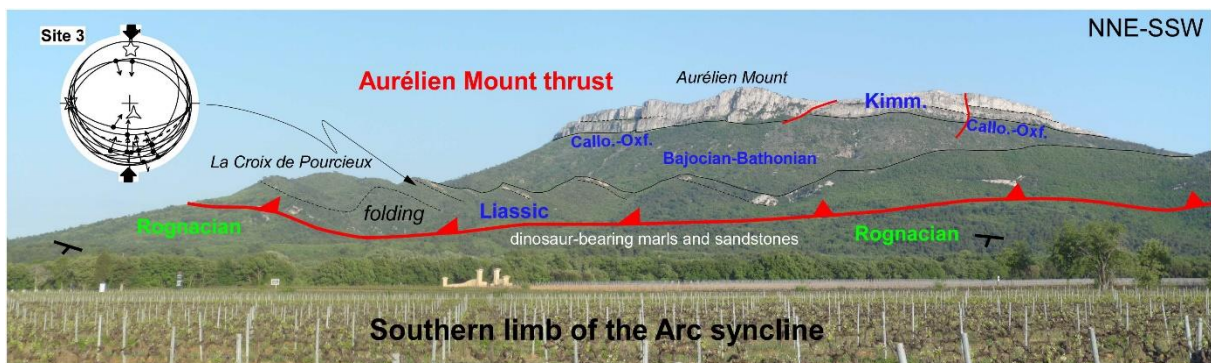
2385  
 2386 **Fig. 8.** Panoramic view of the Bandol thrust and southern limb of the Beausset syncline  
 2387 (modified from Philip et al., 1985 and Espurt et al., 2019b) (view looking eastward;  
 2388  $43.165794^\circ$ ,  $5.709031^\circ$ ). For location, see also Fig. 3. The N-verging Bandol thrust is  
 2389 detached above upper Triassic evaporites (Keuper) embedding upper Muschelkalk carbonate  
 2390 slices (e.g., Pibarnon) and overthrusts Valdonnian-Fuvelian facies strata of the Beausset  
 2391 syncline. In the southern limb of the Beausset syncline, the Saint-Cyr Triassic high is formed  
 2392 by middle Triassic (Muschelkalk) limestones, cargneules and volcano-detritic basaltic facies.

2393 The upper Muschelkalk fossiliferous limestones are unconformably overlain by lower  
 2394 Santonian conglomerates and rudist bearing limestones. Striated faults measured in N-dipping  
 2395 lower Santonian limestones are consistent with a N-trending compression. Fault data and  
 2396 bedding (dashed line) have been projected in an equal area stereogram, lower hemisphere.

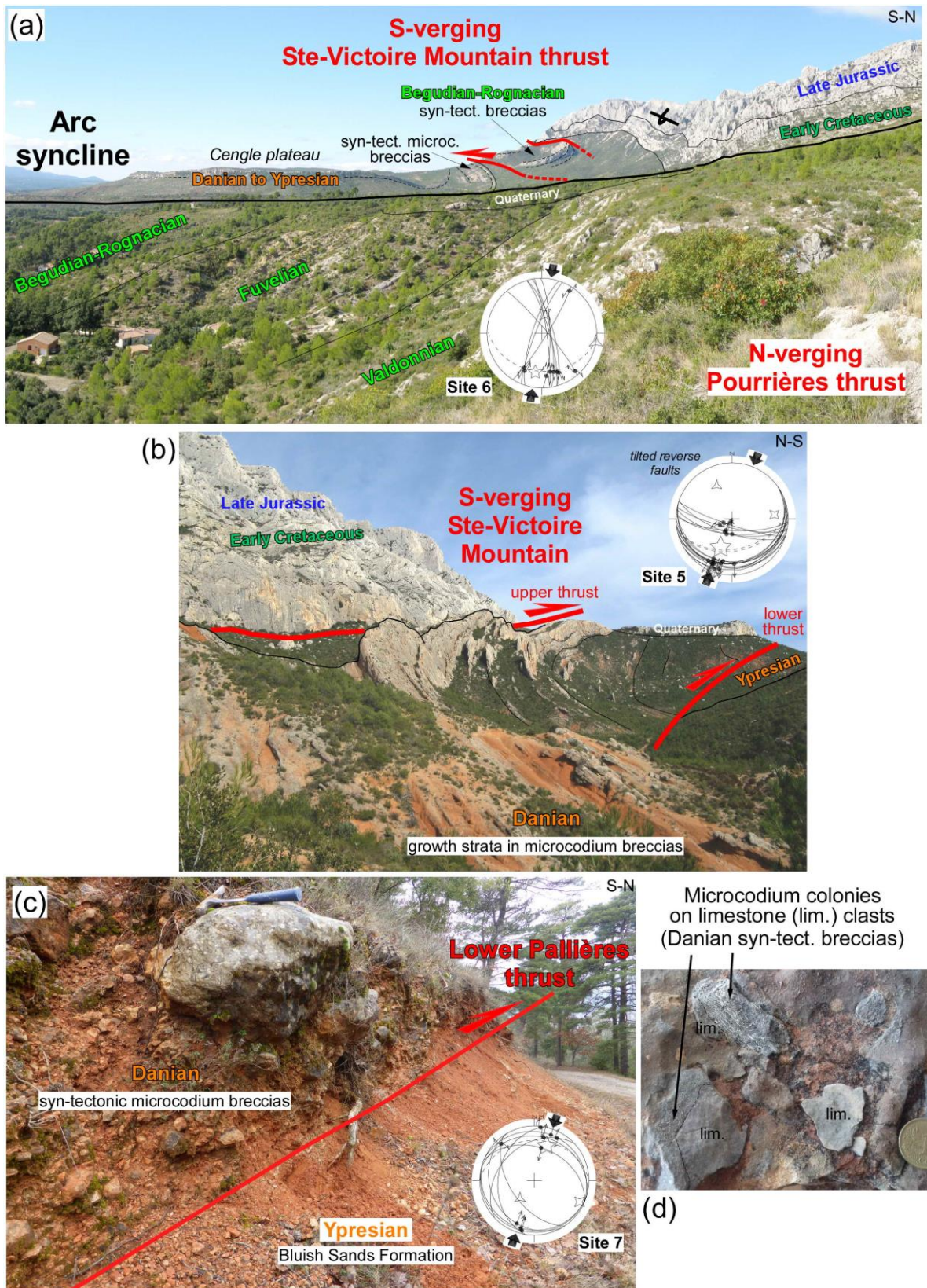


2397 **Fig. 9.** (a) Panoramic view looking eastward of the Sainte-Baume Nappe and its analogous  
 2398 units formed by the Piguière and Liquette slices (view looking eastward;  $43.352896^\circ$ ,  
 2399  $5.615643^\circ$ ). For location, see also Fig. 3. The nappe overthrusts northward Begudian-  
 2400 Rognacian facies strata of the Villecroze zone tectonically separated from the Huveaune  
 2401 Triassic anticlinorium high by the Huveaune fault. Oligocene conglomeratic strata of the La  
 2402 Cauvine basin unconformably rest on the Triassic of the Huveaune high. Under the Sainte-  
 2403 Baume Nappe, the La Lare half-window corresponds to a large autochthonous anticline armed

2405 of upper Jurassic and Cretaceous limestones. Geological data and structural features are from  
2406 Aubagne-Marseille 1:50,000 geological map, 3rd edition, 2018. (b) Panoramic view of the  
2407 southern Plan d'Aups half-window (view looking eastward;  $43.312377^\circ$ ,  $5.660989^\circ$ ). The  
2408 tight Plan d'Aups syncline located under the Pic de Bertagne slice and the Sainte-Baume  
2409 Nappe is cored by Fuvelian facies strata. The northern flank of the Plan d'Aups syncline is  
2410 truncated by the Grande Baume and Pin de Simon slices. Northward, an Oligocene normal  
2411 fault separates the collapsed Sainte-Baume Nappe from these slices. (c) Syn-tectonic breccias  
2412 (Begudian-Rognacian facies) embedding the Grande Baume upper Jurassic unit at the Source  
2413 de Cros (NW Plan d'Aups; view looking westward;  $43.317931^\circ$ ,  $5.689054^\circ$ ). The syn-tectonic  
2414 breccias occur on the northern flank of the Pic des Corbeaux anticline (location on Fig. 9d).  
2415 Photograph from Jean-Claude Tempier. (d) Zoom of the structural cross-section for more  
2416 clarity of the Sainte-Baume Nappe and Aurélien Mount thrust.



2417 **Fig. 10.** Panoramic view of the Aurélien Mount thrust overthrusting Rognacian facies strata  
2418 of the southern limb of Arc syncline (view looking eastward;  $43.479551^\circ$ ,  $5.73129^\circ$ ). For  
2419 location, see also Fig. 3. Striated faults measured in lower Jurassic strata are consistent with a  
2420 ~N-trending compression. Fault data and bedding (dashed line) have been projected in an  
2421 equal area stereogram, lower hemisphere. Geological data and structural features are from  
2422 Aix-en-Provence and Brignoles 1:50,000 geological maps.

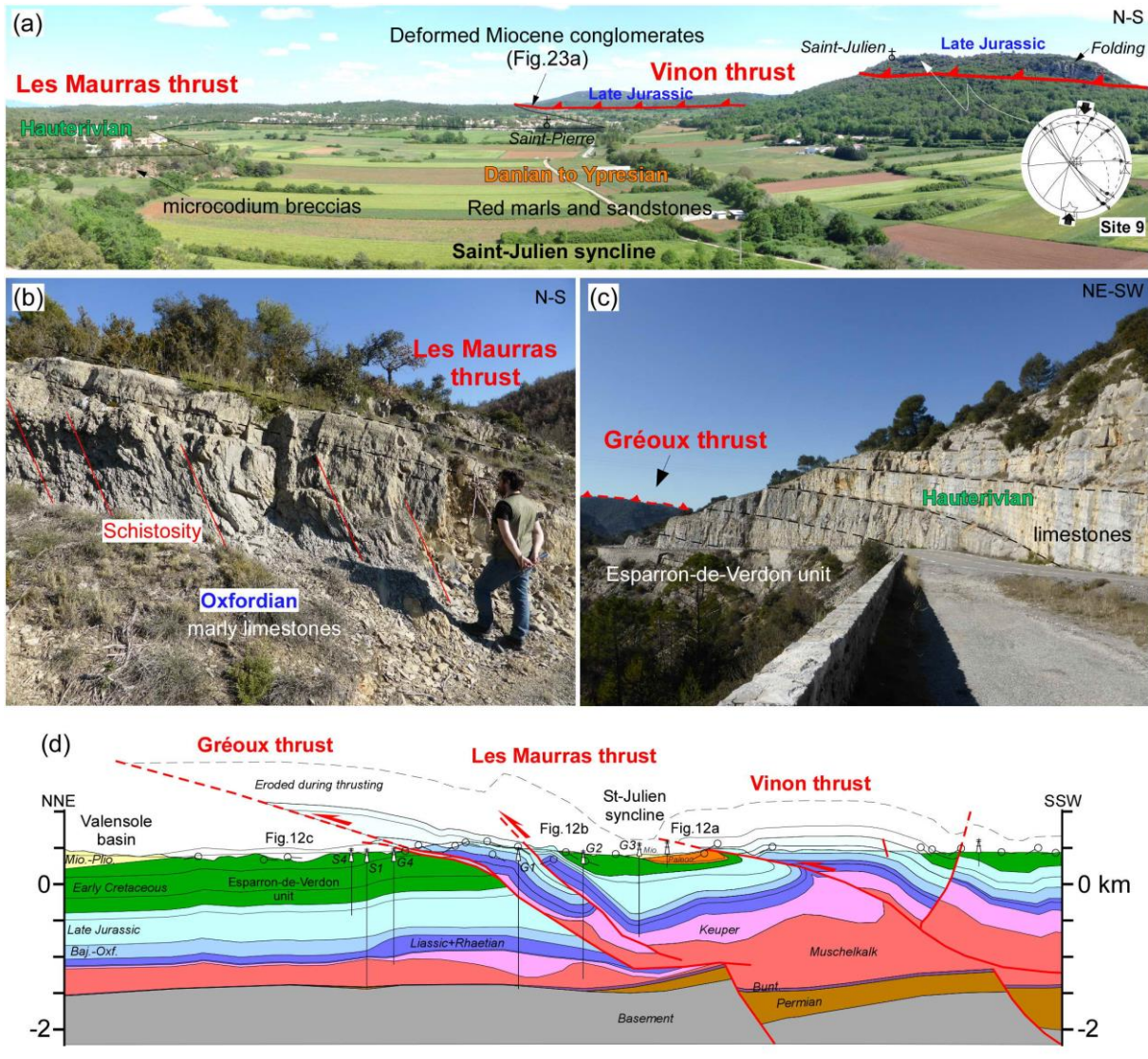


2424

2425 **Fig. 11.** (a) Panoramic view of the northern edge of the Arc syncline (view looking westward;

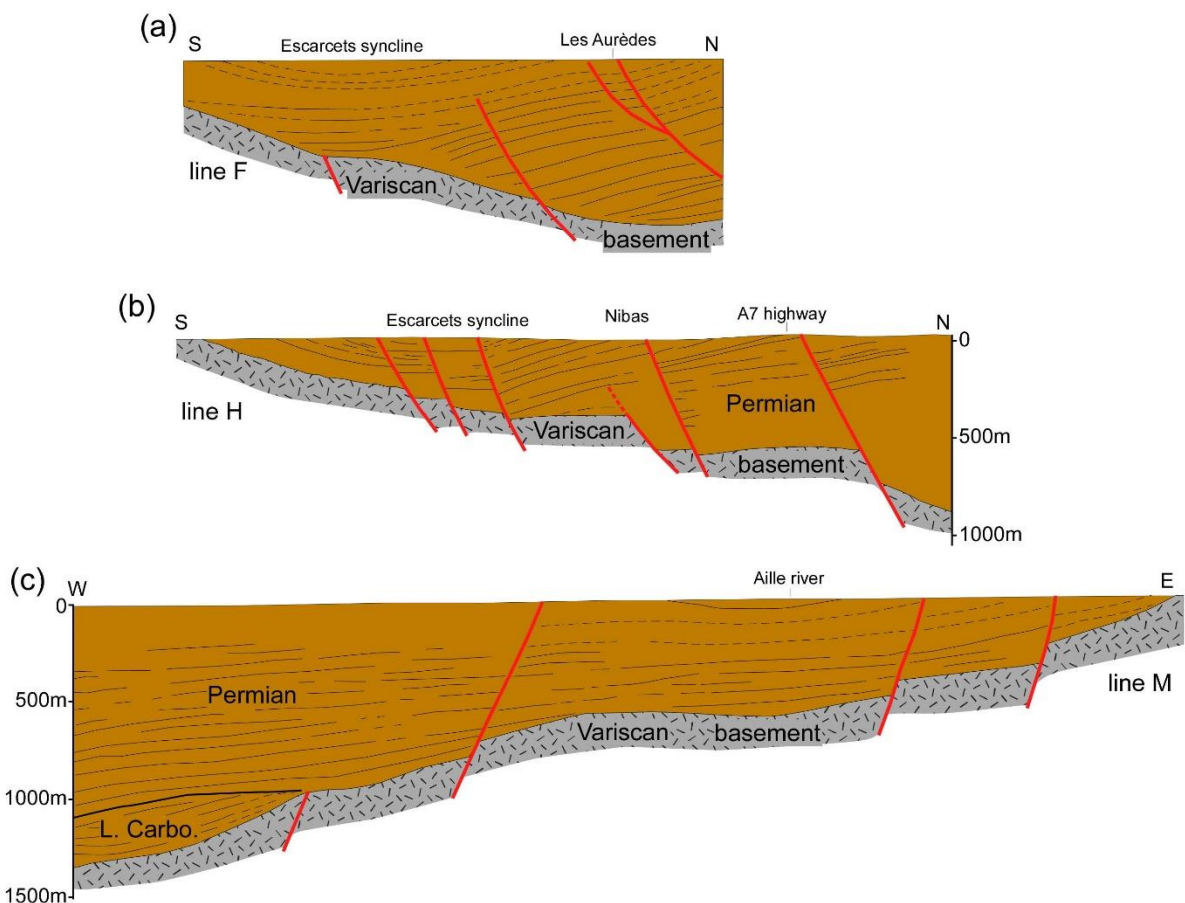
2426 43.529058°, 5.676583°). For location, see also Fig. 3. Westward, the syncline is thrusted by

2427 the S-verging Sainte-Victoire Mountain thrust system, including Begudian-Rognacian and  
2428 Danian microcodium syn-tectonic breccias. Eastward, the upper Cretaceous foreland rocks of  
2429 the Arc syncline pinch-out on lower Cretaceous limestones. The syncline is transported  
2430 northward onto the Pourrières thrust. (b) Panoramic view of the S-verging Sainte-Victoire  
2431 Mountain thrust system with growth strata in Danian microcodium breccias (modified from  
2432 Espurt et al. (2012); view looking eastward;  $43.524806^\circ$ ,  $5.569858^\circ$ ). For location, see also  
2433 Fig. 3. (c) Danian microcodium breccias on the Pallières unit thrusting Ypresian Bluish Sands  
2434 Formation ( $43.590979^\circ$ ,  $5.837873^\circ$ ). (d) Details of the microcodium breccias including  
2435 Mesozoic limestone clasts corroded by microcodium. Striated faults measured in Valdonnian  
2436 limestones and Danian microcodium breccias are consistent with a NNE-trending  
2437 compression. Fault data and bedding (dashed line) have been projected in an equal area  
2438 stereogram, lower hemisphere.

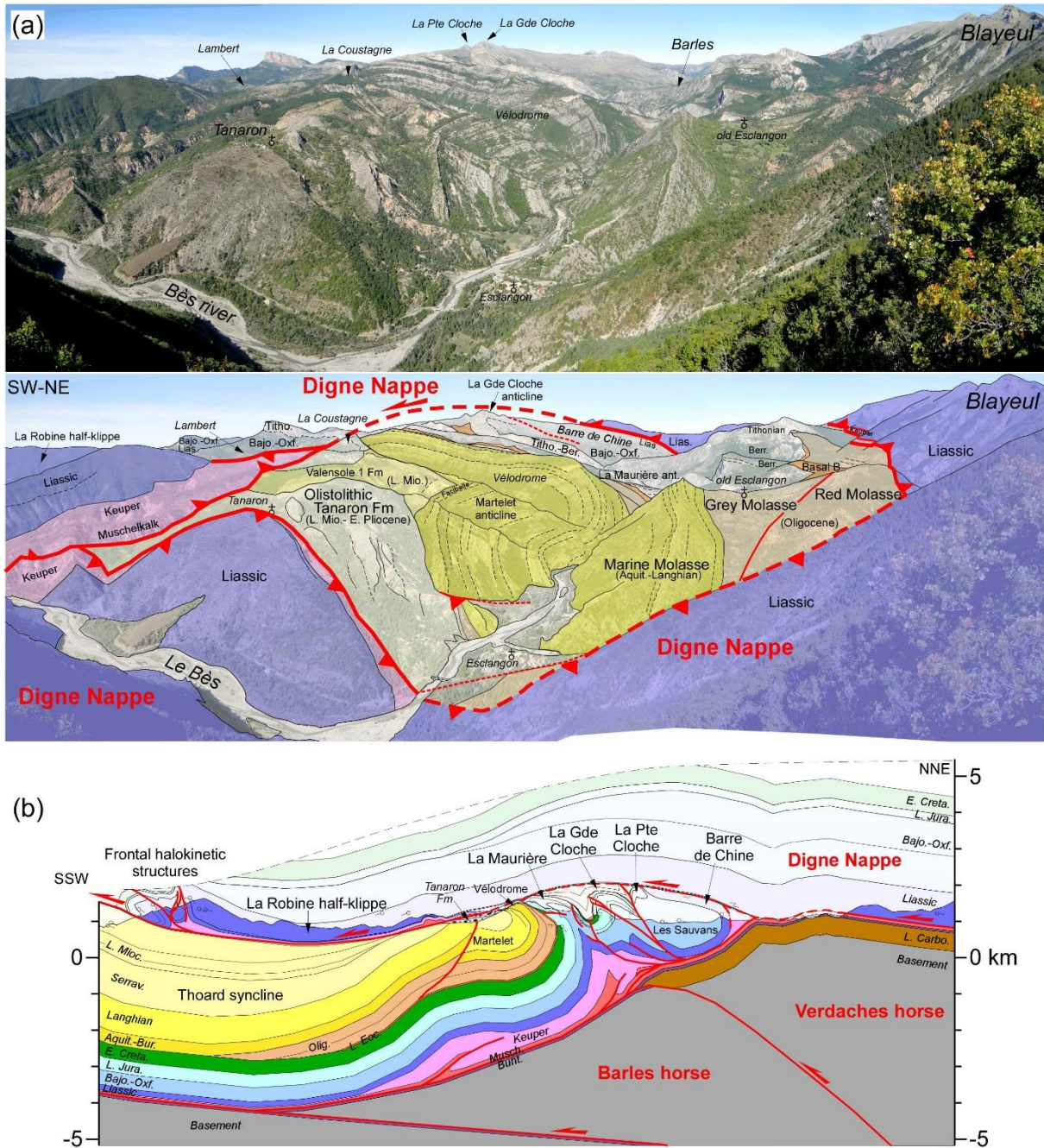


2439 **Fig. 12.** Field observations along the Vinon, Les Maurras and Gréoux thrusts. (a) Panoramic  
 2440 view of the Vinon thrust overlying Paleocene strata in the Saint-Julien syncline (view looking  
 2441 eastward;  $43.702067^\circ$ ,  $5.899911^\circ$ ). For location of the Saint-Julien syncline, see also Fig. 3.  
 2442 The activity of this thrust was recorded at least by Danian microcodium breccias outcropping  
 2443 in the norther limb of the Saint-Julien syncline. Striated faults measured in upper Jurassic  
 2444 limestones of the Vinon thrust are consistent with a NNE-trending compression. Fault data  
 2445 and bedding (dashed line) have been projected in an equal area stereogram, lower hemisphere.  
 2446 Eastward, the Vinon thrust is covered by Miocene conglomerates with sheared and striated  
 2447 pebbles (see Fig. 23a). Geological data and structural features are from Tavernes 1.50 000  
 2448

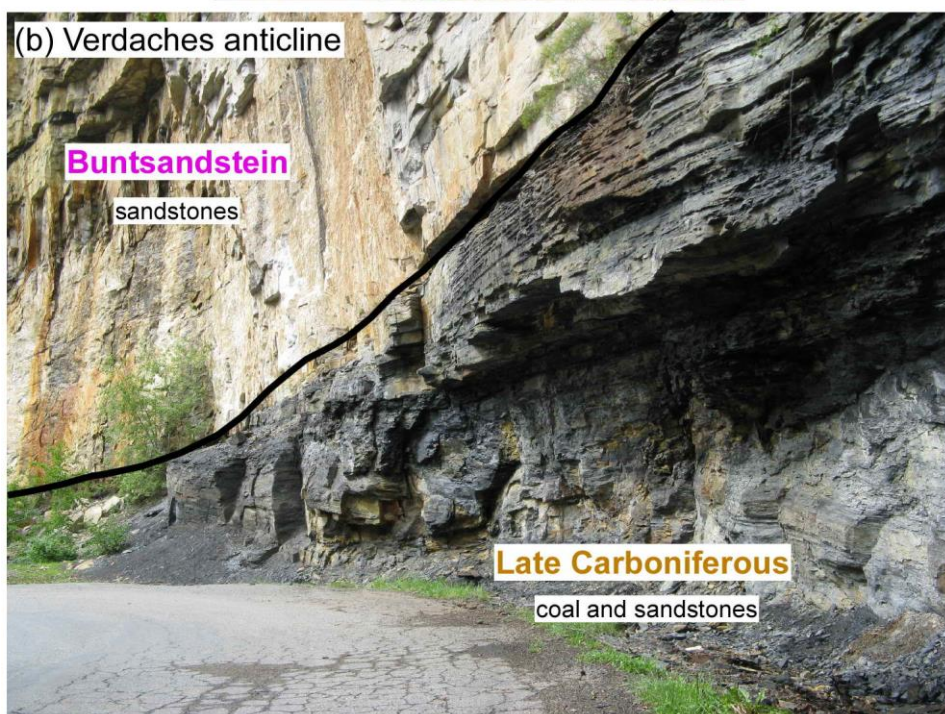
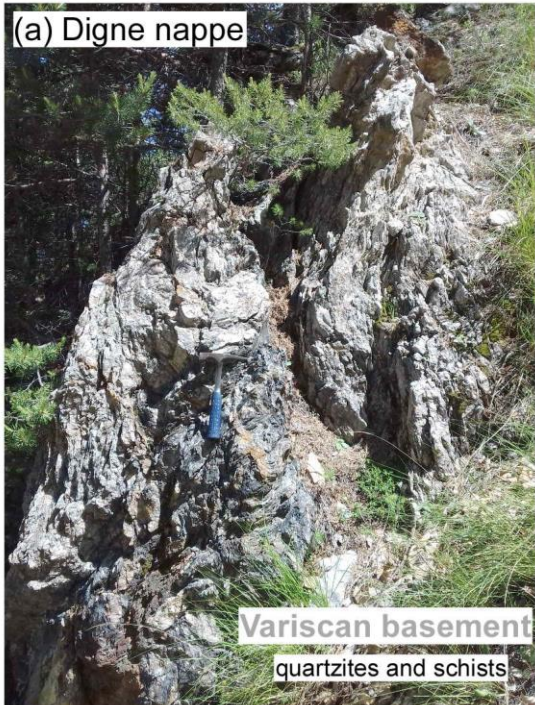
2449 geological map. (b) Sheared middle Jurassic marly limestones in the hanging wall of the Les  
 2450 Maurras thrust ( $43.737375^\circ$ ,  $5.874535^\circ$ ). (c) N-dipping Hauterivian limestones in the footwall  
 2451 of the Gréoux thrust ( $43.764164^\circ$ ,  $5.928908^\circ$ ). (d) Zoom of the structural cross-section for  
 2452 more clarity of the Vinon, Les Maurras and Gréoux thrusts.



2454 **Fig. 13.** Interpreted cross-sections documenting the structure of the Permian extensional basin  
 2455 of Luc along the seismic lines F (a), H (b) and M (c). Modified from Baudemont (1985). For  
 2456 locations, see Fig. 3.



2464 of the Thoard syncline. The Miocene strata of the Vélodrome structure (Marine Molasse and  
2465 conglomerates of the Valensole 1 Formation) show sedimentary wedging. These strata are  
2466 unconformably covered by the upper Miocene-lower Pliocene olistolithic Tanaron Formation,  
2467 a chaotic melange of large middle Jurassic olistoliths with evaporites (Lambert locality),  
2468 upper Jurassic-Berriasiian limestone (e.g., La Coustagne) and Eocene-Miocene olistoliths  
2469 included in red marls, sandstones and conglomerates beds. Geological data and structural  
2470 features are from La Javie 1:50,000 geological map. (b) Zoom of the structural cross-section  
2471 for more clarity of the more clarity of the Barles half-window and Digne Nappe.



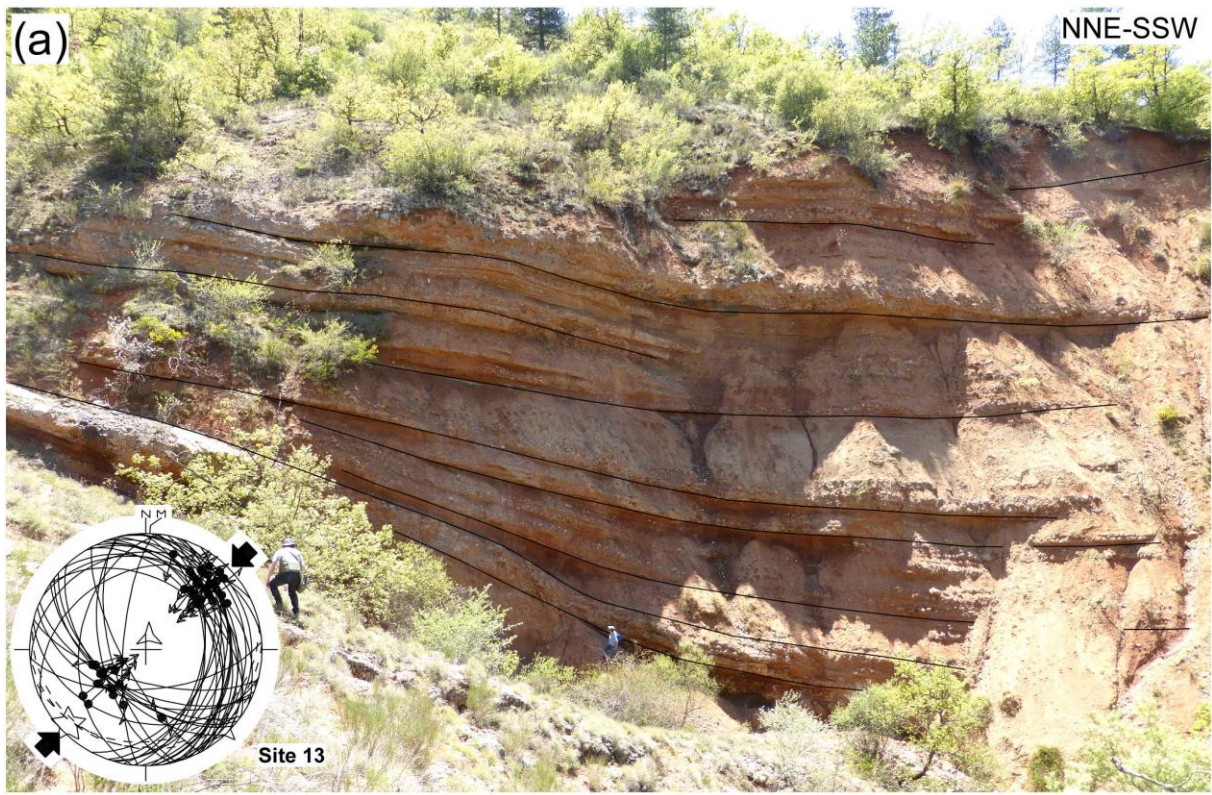
2472

2473 **Fig. 15.** (a) Tectonic slice of Variscan basement at the base of the Digne Nappe (Guimard,  
 2474 1990) ( $44.263578^\circ$ ,  $6.293548^\circ$ ). (b) Upper Carboniferous coal and sandstones unconformably  
 2475 covered by lower Triassic sandstones in the Verdaches basement anticline ( $44.273110^\circ$ ,  
 2476  $6.299909^\circ$ ).



2477

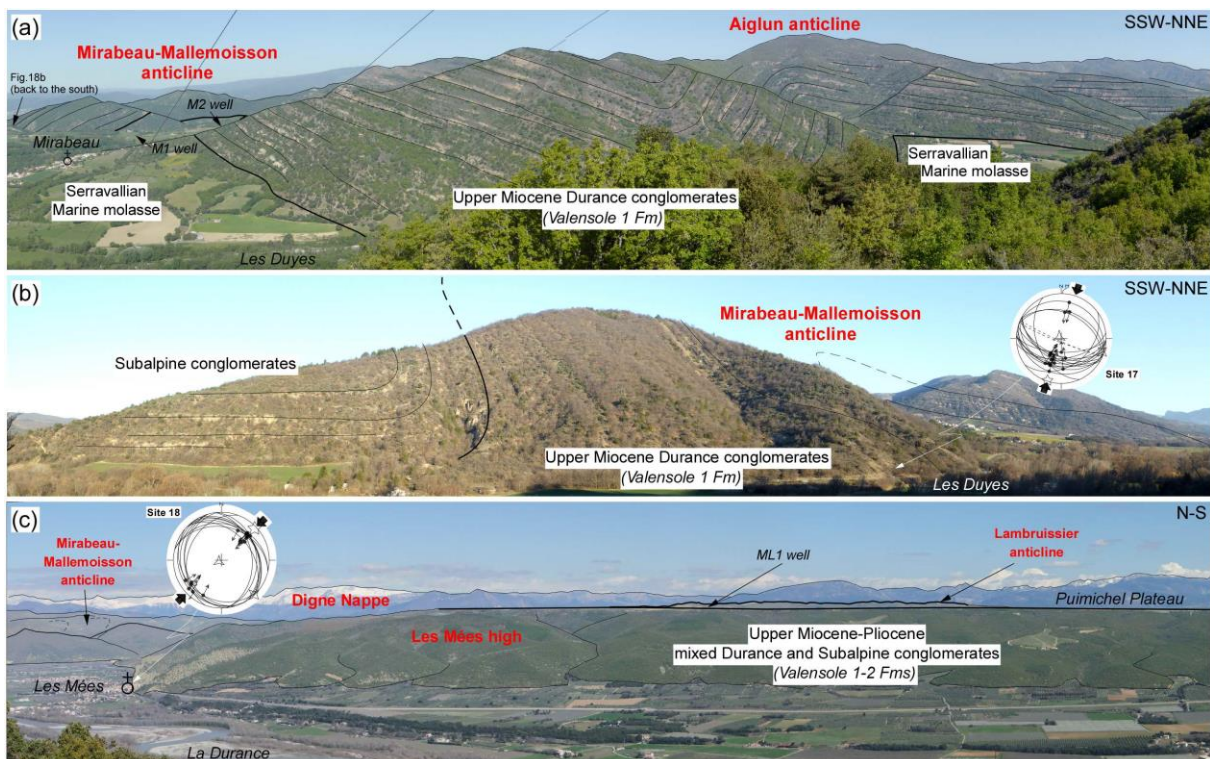
2478 **Fig. 16.** Outcrops of upper Eocene-lower Oligocene Basal Breccia Formation in the erosional  
 2479 Barles half-window. (a) Hauterivian strata unconformably covered by the Basal Breccia  
 2480 Formation on the southern limb of the La Grande Cloche anticline ( $44.228736^\circ$ ,  $6.287899^\circ$ ).  
 2481 (b) Fan-shaped geometry in the Basal Breccia Formation in the northern limb of the Feissal  
 2482 syncline ( $44.246639^\circ$ ,  $6.201392^\circ$ ). Striated faults are consistent with a syn-sedimentary NNE-  
 2483 trending compression. Fault data and bedding (dashed line) have been projected in an equal  
 2484 area stereogram, lower hemisphere. (c) Details of the breccias including Mesozoic limestone  
 2485 clasts (Le Pas de Terre Rouge, southern limb of the La Grande Cloche anticline;  $44.232062^\circ$ ,  
 2486  $6.229132^\circ$ ).



2487

2488 **Fig. 17.** Upper Miocene (Serravallian-Tortonian) Subalpine conglomerate accumulations in  
 2489 the Thoard unit along the Duyes valley west of the La Robine half-klippe (Fig. 3). (a) Growth  
 2490 strata near Thoard town ( $44.164978^\circ$ ,  $6.151822^\circ$ ). Striated faults in these Subalpine

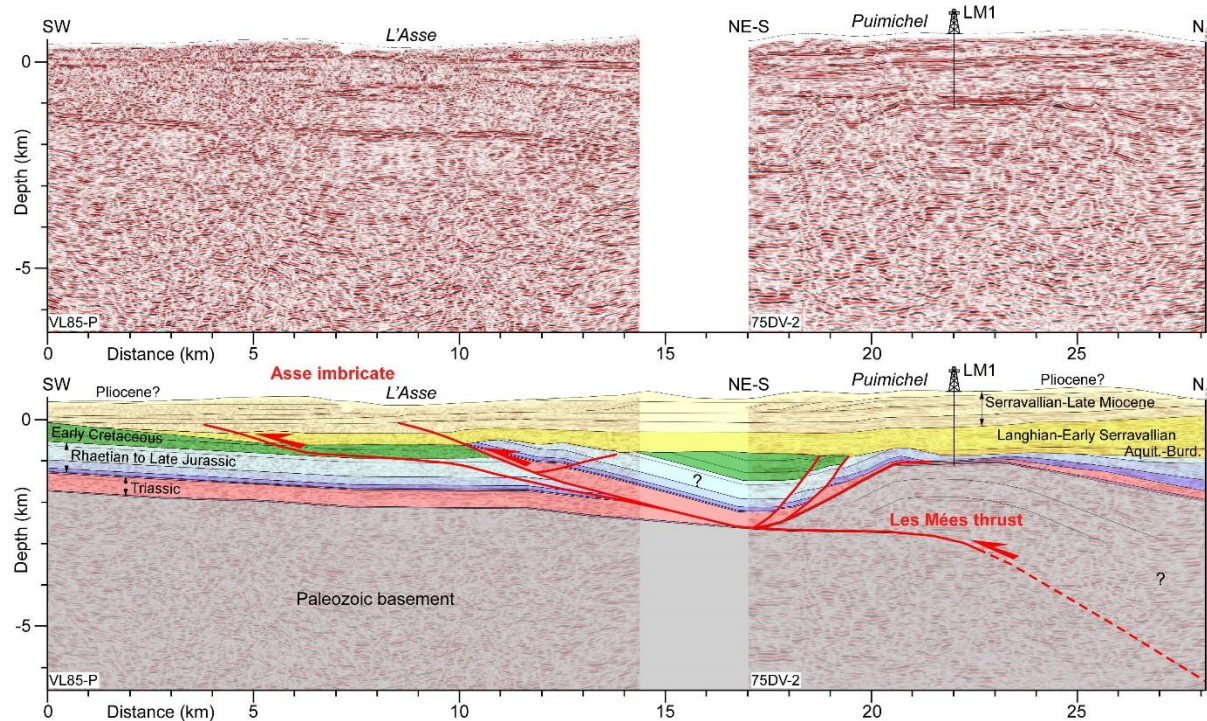
2491 conglomerates are consistent with a NE-trending Alpine compression. The conjugated and  
 2492 tilted reverse faults of the stereogram confirm the tectonic origin of the sedimentary fan. Fault  
 2493 data and bedding (dashed line) have been projected in an equal area stereogram, lower  
 2494 hemisphere. (b) Base of the syn-tectonic Subalpine conglomerates in the Bramefan-Mauduech  
 2495 ravine, high Duyes valley ( $44.181431^\circ$ ,  $6.174494^\circ$ ).



2496

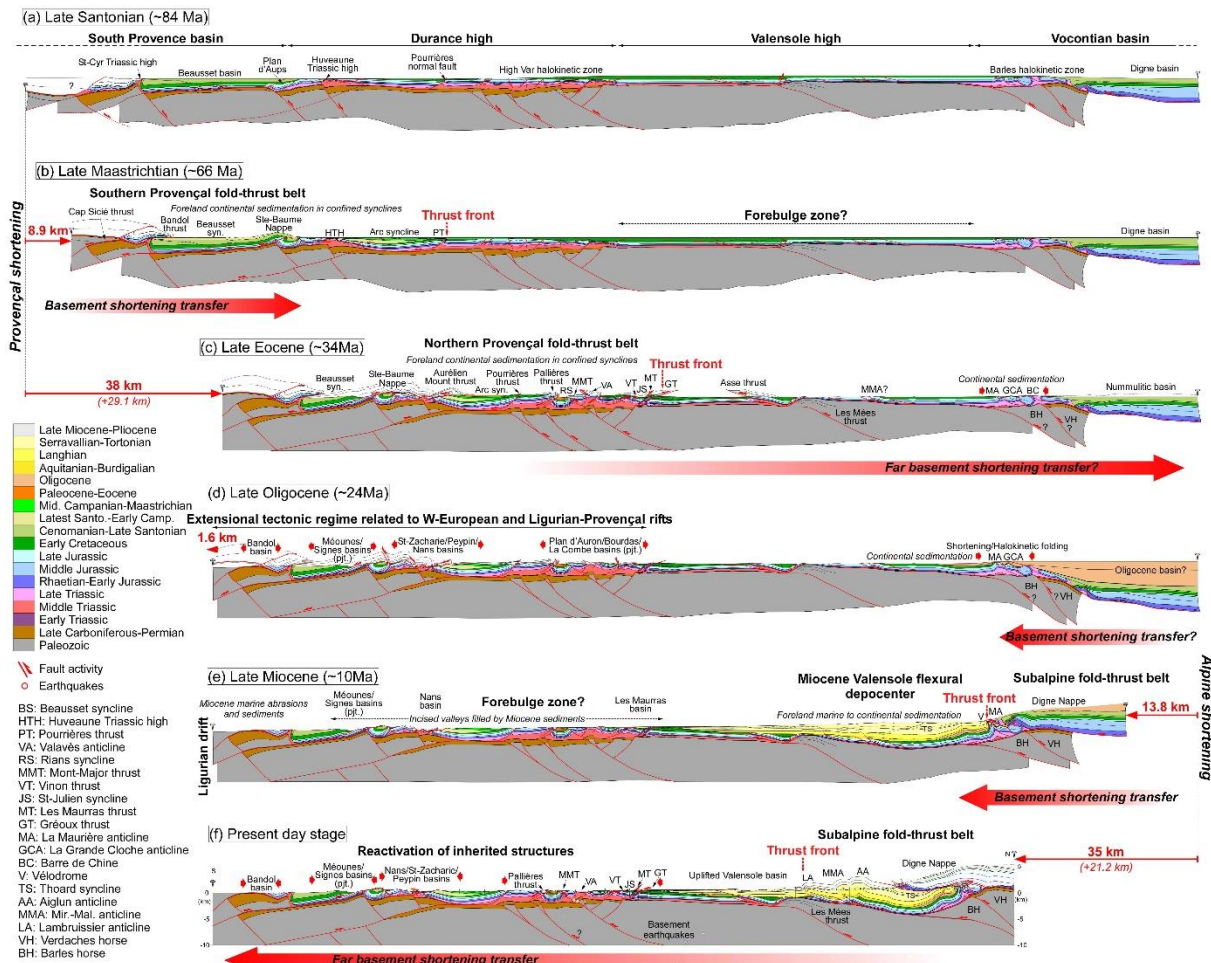
2497 **Fig. 18.** (a-b) Panoramic views of the Aiglun and Mirabeau-Mallemoisson fault-propagation  
 2498 folds armed by upper Miocene conglomerates (Valensole 1 Formation) along the Duyes  
 2499 valley (views looking westward;  $44.066856^\circ$ ,  $6.121088^\circ$ ;  $44.039937^\circ$ ,  $6.103457^\circ$ ). For  
 2500 location, see also Fig. 3. (c) Panoramic view of the southern Valensole foreland basin (view  
 2501 looking NE-ward;  $43.994556^\circ$ ,  $5.906601^\circ$ ). Here, the basin is filled by upper Miocene-  
 2502 Pliocene conglomerates (Valensole 1-2 Formations), topped by slightly S-dipping surface of  
 2503 the Puimichel plateau. Northward, the sedimentary pile is deformed by the Lambruissier and  
 2504 Mirabeau-Mallemoisson anticlines. Striated faults measured in conglomerate beds of the  
 2505 southern limb of the Mirabeau-Mallemoisson anticline and close to the Les Mées town are

2506 consistent with a NE-trending compression. Fault data and bedding (dashed line) have been  
2507 projected in an equal area stereogram, lower hemisphere.



2508

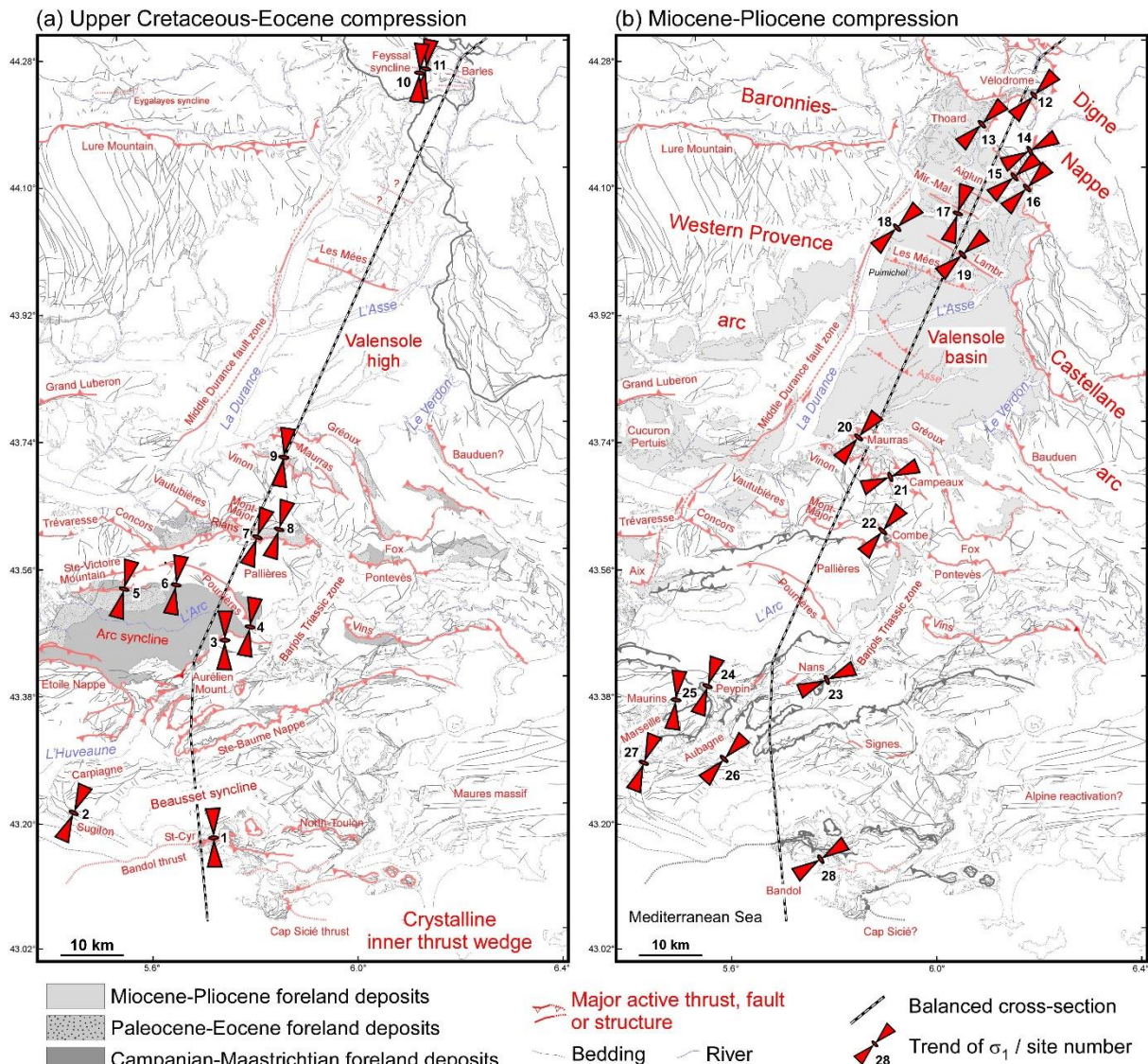
2509 **Fig. 19.** Structural interpretation of southern and central part of the Valensole foreland basin  
2510 using reprocessed seismic profiles VL85-P and 75DV-2 calibrated using the Les Mées-1 well.  
2511 For locations, see Fig. 3. The interpretation of the seismic profiles shows Provençal  
2512 compressional structures (Les Mées basement thrust and upper Asse thrusts) eroded and  
2513 sealed by Miocene strata. These thrusts have been slightly reactivation by the Alpine  
2514 compression.



2515

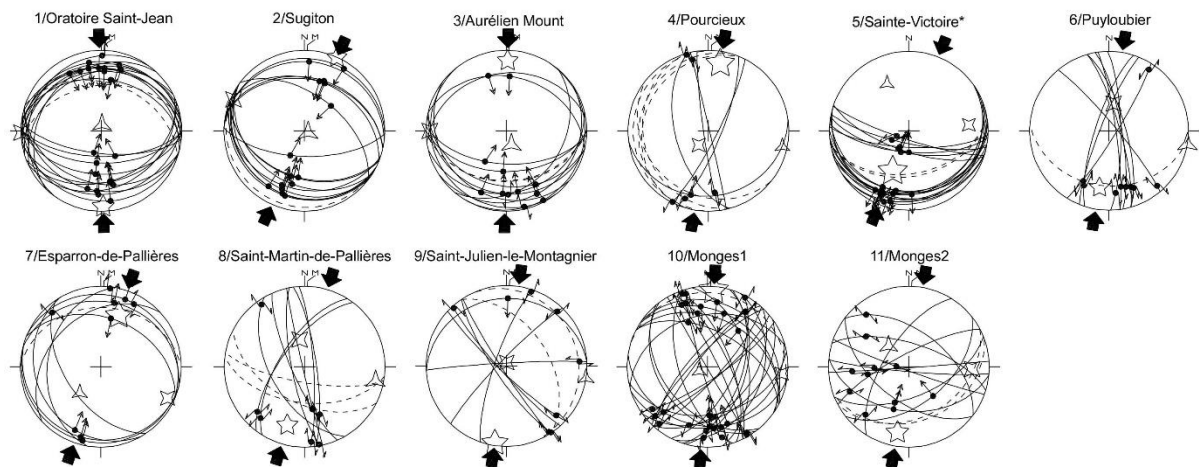
2516 **Fig. 20.** Tectonic evolution of the superimposed Provençal and southwestern Subalpine thrust  
 2517 wedges. (a) Late Santonian restoration showing the structural architecture of the South  
 2518 Provence basin (Beausset basin) and Vocontian basin (Digne basin) separated by the  
 2519 Durance-Valensole high system. (b) Restoration of Provençal belt in Late Maastrichtian with  
 2520 activation of the Bandol thrust and Sainte-Baume Nappe, and sedimentary infill of the Arc  
 2521 depocenter. (c) Restoration of the Provençal belt in Late Eocene with northward transmission  
 2522 of the shortening through the northern part of the Provençal zone, Valensole high, and up to  
 2523 the Barles area. (d) Late Oligocene stage illustrating the deformation of the southern  
 2524 Provençal wedges by extensional faulting and initiation of the Alpine shortening in the Barles  
 2525 area to the north. (e) Growth of the Barles triangle zone during Miocene and concomitant  
 2526 sedimentary infill of the Valensole foreland basin. (f) Late Miocene-Pliocene emplacement of

2527 the Digne Nappe and southward propagation of the Subalpine thrust front into the Valensole  
 2528 foreland basin in cover and up to Mediterranean coast (Bandol basin) through the basement.

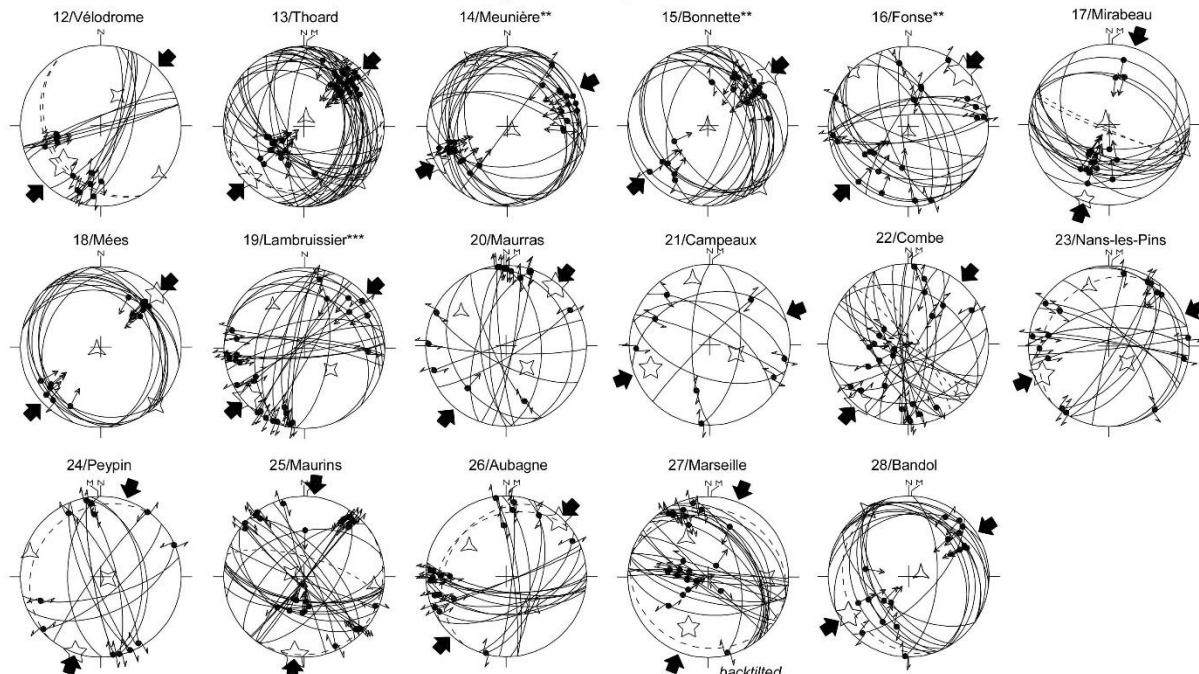


2529 **Fig. 21.** Reconstruction of compression directions (trend of  $\sigma_1$  is shown by red double arrow).  
 2530 (a) Provençal compressional stress field. (b) Alpine compressional stress field. Site numbers,  
 2531 fault slip data and computed principal stress axes are shown in Fig. 22 and Table 1. The  
 2532 names of the major active structures are indicated in red. Thick dashed black and white line  
 2533 shows the trace of the balanced and restored cross-section of Fig. 6.  
 2534

### Provencal compression



### Alpine compression

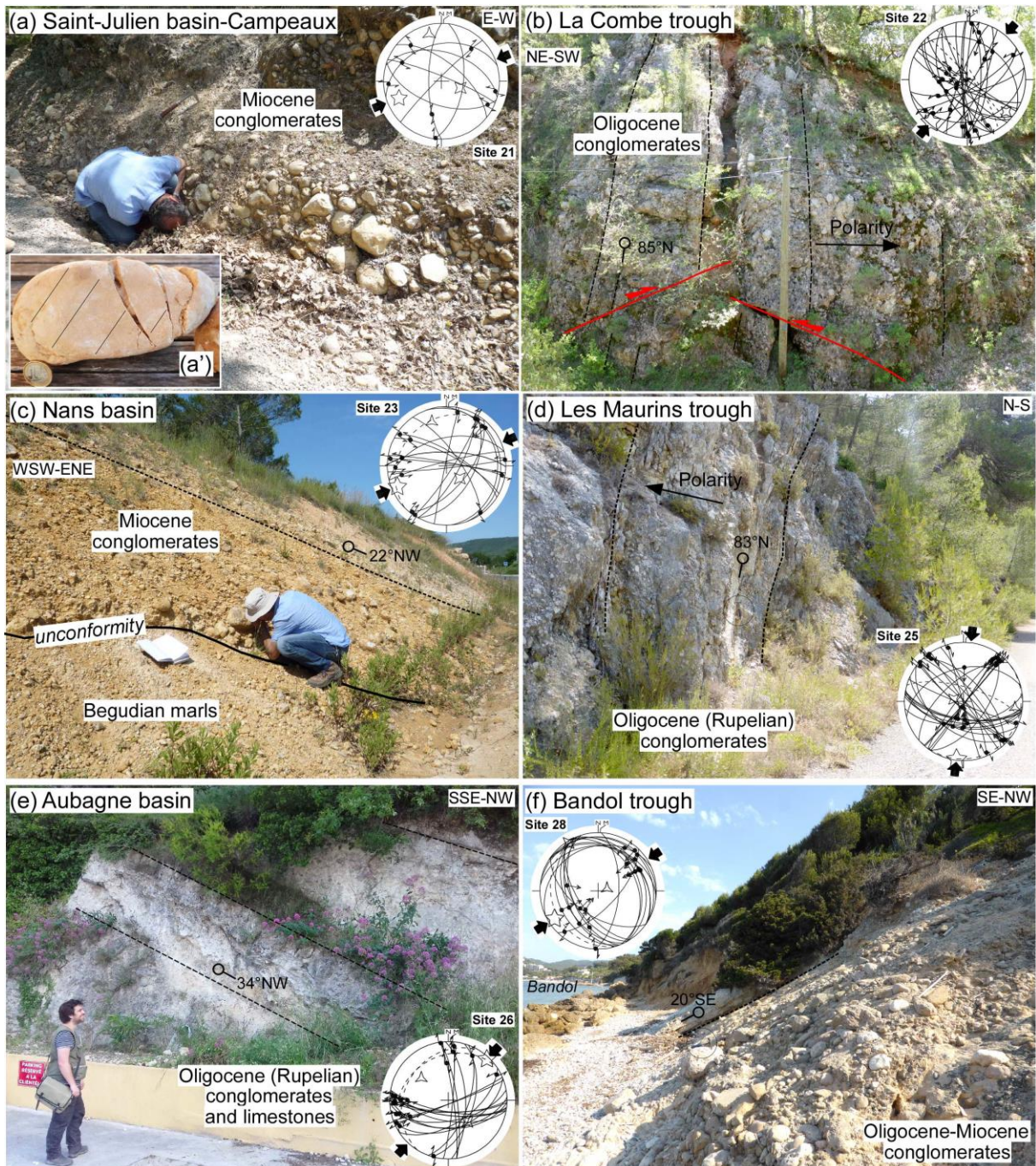


2535

2536 **Fig. 22.** Fault data and principal computed stress axes (see Angelier (1990) for more details).

2537 Principal stress axes ( $\sigma_1$ ,  $\sigma_2$ , and  $\sigma_3$ ) are symbolized by five-branch, four-branch, and three-  
2538 branch stars, respectively. Trend of  $\sigma_1$  is shown by arrows. For locations, see Fig. 21. Data are  
2539 projected in an equal area stereogram, lower hemisphere (see Table 1). Dashed line  
2540 corresponds to the projection of bedding dip in the stereogram. \*Espurt et al. (2012).

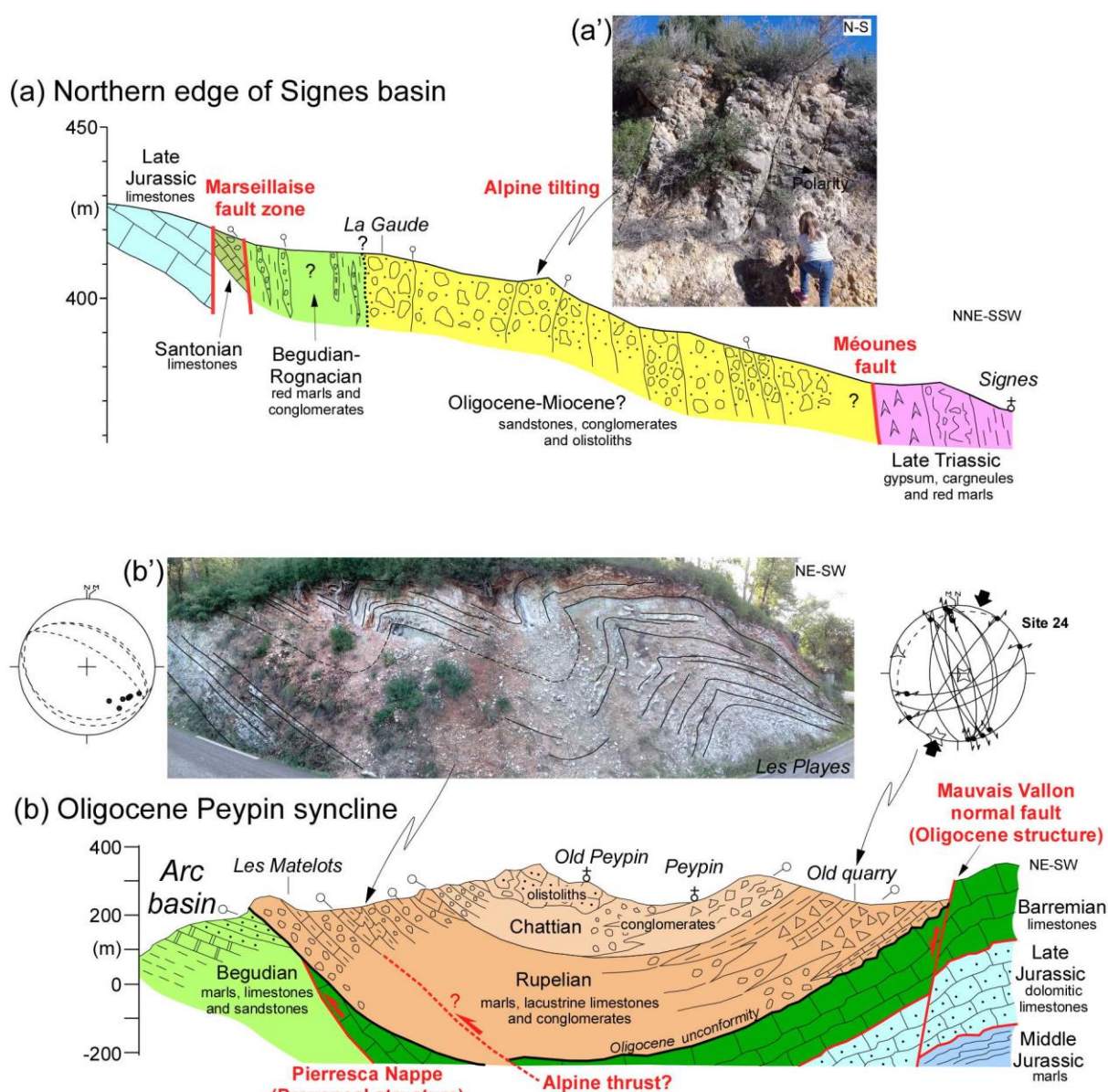
2541 \*\*Hippolyte et al. (2012). \*\*\*Hippolyte and Dumont (2000).



2542

2543 **Fig. 23.** Field evidence for Alpine contractional deformations in the Provençal zone. For  
 2544 location, see Fig. 2. (a) Striated and sheared Miocene conglomerates above the Vinon thrust,  
 2545 eastern edge of the Saint-Julien basin-Campeaux ( $43.677722^\circ$ ,  $5.946401^\circ$ ; Figs. 3 and 12a).  
 2546 (a') Zoom on a sheared and striated (thin black lines) limestone pebble. (b) Overturned  
 2547 Oligocene strata in the La Combe trough, eastern edge of the Rians basin ( $43.600228^\circ$ ,  
 2548  $5.927771^\circ$ ; modified from Espurt et al., 2019b). (c) Tilted Miocene strata in the Nans basin,

2549 southern edge of the Barjols Triassic zone ( $43.392411^\circ$ ,  $5.798388^\circ$ ). (d) Tilted Oligocene  
 2550 (Rupelian) conglomerate beds in the Les Maurins trough ( $43.363886^\circ$ ,  $5.512575^\circ$ ). (e) NW-  
 2551 dipping Oligocene (Rupelian) conglomerate and limestone beds in the southern edge of the  
 2552 Aubagne basin ( $43.282596^\circ$ ,  $5.597940^\circ$ ). (f) SE-dipping Oligocene-Miocene conglomerate  
 2553 beds in the Bandol trough ( $43.133639^\circ$ ,  $5.779645^\circ$ ). Striated faults in these Oligocene and  
 2554 Miocene strata are consistent with a ~NE-trending Alpine compression. Fault data and  
 2555 bedding (dashed line) have been projected in an equal area stereogram, lower hemisphere.



2556

2557 **Fig. 24.** Surficial cross-sections and field evidence showing Alpine contractional  
 2558 deformations in the southern part of the Provençal domain. For location, see Fig. 3. (a)  
 2559 Surface cross-section across the northern part of the Signes basin ( $43.295733^\circ$ ,  $5.867607^\circ$ ).  
 2560 (a') Photograph of overturned beds of Oligocene-Miocene conglomerates is shown. (b)  
 2561 Surface cross-section of the Peypin syncline ( $43.381589^\circ$ ,  $5.575817^\circ$ ). Photograph of SE-  
 2562 trending folds in Oligocene limestone and conglomerate beds on the northern limb of the  
 2563 Peypin syncline is shown ( $43.386835^\circ$ ,  $5.603627^\circ$ ). Striated faults and fold axis in these  
 2564 Oligocene strata are consistent with a NE-trending Alpine compression. Fault data, fold axis  
 2565 (point) and bedding (dashed line) have been projected in equal area stereograms, lower  
 2566 hemisphere.

Site number/name	Latitude (m)	Longitude (m)	Elevation (masl)	Age/Lithology	Number of faults	$\sigma_1$		$\sigma_2$		$\sigma_3$		$\Phi$	ANG	RUP	Stress regime
						Trend	Plunge	Trend	Plunge	Trend	Plunge				
1/Oratoire Saint-Jean	43.166772	5.719908	139	Santonian/Limestones	22	179	6	269	1	5	84	0.448	10	30	reverse
2/Sugiton	43.217049	5.450640	208	Berriasian/Limestones	15	24	0	294	4	115	86	0.559	6	27	reverse
3/Aurélien Mount	43.455585	5.775748	631	Early Jurassic/Limestones	12	1	14	270	5	160	75	0.524	14	34	reverse
4/Pourcieux	43.475319	5.796727	351	Late Jurassic/Limestones	12	1	14	270	5	160	75	0.524	14	33	strike-slip
5/Sainte-Victoire*	43.524806	5.569858	334	Danian/Conglomerates	17	202	45	284	25	335	35	0.08	8	31	reverse
6/Puyloubier	43.528522	5.675310	396	Early Campanian/Limestones	9	190	28	10	62	100	0	0.569	8	36	reverse
7/Esparron-de-Pallières	43.590707	5.838716	495	Danian/Conglomerates	9	19	33	115	9	219	55	0.207	9	39	strike-slip reverse
8/Saint-Martin-de-Pallières	43.601974	5.887519	400	Danian/Conglomerates	8	197	25	350	62	101	11	0.489	14	36	strike-slip
9/Saint-Julien-le-Montagnier	43.692550	5.905738	565	Late Jurassic/Limestones	8	189	3	6	87	99	0	0.238	10	32	strike-slip reverse
10/Monges1	44.242379	6.192825	1450	Late Eocene-Oligocene/Conglomerates	29	5	5	95	8	243	80	0.106	10	38	strike-slip reverse
11/Monges2	44.246639	6.201392	1535	Late Eocene-Oligocene/Conglomerates	11	190	18	92	22	316	60	0.418	17	44	strike-slip reverse
12/Vélodrome	44.203386	6.256325	1191	Late Miocene/Conglomerates	12	224	34	29	55	130	7	0.113	9	33	strike-slip
13/Thoard	44.171178	6.151978	785	Miocene/Conglomerates	38	226	8	135	5	14	81	0.356	8	24	reverse
14/Meunières**	44.123561	6.245412	866	Pliocene/Conglomerates	25	242	2	332	6	134	83	0.34	10	38	strike-slip reverse
15/Bonnette**	44.093349	6.221008	767	Pliocene/Conglomerates	21	50	0	140	0	249	90	0.29	10	32	strike-slip reverse
16/Fonse**	44.072696	6.249599	1050	Pliocene/Conglomerates	21	45	4	315	4	177	85	0.01	11	34	strike-slip reverse
17/Mirabeau	44.043538	6.105934	536	Miocene/Conglomerates	17	192	2	108	4	309	85	0.605	7	18	reverse
18/Mées	44.030339	5.980524	424	Miocene/Conglomerates	15	46	5	137	1	238	85	0.407	8	36	reverse
19/Lambruissier***	43.981107	6.105508	845	Miocene/Conglomerates	26	229	6	130	55	323	34	0.083	10	39	strike-slip reverse
20/Maurras	43.733025	5.891955	458	Miocene/Conglomerates	14	40	4	137	59	307	90	0.223	11	35	strike-slip reverse
21/Campeaux	43.677643	5.946504	522	Miocene/Conglomerates	8	248	22	109	62	345	17	0.393	15	37	strike-slip
22/Combe	43.600039	5.927321	337	Oligocene/Conglomerates	23	221	4	129	15	327	75	0.162	17	45	strike-slip reverse
23/Nans-les-Pins	43.392464	5.798273	369	Miocene/Conglomerates	8	251	18	54	71	159	5	0.434	11	36	strike-slip
23/Peypin	43.381959	5.573757	303	Oligocene/Conglomerates	12	199	1	105	82	289	8	0.389	11	29	strike-slip
25/Maurins	43.366172	5.506941	300	Oligocene/Conglomerates	27	187	2	283	76	97	14	0.17	11	30	strike-slip reverse
26/Aubagne	43.282650	5.597922	114	Oligocene/Conglomerates	19	43	4	138	49	309	40	0.288	13	30	strike-slip
27/Marseille	43.279588	5.444457	97	Oligocene/Conglomerates	23	201	26	82	44	311	35	0.324	13	32	strike-slip reverse

28/Bandol	43.133639	5.779645	1	Oligocene-Miocene/Conglomerates	18	237	12	328	4	76	77	$\frac{0.4}{54}$	13	33	reverse
-----------	-----------	----------	---	---------------------------------	----	-----	----	-----	---	----	----	------------------	----	----	---------

2567 **Table 1.** Paleo-stress tensors computed from fault slip data. See location of sites in Fig. 21.

2568 Fault data and principal computed stress axes are shown in Fig. 22.  $\sigma_1$ ,  $\sigma_2$ ,  $\sigma_3$ : maximum,

2569 intermediary, and minimum principal stress axis, respectively.  $\Phi=(\sigma_2-\sigma_3)/(\sigma_1-\sigma_3)$ .

2570 ANG=average angle between computed shear stress and observed slickenside lineation (in

2571 degrees). RUP=quality estimator ( $0 \leq RUP \leq 200$ ) taking into account the relative magnitude of

2572 the shear stress on fault planes (see Angelier (1990) for more details). \*Espurt et al. (2012).

2573 \*\*Hippolyte et al. (2012). \*\*\*Hippolyte and Dumont (2000).